DISSERTATION

A PHARMACOKINETIC INVESTIGATION OF CHLOROQUINE ANALOGUES IN CANCER AUTOPHAGY MODULATION

Submitted by

Keagan P. Collins

School of Biomedical Engineering

In partial fulfillment of the requirements

For the Degree of Doctor of Philosophy

Colorado State University

Fort Collins, Colorado

Fall 2020

Doctoral Committee:

Advisor: Daniel Gustafson

Ashok Prasad
TingTing Yao
Douglas Thamm
Andrew Thorburn

ABSTRACT

A PHARMACOKINETIC INVESTIGATION OF CHLOROQUINE ANALOGUES IN CANCER AUTOPHAGY MODULATION

Hydroxychloroquine (HCQ) is currently being investigated for safety and efficacy as an autophagy inhibitor in Phase I/II cancer clinical trials. It is the only clinically-approved autophagy inhibitor for use in cancer clinical trials in the United States. HCQ is used in combination with other chemotherapeutics to augment their efficacy and has shown moderate success in treating patients with late stage cancers. While HCQ has a good safety index and shows promise as an addition to standard of care treatment regimens, it suffers from several critical pharmacologic shortcomings which we take steps to address herein. The primary issues with usage of HCQ addressed in this work are the metrics used to predict patient tumor concentration of the drug following various dosing regimens.

HCQ pharmacokinetics (PK) are highly variable in patients, with no correlation between traditional plasma:tumor concentrations. The first step taken to address this problem is to characterize likely sources of interindividual variability in HCQ PK. To do this a physiologically-based pharmacokinetic (PBPK) model was developed to investigate absorption, distribution, metabolism, and toxicity (ADMET) factors relating to HCQ in a mathematical system representative of the human body. This model was developed based on physiological and biochemical parameters relevant to HCQ

ADMET in mice and scaled to represent humans. The model was capable of simulating single and multiple dosing regimens in humans, that would be characteristic of a cancer clinical trial.

PBPK modeling addressed variability that would be associated with the macrophysiologic scale, but intrinsic and extrinsic factors on the cellular scale needed to be further defined to strengthen the understand of HCQ PK. To investigate factors that affect cellular uptake and sub-compartment localization of HCQ, a base PK model of lysosomotropic agents like HCQ was applied. Model specific parameters were identified for a panel of four human breast cancer cell lines, and a majority of differences in cellular uptake of the drug could be attributed to differences in the relative lysosomal volume fraction of each cell line. The model was able to characterize HCQ PK under different extracellular pH conditions, and identified a positive-feedback loop, related to transcription factor EB (TFEB) activation. This feedback loop caused the cell to increase its lysosomal volume over time of exposure to HCQ, resulting in a continuous increase of HCQ concentration within the cell.

Through sensitivity analysis of the model, acidic extracellular pH was identified as a critical limiting factor of HCQ uptake into cells – which is particularly important as the tumor microenvironment is physiologically acidic. HCQ concentrations in cells cultured in an acidic microenvironment are decreased up to 10-fold, which cannot be overcome without the aid of agents that neutralize this pH. Dimeric analogues of HCQ, Lys05 and DC661, have been reported to maintain potency in acidic conditions and so were investigated in a comparative context to HCQ. Lys05 and DC661 were found to behave similarly to HCQ pharmacokinetically – i.e. highly dependent on the lysosomal

profile of the cell. These drugs exhibited similar kinetic uptake curves as HCQ, and also induced the lysosomal biogenesis PK feedback loop. Unlike HCQ, Lys05 and DC661 uptake was not completely inhibited by acidic extracellular pH, and they were able to maintain activity under these conditions. PK of these drugs was characterized in a murine model to investigate their potential as *in vivo* agents, suggesting they could maintain high concentrations for a longer duration than HCQ. Lys05 and DC661 share many pharmacologic similarities to HCQ, while not sharing significant shortcomings such as inactivity under acidic extracellular conditions suggesting they should be investigated for further application as next generation autophagy inhibitors.

ACKNOWLEDGEMENTS

Of the 200+ pages that compose this dissertation, this is probably the most difficult part to write as there are many people whose continued support and guidance have helped me accomplish the research outlined herein. First and foremost, I'd like to thank my advisor and mentor, Dr. Daniel Gustafson, whose continued enthusiasm for the ideas we've pursued has been a constant source of motivation throughout the ups and downs of research. Dan, you offered me the chance to give graduate school a try, a commitment I was initially unsure about, and ultimately inspired me to pursue a PhD. Thank you for your continued guidance in approaching challenging problems.

I also owe a great deal of thanks to those on my committee, Drs. Ashok Prasad, Douglas Thamm, TingTing Yao, and Andrew Thorburn, for serving as mentors and offering a broad degree of insight in our brief, but thought-provoking meetings that led me to approach problems in often unique ways. I'd also like to offer thanks for those who went out of their way to offer me guidance and served as invaluable mentors and role models – Dr. Daniel Regan and Paul Lunghofer. Dr. Regan, your expertise has been invaluable, and in many ways I've seen you as a second mentor. Paul, your technical skills in analytical chemistry are second to none. I appreciate everything you've taught me along the way, and have definitely enjoyed the laughs we've shared over the past few years. Other members of the ACC - Josh "Shmoop" Mannheimer, Dominique "Armadillo" Ramirez, Jade Kurihara, and Kathryn "Eenis" Cronise you have been incredible friends and colleagues.

Most of all I want to give thanks to my friends and family for continuing to support me through what has often felt like an endless endeavor. Mom, Dad, I made it and I couldn't have done it without you. Kevin and Jessi, thank you for coming in and out of my life for the past few years. You're the glue that has held this all together. A big thank you to all!

TABLE OF CONTENTS

Chapter One

Introduction

Autophagy and Cancer

Overview

Autophagy is a naturally occurring catabolic process that involves recycling of a cell's own proteins, organelles, and other cellular debris. Serving as a key regulator of cellular homeostasis, autophagy constantly operates at a basal level and shifts activity in response to cellular stress, which can include nutrient-deprivation, hypoxia, pharmacologically-induced stress, and rise of reactive oxygen species (ROS) to name a few. Autophagy exists in three main forms – macroautophagy, microautophagy, and chaperone-mediated autophagy (CMA). Macroautophagy is the primary autophagic pathway and serves as a recycling mechanism for damaged proteins and organelles. It involves a double-membraned vesicle (phagophore) engulfing the substrate of interest to form an autophagosome. Autophagosomes are shuttled through the cytoplasm to the lysosome, a highly acidic organelle responsible for many cellular degradation processes, fusing together to form an autolysosome wherein autophagosome contents are degraded by acid hydrolases. Microautophagy involves contents of the cytosol

directly taken up into the lysosome through invaginations in the membrane. CMA is a more complex process involving substrate tagging, transport to, and entry into the lysosome by a protein called heat shock cognate 70 (hsc70). Each process is involved in maintaining cellular homeostasis, but most of this dissertation will focus on macroautophagy, which will simply be referred to as “autophagy” for the remainder of this work.

Mechanism

The molecular mechanism of autophagy is primarily governed by a family of autophagy-related genes (ATG) and consists of three main steps – autophagy initiation and autophagosome nucleation, autophagosome maturation, and lysosomal fusion and degradation.

Autophagy initiation (*step 1*) begins with the mTORC1 complex, located on the lysosomal membrane and often regarded as the primary regulator of autophagy. Under nutrient-rich conditions mTORC1 maintains phosphorylation of the ULK1 (ATG1) complex which suppresses autophagy (active at a basal level). Class I PI3K activates mTORC1 through Rag and Rheb GTPases, whose signaling is driven by amino acids, glucose, O2, ATP, growth factors (including cytokines), and hormones (including insulin) (Dibble and Cantley, 2015). Abundant levels of these signaling factors maintain mTORC1 activation, which inhibits autophagy (*step 1a*). mTORC1 can be pharmacologically inhibited by drugs like rapamycin or temsirolimus to induce autophagy (Chude and Amaravadi, 2017). The activated ULK1 complex targets Vps34 on the downstream class III PI3K complex (*step 1b*). Vps34 is attached to the tumor suppressor Beclin 1 (BECN1) (Liang et al., 1999), and activates another attached

protein, BECN1-regulated autophagy protein (AMBRA1), to drive autophagosome biogenesis and maturation (Wu et al., 2010; Dowdle et al., 2014). Autophagosome formation can be pharmacologically inhibited by Vps34 inhibition using SAR405, or by inhibition of the PI3K class III complex as a whole using 3-methyladenine (3-MA), wortmannin, and LY294002 (Chude and Amaravadi, 2017).

Autophagosome maturation (*step 2*) involves conjugation of ATG16L1 with the ATG5-ATG12 complex, driven by ATG7 and ATG10, causing membrane expansion (*step 2a*). Additionally, microtubule-associated protein light chain 3 (LC3) is incorporated into the autophagosome membrane to promote vesicle growth (*step 2b*). This process involves LC3-II formation that occurs when LC3-I is lipidated with phosphatidylethanolamine (PE) by ATG4B and ATG7, after which LC3-II is incorporated into the autophagosome membrane (Levy et al., 2017). Buildup of LC3-II, also referred to as MAP1LC3B, is one of the common markers of autophagic flux (Klionsky et al., 2016). LC3-II buildup can be prevented by inhibiting ATG4B, which blocks catalyzation of LC3-I lipid conjugation (Chude and Amaravadi, 2017).

The final step of autophagy (*step 3*) involves fusion of the autophagosome with the lysosome, forming an autolysosome, and subsequent degradation of the intravesicular products by lysosomal acid hydrolases. Degradation products are recycled and used to power other cellular metabolic processes (Levy et al., 2017). Adaptor protein sequestosome 1 (p62, SQSTM1), a substrate-to-autophagosome targeting protein, is degraded during lysosomal fusion along with LC3-II (Levy et al., 2017). Both p62 and LC3-II protein levels are commonly used as markers of autophagic flux (Klionsky et al., 2016). Lysosome-autophagosome fusion and

degradation is a function of multiple factors including lysosomal Ca^{2+} content, lysosomal membrane permeability, and lysosomal pH, just to name a few (Lu et al., 2017). Inhibition of this step is the primary target of pharmacologic autophagy inhibition in the clinic, and can be achieved with the clinically-approved autophagy inhibitors chloroquine (CQ) and hydroxychloroquine (HCQ), and other non-approved drugs such as bafilomycin A1 (BafA1), Lys05, quinacrine, mefloquine, and others (Chude and Amaravadi, 2017). A detailed description of this process, and steps which can be inhibited, are outlined in Figure 1.1.

Recovery of lysosomes from autophagy involve the formation of new lysosomes that bud off autolysosomes that have completed autophagic degradation. These proto-lysosomes mature in the Golgi where they acquire acid hydrolases and vacuolar ATPase (V-ATPase), which are lysosomal membrane-bound proton pumps that maintain acidic luminal pH (Rubinsztein et al., 2012; Yin et al., 2016). Additionally, lysosomal biogenesis can be directly initiated by the coordinated lysosomal expression and regulation (CLEAR) network through master lysosomal transcription factor EB (TFEB), which is bound to mTORC1 on the lysosomal membrane. This mechanism as it relates to autophagy and lysosomal dynamics will be discussed in detail in Chapter 2.

Role of Autophagy in Cancer

Autophagy in cancer has often been referred to as a “double-edged sword”. As more recent research has suggested, it serves a suppressing or promoting role depending on the stage of tumor progression. In early stages of cancer progression autophagy serves as a suppressing mechanism, increasing rapidly to counteract the rise of reactive-oxidative species (ROS) and associated genomic instability (Amaravadi,

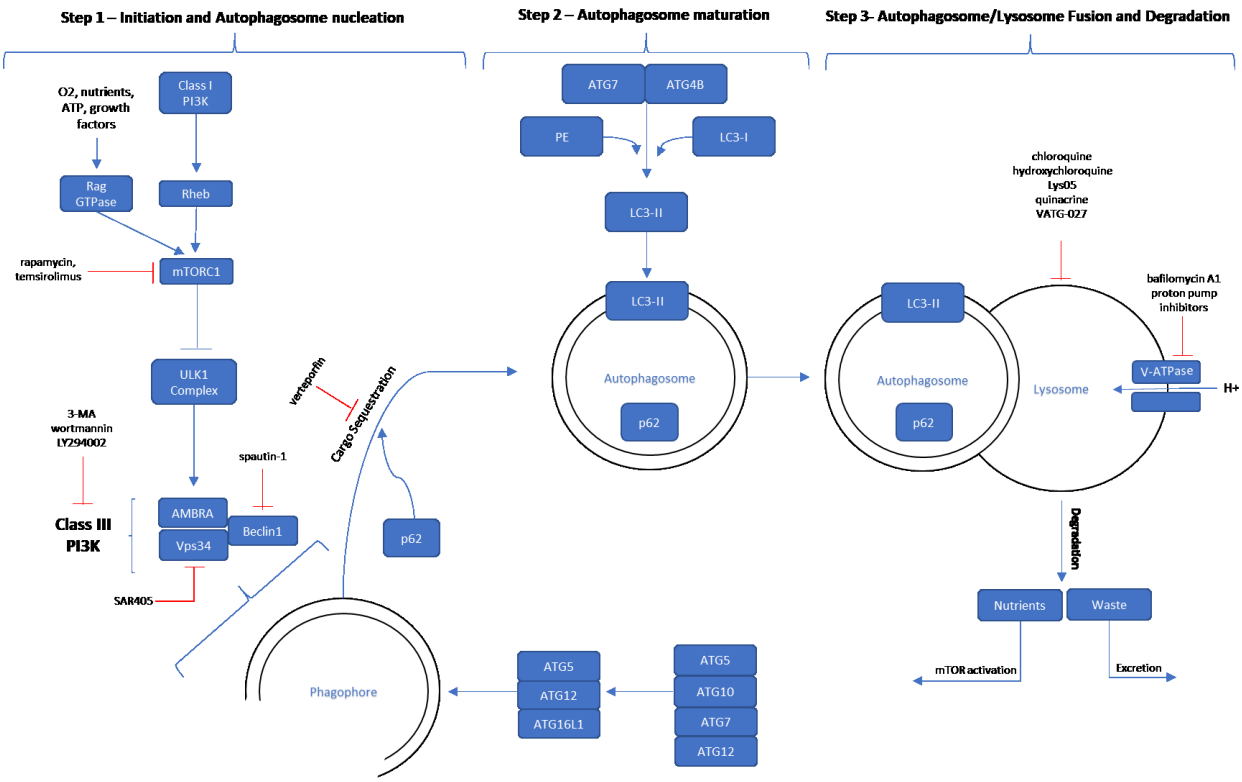

Figure 1.1. Mechanism of autophagy and inhibitors of each step. Step 1 (left): Autophagy initiation occurs when the mTORC1 complex is inhibited. This can happen through inhibition of Class I PI3K, nutrient deprivation, or pharmacologic inhibition through rapamycin analogs. Inhibited mTORC1 releases its hold on the ULK1 complex, which then activates Class III PI3K to begin autophagosome nucleation. Components of Class III PI3K can be inhibited through spautin-1 or SAR405, or directly by 3-MA, wortmannin, or LY294002. Step 2 (center): The phagophore begins to sequester its cargo, including p62-tagged substrates, and transitions into an autophagosome. This can be inhibited by verteporfin. The autophagosome matures as LC3-1 is lipidated with PE by ATG7 and ATG4B to form LC3-II. LC3-II is then incorporated into the membrane of the mature autophagosome. Step 3 (right): Lysosome/autophagosome fusion begins, forming an autolysosome. Fusion can be inhibited by deacidifying the lysosome using clinically-approved autophagy inhibitors chloroquine and hydroxychloroquine, or by Lys05, quinacrine, and VATG-027. Fusion can also be inhibited by blocking the proton pump on the lysosomal surface, V-ATPase, by bafilomycin A1 or proton pump inhibitors. When fusion occurs successfully the contents of the autophagosome are degraded by acid hydrolases. Waste is excreted extracellularly, and nutrients are recycled for use within the cell.

2011). As the premalignancy transitions to the primary tumor stage, autophagy is suppressed allowing for rapid tumor growth and maintenance. The tumor will continue to progress to later stages, which are associated with harsh microenvironmental conditions such as nutrient deprivation and hypoxia, causing a subsequent rise in autophagy to promote survival in this environment (Lazova et al., 2012). Roles of autophagy in the survival of these late stage tumor cells include providing nutrients through catabolism and recycling organelles and proteins damaged by attempted cancer treatments, promoting resistance to drug therapies (Amaravadi and Thompson, 2007).

Preclinical Studies

The role of autophagy in late stage cancer has been investigated in many preclinical studies using clinically-approved autophagy inhibitors CQ and HCQ, and others that are not approved for clinical studies, like BafA1 and Lys05. The tumor suppressing role of autophagy was first demonstrated in mice with allelic loss of BECN1/ATG6, which was associated with development of hepatocellular carcinomas in aged mice and eventually led to BECN1 classification as a tumor suppressor (Qu et al., 2003). The role of autophagy in tumorigenesis has also been investigated *in vitro* in the context of p62 accumulation. Autophagy suppresses rise of ROS through sources like old/damaged mitochondria and defective proteins. Buildup of p62 is associated with activation of NRF2, which is normally activated during inflammation and injury to express antioxidant proteins (White, 2013). When these scenarios occur and autophagy is significantly suppressed, NRF2-promoted antioxidant effects are not sufficient to quell the rise of ROS, describing why inflammation and tumorigenesis are

linked when autophagy is inhibited, and observed by p62 accumulation (Degenhardt et al., 2006; Mathew et al., 2009). On the other hand, lower incidence of cancer has been linked to autophagy induction in cases of caloric restriction and exercise (Blagosklonny, 2010). Amaravadi et. al. (Amaravadi, 2011) examines this tumor suppression role further to show that autophagy is important in suppressing early stages of tumorigenesis, but the role reverses at later stages to serve as a survival mechanism.

Later stages of cancer increase autophagy as a survival mechanism in response to the harsh tumor microenvironment, which includes conditions such as hypoxia, nutrient and growth factor deprivation, extracellular acidity, and cancer treatment-induced stress (Hanahan and Weinberg, 2011; White, 2013). Basal autophagy also shifts in late stage cancers, specifically being much higher than normal cells, even under nutrient-rich conditions (Mizushima et al., 2004; Mizushima, 2009). This observation has fueled attempts to classify types of cancer as autophagy-dependent or independent, either in terms of molecular signaling mutation/expression or histologically. As outlined by Levy et. al. (Levy et al., 2017), autophagy-dependence is currently being investigated in activation/mutation of four main signaling pathways – RAS, PI3K, JAK-STAT, and p53. RAS is a known oncogene, and when activated causes a significant increase in autophagy (Guo et al., 2011; Lock et al., 2011). Specifically, sensitivity to autophagy inhibition has been linked to pancreatic cells exhibiting KRAS mutation (Guo et al., 2011; Yang et al., 2011; Perera et al., 2015), BRAF V600E mutant melanoma and lung cancer (Levy et al., 2014), and JNK1 expression in the presence of hypoxia (Jin et al., 2016). PI3K signaling, especially in the context of EGFR mutation/amplification, influences autophagy through downstream pathways like PI3K-AKT-mTOR (Jutten and

Rouschop, 2014). The relationship of JAK-STAT signaling in autophagy was shown in breast cancer cells that were autophagy-dependent by way of signal transducer and activator of transcription 3 (STAT3) and IL-6 secretion (Maycotte et al., 2015). Finally, tumor promoter 53 (TP53, p53) activation has been linked with autophagy dependence, though the role is unclear in that p53 located in the nucleus is associated with the autophagy dependence, whereas if located in the cytoplasm is associated with autophagy inhibition (Levine and Abrams, 2008; Tang et al., 2015). Overall, classifications of autophagy-dependent vs. independent tumor types are still being investigated.

Currently, the only clinically approved autophagy-inhibitors in cancer therapy are chloroquine (CQ) and hydroxychloroquine (HCQ). Preclinical treatment efforts using these two inhibitors in combination with a multitude of other treatment methods have shown moderate to high success in a significant amount of studies. To name a few, in the case of renal cell carcinoma (RCC) HCQ has been shown to promote cell death as a single agent (Lee et al., 2015), and synergistically in combination with the mTOR inhibitor temsirolimus (Bray et al., 2012). Results from this combination have been recapitulated in melanoma spheroids and xenografts (Xie et al., 2013). In breast cancer HCQ increased sensitivity to gefitinib (Dragowska et al., 2013) and estrogen receptor positive breast cancer cells to tamoxifen (Cook et al., 2014). Gemcitabine toxicity in LM7 osteosarcoma cells was amplified with HCQ treatment as well (Farrill et al., 2017). HCQ has been shown to amplify chemotherapy regimens in myeloid leukemia (Helgason et al., 2013), myeloma, lymphoma, and hepatocellular carcinoma cells (Pan et al., 2011; Li et al., 2013a). In contrast to these findings, some treatments with CQ

and HCQ have shown antagonistic effects in combination with other drugs. One study of note was cisplatin/CQ combination in relation to tumor progression. This study showed neoadjuvant CQ treatment in metastatically induced cells delayed metastatic development, but adjuvant treatment did not. On the contrary, trehalose, an autophagy inducer, caused metastatic development to occur much more quickly (Barnard et al., 2016). Clinical observations in the usage of HCQ for other diseases, like rheumatoid arthritis and lupus, suggest it accumulates readily in inflamed tissues, acting as an anti-inflammatory agent, and also inhibits immune system activity through reduction of T-cell cytokine production and toll-like receptor signaling (Schrezenmeier and Dorner, 2020). These mechanisms are likely to have an impact in cancer treatment as well.

Clinical Studies

The first round of phase I clinical trials using HCQ to augment primary cancer treatment, published in 2014, showed the potential benefit of autophagy inhibition as a supplement to treatment. Clinical trials looked at increasing doses of HCQ up to the FDA-allowed maximum of 600mg twice per day. The results were very positive for four of the six trials. The trial using temozolomide in combination with HCQ in patients with solid tumors recorded no dose-limiting toxicity (Rangwala et al., 2014b). Temsirolimus and HCQ was a combination that showed synergistic activity in preclinical models, and reported a 74% stable disease rate in patients (0% in temsirolimus alone) with autophagy inhibition shown in PBMCs at 1200mg/day (although this biomarker was later shown not to be indicative of autophagy inhibition in the tumor) (Rangwala et al., 2014a). A trial in myeloma used the proteasome inhibitor bortezomib with HCQ and reported 45% stable disease rate with some cases of grade 2 GI toxicity and cytopenia,

but a maximum tolerated dose (MTD) of HCQ was not achieved (Vogl et al., 2014). A trial in canine lymphoma patients using doxorubicin (DOX) in combination with HCQ allowed for dose de-escalation of the primary treatment (DOX), while observing 100% clinical benefit (Barnard et al., 2014). On the contrary the two other trials did report an MTD for HCQ. Vorinostat (HDAC inhibitor) and HCQ combination treatment reported fatigue and GI toxicity at 600mg/day of HCQ, but noted these were known side-effects of vorinostat (Mahalingam et al., 2014). A second temozolomide trial in patients with glioma reached HCQ MTD at 800mg/day and observed no significant improvement with the combination in patients (Rosenfeld et al., 2014). The overall conclusion from the six trials was that inhibiting autophagy was not automatically too toxic in patients, opening the door to the 75+ cancer clinical trials that have or are using HCQ either alone or in combination with another chemotherapeutic regiment (ClinicalTrials.gov, May 10th, 2018).

Results from the next round of clinical data with HCQ are starting to be reported. To name a few – in a patient with BRAF V600E mutant brain cancer, CQ treatment has been shown to overcome acquired resistance to vemurafenib (Levy et al., 2014). HCQ is currently being used in combination with BRAF autophagy and MEK inhibition in metastatic melanoma expressing BRAF V600E and BRAF V600K [NCT02257424]. On the negative side of things, a trial using HCQ alone in patients with pancreatic cancer showed negative results, indicating that HCQ should be used in combination (Wolpin et al., 2014). However, another phase I/II clinical trial using HCQ and gemcitabine in patients with pancreatic adenocarcinoma showed partial response and no dose limiting toxicity at 1200mg/day HCQ (Boone et al., 2015). An additional phase I/II trial

investigated everolimus, an mTOR inhibitor and thus autophagy-inducer, in combination with HCQ in patients with late-stage renal cell carcinoma. The study was able to achieve dosing of 600mg HCQ BID (1200mg/day), which is the highest achievable dose in phase I cancer clinical trials. This study reported stable disease and partial response in 67% of patients tested and a progression-free survival of greater than 6-months in 45% of patients (Haas et al., 2019).

The major route of toxicity causing patients to discontinue long term treatment with CQ and HCQ is retinopathy. In the past, retinopathy has been relatively rare in patients taking the drug for extended periods of time, 5-10 years, but is irreversible (Pandya et al., 2015). Between the cancer treatment strategies requiring high doses and the development more sensitive detection techniques, retinopathy in cancer trials has been observed in as many as 7.5% of patients (Melles and Marmor, 2014). Current HCQ dosing regiments have resulted in retinal toxicity reported within 11 months of starting treatment during clinical trials of HCQ and erlotinib for non-small cell lung cancer (Leung et al., 2015). Actual concentrations associated with retinopathy are unknown, but patients classified as high risk are categorized as those receiving >6.5 mg/kg per day for >5 years (Pandya et al., 2015).

Pharmacodynamic (PD) evaluation of autophagy in the clinic is another source of problems for treatment. Barnard et. al. (Barnard et al., 2014) showed LC3-II increase and accumulation of p62 in HCQ-treated tumor samples vs. control, but this required tumor resection, which is not always an option. Peripheral blood mononuclear cells (PBMCs) were another biomarker used in early clinical trials, analyzed via TEM for autophagosome buildup, but this method was unreliable as it was not correlated with

autophagy inhibition in tumor samples (Mahalingam et al., 2014). Current clinical trials and preclinical studies are heavily focused on establishing better biomarkers.

Multiple works have attempted to develop population-based pharmacokinetic models for HCQ, albeit with differing results among studies. An older study investigated a population pharmacokinetics (popPK) model of HCQ in rheumatoid arthritis patients and was supported by a one-compartment model with estimated bioavailability of 0.75 (Carmichael et al., 2003). Another study looked at HCQ popPK in Japanese patients with cutaneous or systemic lupus erythematosus and reported a one-compartment model. The model was characterized by first-order absorption and absorption lag time and the major covariate was body-weight, although this was hypothetically likely to be significant as they dosed HCQ based at 200-400mg daily rather than dosing on a mg/kg basis (Morita et al., 2016). Furthermore, a recent Phase I/II trial with HCQ and everolimus (Haas et al., 2019) also developed a popPK model for HCQ in blood. They reported a 2-compartment model with first-order absorption and no lag time, and also did not identify any covariates that improved model fit. The population data emphasized large interpatient variability in HCQ pharmacokinetics. Even though previous studies suggested body weight should have a significant effect on HCQ disposition, these were not observed in this cancer popPK model. There has been one recent attempt to characterize HCQ PK in the context of SARS-CoV-2 treatment through development of a physiologically-based pharmacokinetic (PBPK) model using SimCyp commercial software. but did not report model covariates, sensitivity of parameters, or characterization of residual or interindividual variability (Yao et al., 2020).

Inconsistent PK/PD relationships with CQ and HCQ in tumor tissue is another issue the clinic is facing at the moment (Barnard et al., 2014). First, autophagy dependence of tumor cells vs. peripheral cells are likely different, and so inhibition of autophagy may require more or less drug exposure in the tumor. Differences may also be due to pharmacokinetic relationships of HCQ. PK studies with HCQ have shown up to 10-fold higher concentrations in tissue vs. blood (Collins et al., 2018), and up to 100-fold higher in tumor vs. plasma (Barnard et al., 2014). HCQ and CQ uptake and activity is also highly dependent on tumor pH, the driver of HCQ and CQ volume of distribution, has been shown to be markedly variable in tumor cells (Barnard et al., 2014; Koltai, 2016). Overall, better *in vivo* biomarkers are needed to evaluate autophagy inhibition, as well as a stronger understanding of the PK/PD relationship of currently used autophagy inhibitors.

Pharmacology of Autophagy Inhibitors

Mechanistically, CQ derivatives are weakly basic compounds that alkalinize the highly acidic lysosome, preventing the autophagosome-lysosome fusion step of autophagy (de Duve, 1983; Lu et al., 2017). This mechanism drives their pharmacokinetics (PK), primarily through an ion-trap accumulation observed in lysosome and other acidic compartments, which can be seen in Figure 1.2.

HCQ PK has been well characterized in multiple species, and the PK profile appears to scale linearly with dose escalation, though exhibits a significant amount of intersubject variability (McChesney, 1983; Tett et al., 1988; Furst, 1996; Lim et al., 2009; Fan et al., 2015). Sources of variability are likely due to these studies having been done by different research groups over the course of decades, as well as variance

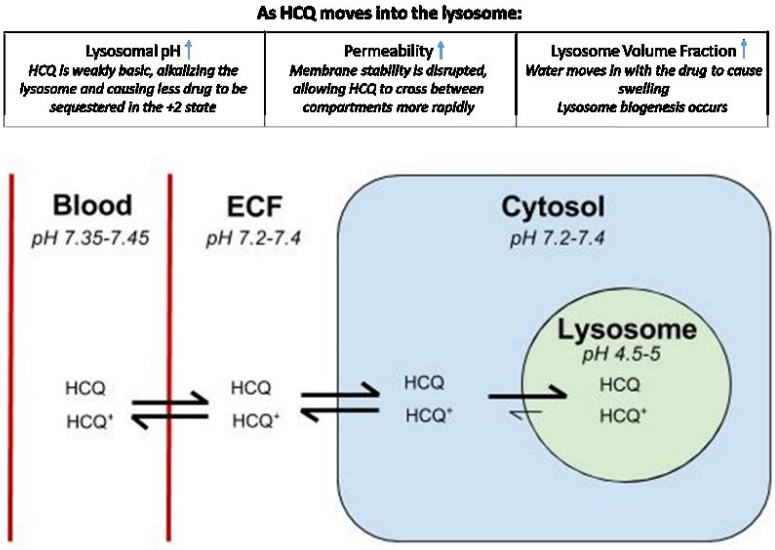

Figure 1.2. Intracellular mechanism of HCQ PK with pH dependence. HCQ crosses membranes readily, but accumulates in acidic compartments due to being non-permeable in its +2 state.

in absorption, distribution, metabolism, and elimination (ADME) factors related to the physicochemical properties that drive HCQ PK. Of note HCQ and CQ have similar potency and PK properties, but HCQ has been shown to be less toxic in long term dosing than CQ (Shi et al., 2017).

HCQ is typically administered as an oral tablet, in doses ranging from 100 to 1200 mg daily, by which it is readily absorbed within 2–4 hours (Browning, 2014). The fraction absorbed is estimated to be 74% (Tett et al., 1989; Browning, 2014). HCQ blood concentration peaks shortly after the absorption phase and falls relatively quickly due to rapid partitioning into organs. Accumulation in lysosomes appears to drive the large volume of distribution in plasma, whereas binding to melanin contributes to the long terminal half-life ($t_{1/2}$) (Tett et al., 1990). It is approximately 50% bound to plasma

protein in the blood (Furst, 1996). Metabolism appears to be the primary driver of HCQ clearance. It occurs in the liver through CYP3A4- and CYP2C3-driven dealkylation to form desethylhydroxychloroquine, desethylchloroquine, and bisdesethylchloroquine, the former that exhibits therapeutic activity and PK thought to be comparable to HCQ (McChesney et al., 1965; Kim et al., 2003; Browning, 2014; Qu et al., 2015). Rate of metabolism varies tremendously across species, leading to significant cross-species differences in $t_{1/2}$ that ranges from hours in mice to days in humans (Tett et al., 1988). Excretion takes place primarily in the kidneys, accounting for about 22% of HCQ total blood clearance, with liver clearance assumed to account for the rest (Tett et al., 1988). Mean renal clearance from plasma is reported as three to four times greater than glomerular filtration rate (GFR) corrected for protein binding, suggesting the drug is secreted in addition to filtration (Tett et al., 1988).

Regarding actual ability to inhibit autophagy CQ derivatives work well, but fall short of the mark in terms of potency. To achieve an LC3-II/I increase, 1μM CQ must be reached and climbs linearly to maximize at 100μM. Cell death with HCQ alone begins at 50μM and scales linearly to 100μM, and cell death with HCQ and another stressor begins at 10μM and scales linearly to 100μM. Putting this into perspective, clinically achievable concentrations of HCQ peak at about 10μM in the blood with roughly five to six weeks of dosing required due to the extremely long half-life. It is of note that HCQ has been reported as much as 100-fold higher in the tumor vs. blood, but there is not yet a reliable biomarker to consistently determine this (Barnard et al., 2014).

Next generation autophagy inhibitors are currently being investigated as future alternatives to CQ and HCQ. One of the more well-known is Lys05, which is a dimeric

version of CQ shown to be up to 10x more potent at inhibiting autophagy both *in vitro* and in human xenografts *in vivo* (Amaravadi and Winkler, 2012). Additionally, Lys05 was reported to have a much more pronounced cytotoxic effect in cell lines known to be resistant to HCQ alone, showing that it has significant anti-tumor capabilities on its own (Amaravadi and Winkler, 2012). This carried over to *in vivo* studies where 10mg/kg Lys05 dosed intraperitoneally (i.p.) caused significant antitumor activity alone, whereas HCQ autophagy inhibition is rather inconsistent and single agent antitumor activity is much less pronounced (McAfee et al., 2012). Lys05 was also shown to be a more potent lysosomal deacidifier, as 50μM could completely deacidify the lysosome whereas doses as high as 100μM HCQ could not (McAfee et al., 2012). The only reported side effect of Lys05 in *in vivo* studies was GI toxicity due to Paneth cell destruction in mice observed at only the highest dose of 80mg/kg (McAfee et al., 2012). Some other next generation autophagy inhibitors being investigated for potential future use include the Vps34 inhibitors SAR405 (Pasquier, 2015) and spautin-1 (Shao et al., 2014); the inhibitor of autophagosome formation verteporfin (Donohue et al., 2011); and antimalarials mefloquine (Sharma et al., 2012), quinacrine, and VATG-027 (Goodall et al., 2014). On the unconventional side structurally, ferroquine (FQ) is an organometallic chloroquine structural derivative with increased potency both as a single agent or in combination with other chemotherapeutics *in vivo* (Kondratskyi et al., 2017).

Further investigation into dimeric quinoline-based compounds like Lys05, has been investigated by the Amaravadi and Winkler group and ultimately elucidated mechanistic targets of these drugs. Recent reports suggest that dimerization of multiple quinoline compounds, including quinacrine, mefloquine, and primaquine, all led to an

increase in potency relative to the monomeric versions (Nicastri et al., 2018; Rebecca et al., 2019). The study by the Amaravadi group identified a highly potent version, dimeric quinacrine 661 (DQ661), and investigated its molecular target as PPT1 (Rebecca et al., 2017). Inhibition of PPT1 mechanistically works to both inhibit mTORC1 while simultaneously inhibiting autophagy to block autophagosome-lysosome fusion. Presence of a methyl group on the carbon-chain linker (indicated by a 1 for a methyl group or 0 for no methyl group) indicated whether the dimeric quinacrine had affinity for PPT1 on the lysosomal membrane, or accumulated in the nucleus of the cell. Further investigation of the role of PPT1 in cancer suggests that it is correlated with reduced patient survival, and its genetic inhibition is significant in reducing tumor progression (Rebecca et al., 2019). Investigation of structure activity relationship (SAR) of dimeric quinolines ultimately found dimeric chloroquine 661 (DC661) to be the most efficacious version of these compounds in vitro. DC661 was reported to have much higher potency than Lys05 and HCQ, with strong growth inhibition and autophagy blocking potential between 0.1-1uM, where the formers are 0.5-5uM and 5-30uM based on in-house data. Additionally, DC661 was shown to be capable of overcoming a major shortcoming of HCQ, which is efficacy under acidic extracellular conditions (Rebecca et al., 2019).

Overall autophagy has been shown as a double-edged sword in tumor development, in that it serves as a tumor suppressor in early stages and a tumor promoter at later stages. Preclinical treatment methods have shown that autophagy inhibition can be highly beneficial as an adjuvant to primary chemotherapy, although classifications of autophagy-dependence are still becoming clear. These studies have led to 75+ clinical trials involving autophagy inhibition using CQ or HCQ, which have

shown mostly positive results when used in combination with the primary treatment. Autophagy inhibition remains a promising strategy to improve cancer patient outcomes, which will surely evolve with discovery of better clinical biomarkers of autophagy-dependence and development of more potent autophagy inhibitors.

Lysosomal Dynamics and Cancer

Overview

Lysosomes, the primary organelle involved in autophagy, were first discovered by Christian de Duve in 1955. They are described as vesicles of roughly 100-500nm in diameter (Xu and Ren, 2015) with characteristic acidic pH between 4.6-5.0, and a variety of different acid hydrolases optimized to function in these conditions (Mellman et al., 1986). Lysosomes are often regarded as the garbage disposal of the cell due to their role as the autophagy mediator, as well as their involvement in endocytic and phagocytic degradation, cytosolic protein proteolysis (Lawrence and Brown, 1992), and cholesterol homeostasis (Guillaumot et al., 2010). They serve many other functions, including regulation of calcium homeostasis by serving as the calcium store of the cell (Feng and Yang, 2016). The key role of interest in the context of autophagy is lysosomal adaptation during nutrient starvation conditions. Specifically, lysosomes fuse with each other resulting in many less (~100/cell to <50) but larger lysosomes (up to 1500nm diameter) that redistribute from their uniform cellular distribution to a perinuclear concentration wherein autophagosome-lysosomal fusion takes place (Xu and Ren, 2015).

Lysosome formation, functional maintenance, and trafficking through the cell are dynamic, complicated processes that are critical to their cellular role. Briefly, lysosomes formation occurs within the Golgi network, wherein newly formed vesicles are fused with endosomes (Cooper, 2000). Acidic lysosomal pH is maintained by proton pumps located on the membrane, referred to as vacuolar-type H+ ATPase (V-ATPase), in combination with a lysosomal membrane potential of -20 to -40 mV (Ohkuma et al., 1983; Steinberg et al., 2010). This results in a proton homeostatic concentration of roughly 100-1000 times higher than that of the cytosol. Lysosomal trafficking, the processes involved in lysosomal fusion and fission, throughout the cell is highly regulated and involves lysosomal degradation of autophagy substrates, supply of hydrolases, export of catabolites, and lysosomal recycling and biogenesis. Trafficking is regulated by the H+ homeostasis / membrane potential interplay, but primarily by Ca^{2+} storage and efflux (Luzio et al., 2007; Li et al., 2013b). Impairment of lysosomal trafficking, along with other lysosomal processes, can lead to a number of issues including cell impairment and disease.

There is a large group of relatively uncommon genetic diseases that are caused by lysosomal dysfunction, known as lysosomal storage diseases (LSDs). They tend to come about most often due to a deficiency in one or more lysosomal enzymes, resulting in a buildup of the enzyme-targeted substances in the lysosome. LSDs are further classified by alteration of the following: signaling pathways, intracellular calcium homeostasis, lipid biosynthesis, and endosomal/lysosomal trafficking (Ballabio and Gieselmann, 2009). Autophagy is almost always involved in LSDs, as it relies on the lysosome. Blocking or inducing autophagy due to the specific feature of the LSD results

in autophagosome accumulation, which is a result of issues with lysosome-autophagosome fusion (Ballabio and Gieselmann, 2009). The proposed mechanism for cell death in LSDs is similar to the proposed mechanism by which lysosomotropic autophagy inhibitors, like HCQ, cause tumor cell death. Specifically, defective autophagosome-lysosome fusion observed in these diseases prevents autophagosome degradation. Consequently, substrates of the autophagosome, like ROS, defective proteins, and aberrant mitochondria, accumulate within the cell. Cell death ultimately occurs through subsequent damage and inflammation (Ballabio and Gieselmann, 2009).

Lysosomal involvement in cancer has been recently investigated, and while still not clearly defined, it is known to play a dual role in both cancer treatment and progression. Extending from the cancer-treatment role in autophagy-inhibition and death related to overwhelming autophagosome accumulation, lysosomes can serve as a target for tumor cell death due to lysosomal membrane destabilization (LMD) associated with cathepsin release and subsequent caspase activation (Foghsgaard et al., 2001), or oppositely a source of multi-drug resistance (MDR) due to their protective effects against hydrophobic weak bases. Lysosomes dual role in tumor progression is a bit more complicated, specifically in regard to location of cathepsin release. Cathepsins released into the extracellular space are associated with tumorigenesis (Ilan et al., 2006; Mohamed and Sloane, 2006; Palermo and Joyce, 2008), but if released into the cytosol promote apoptotic cell death (Foghsgaard et al., 2001; Kirkegaard and Jaattela, 2009). This can by visualized directly through lysosome migration and dispersion within the cell. Peripheral concentration of lysosomes is correlated with tumor progression, as compared to the normally observed perinuclear concentration (Koblinski et al., 2000).

Regarding tumorigenesis – higher expression levels of cathepsins B, D, and L in the extracellular space have been linked to tumor progression (Kos and Lah, 1998), while pharmacologic inhibition of cathepsins is associated with delayed tumor progression in mouse models and increased cell sensitivity to additional chemotherapeutic agents *in vitro* (Shree et al., 2011). The proposed mechanism involves cathepsin-mediated degradation of ECM components, promoting metastasis (Kirkegaard and Jaattela, 2009). Alternatively, cathepsin release into the cytosol is associated with apoptotic cell death. Lysosomal membrane destabilization (LMD) is the proposed mechanism of cathepsin release, leading to cytochrome c transport out of the mitochondria, causing downstream activation of caspases, specifically caspase-8 (Stoka et al., 2001). LMD can be caused by such apoptotic stimuli as TNF, activation of p53, ROS production, and lysosomotropic agents (Halaby, 2015). Treatment with CQ has been shown to cause lysosomal membrane damage, associated with recruitment of Galectin-3 to lysosomal sites and swelling of lysosomes up to a 3-fold increase in diameter. Lysosomal membrane damage appears to be linked to glucose, as glucose starvation, regardless of serum concentration, could prevent CQ-induced lysosomal damage (Gallagher et al., 2017). Overall, the exact mechanism of LMD, its associated factor, and its involvement in apoptotic cell death remain unclear.

Lysosomal Displacement of Drugs

Another signature feature of lysosomes is their ability to sequester weakly basic chemicals, which, depending on how you look at it, poses a challenge or solution to many of the hurdles that must be overcome in cancer treatment. Commonly referred to as “lysosomal trapping”, the highly acidic environment of the lysosome can protonate a

majority of weak bases that passively diffuse into it, massively reducing their rate of diffusion back into the cytosol by reducing their effective permeability. This mechanism, as discussed previously for dibasic HCQ, causes lysosomes to serve as a drug sink for many other mono-, di-, and tri-basic drugs. The actual extent to which bases are sequestered is a factor of both permeability as well as pKa. Contributions of each factor were investigated by Ishizaki et. al. (Ishizaki et al., 2000) using three known lysosomotropic agents including imipramine, chlorpromazine, and propranolol. They found that uptake of imipramine into isolated rat liver lysosomes was approximately 140-fold higher than pH-partition theory predicted, attributing extra uptake to lipidic binding, and simulating this contribution with a simplistic mathematical model. This concept was extended even further, differentiating between drugs whose permeabilities were reduced when ionized preferentially accumulating in the lysosome versus drugs whose permeabilities were not reduced preferentially accumulating in the mitochondria. Permeability-related lysosomal affinity was attributed to acid polysaccharides and glycolipids that make up the lysosome (Duvvuri et al., 2004; Duvvuri and Krise, 2005). Interplay between acidic macromolecule binding and drug pKa/permeability has been incorporated on a more general level into recently developed theories used in practice to predict drug-tissue partitions for pharmacokinetic modeling (Schmitt, 2008; Peyret et al., 2010).

Concepts from these cell-based models of lysosomal-sequestering translate well when considering the role of lysosomes in tissue distribution, particularly in the case of known lysosomotropic (lysosomal-targeting) agents. MacIntyre and Cutler (MacIntyre and Cutler, 1988) calculated that basic compounds would accumulate around 400 times

the concentration of the cytosol for monoacidic bases, and up to 16,000 times for diacidic bases. Taking the volume fraction of lysosomes of the hepatocyte as 0.68%, the physical amount of drug in the lysosomal compartment would be roughly 3 or 1100 times that of the cytosol, respectively. This theory holds ground when comparing apparent volumes of distribution (VDss) between lysosomotropic compounds and other chemicals. Assuming a VDss of 0.7 L/kg is representative of total body water (Obach et al., 2008) and VDss of 10 L/kg is indicative of very high tissue partitioning, in a panel of 670 lipophilic drugs (logP = 2-4) the median unbound VDss (VDss/fu) was 13 and for very lipophilic drugs (logP > 4) was 77. As a whole, basic drugs exhibited a median unbound VDss of roughly 9. Of all 670 drugs screened, the lipophilic hydroxychloroquine showed an unbound VDss of roughly 1300 L/kg (Obach et al., 2008). Drugs exhibiting a VDss > 25 fit the profile for lysosomally-sequestered chemicals, as characterized in immortalized hepatocytes (Kazmi et al., 2013).

The extent to which lysosomal ion trapping affects cellular uptake has been examined by numerous studies testing weakly basic lipophilic drugs in the presence of inhibitors of lysosomal trapping. These include chemicals that deacidify the lysosome directly by acid-quenching (NH_4Cl, CQ/HCQ, ionophores nigericin and monensin), or indirectly by inhibiting V-ATPase function (bafilomycin A1, omeprazole). Ishizaki et. al. (Ishizaki et al., 2000) demonstrated dose-dependent neutralization of lysosomal pH with chlorpromazine, imipramine, propranolol, and NH_4Cl within the low μM to low mM range, and were able to mathematically define lysosomal buffering capacity against basic drugs (Ishizaki et al., 2000). The validity of this buffering capacity was verified by Yokogawa et. al. (Yokogawa et al., 2002) when mathematically-simulating and

validating the pretreatment of imipramine and methylamine with dose-escalating chlorpromazine, propranolol, and NH_4Cl. Additionally, Ishizaki et. al. showed tissue affinity of lipophilic basic drugs was decreased between 20-80% by NH_4Cl treatment (Ishizaki et al., 2000). Kazmi et. al. (Kazmi et al., 2013) examined this effect in immortalized hepatocytes using imipramine and propranolol, finding that uptake of these two drugs was inhibited >40% by NH_4Cl, nigericin, and monensin, and >50% by CQ where non-lysosomotropic agents exhibited no effect on uptake. Of particular note was the lengthy washout time required to reverse the CQ effect on imipramine and propranolol uptake compared to NH_4Cl, representative of CQ's long half-life *in vivo* (Kazmi et al., 2013). For imipramine in particular, pretreatment with 2.5μM nigericin showed significantly decreased cellular uptake, whereas treatment with 1mM ATP caused massive increase in cellular uptake – likely due to the more readily available ATP source required by the V-ATPase pumps to maintain acidity of the lysosome. This was verified in that 10nM bafilomycin A1, a V-ATPase inhibitor, negated the effect of 1mM ATP in increasing imipramine uptake (Ishizaki et al., 2000). Examining the influence of lysosomal sequestration even further, a cell model representative of lysosomal uptake based on pH-perturbing, permeability-altering, and acidic macromolecule binding dynamics was developed and validated in lipophilic weak bases (Trapp and Horobin, 2005; Trapp et al., 2008), eventually looking directly at drug displacement dynamics by investigating displacement of the pH-dependent fluorescent lysosomal marker LysoTracker with four different lipophilic weakly basic drugs tested at therapeutically-relevant concentrations (Kornhuber et al., 2010).

A similar experimental method to characterize lysosomal sequestration of weak bases based off of chemical pKa was recently established by Schmitt and colleagues (Schmitt et al., 2019). This methodology compared LCMS/MS concentrations from rat hepatocytes treated with different drugs to displacement of LysoTracker Red, correlating decreased fluorescence directly to an increase in lysosomal concentration of the agent described. In rat hepatocytes the lysosomal pH was found to be a Gaussian distribution around mean pH of 5.53, suggesting the variation of pH that occurs throughout the endo/lysosomal system. Overall, they observed lysosomal pH and lysosomal volume fraction of cells to be the most important factors in uptake of lysosomotropic agents. On the basis of determining cellular uptake of drugs based on lysosomal profiles, it is of note that both lysosomal pH and lysosomal volume fraction of cells have been reported with an extremely large variation among cell types, with pH ranging from ~4.5-5.5 and volume fraction ranging from ~0.2-8% in cell lines (Schmitt et al., 2019). Additionally, lysosome pH and lysosomal turnover is a dynamic process that is responsive to cellular intrinsic and extrinsic factors, adding another level of difficulty to characterizing drug/lysosome interplay.

Mechanistically, the lysosomal drug sink effect is why a number of lysosomotropic drugs, like HCQ, exhibit their activity, but could also be a reason why other drugs actually exhibit diminished activity. Lysosomal sequestration of weakly basic chemotherapeutics away from their target sites throughout the cell, effectively reducing their activity, has been identified as a form of MDR (Duvvuri and Krise, 2005). Numerous studies are involved with investigating the actual magnitude of this effect. In comparison of drug sensitive versus resistant MCF-7 cells (MCF-7 vs. MCF-7/ADR),

DOX lysosomal sequestration was observed in resistant, but not sensitive cells. This was correlated to a much more acidic lysosomal pH in the resistant cells, as well as the cytosolic pH being roughly 0.4 units lower in the resistant cells – a trend also observed in MDA-MB-231 and SW-48 cell lines. Subsequent decreased DOX uptake/sensitivity was reversed by treatment with BafA1 and monensin (Altan et al., 1998). This sequester-release effect of DOX and lysosome-targeting agents was also observed in a different study using CQ, OMZ, and BafA1 as alkalinizing agents. Specifically, dose-dependent lysosomal alkalization was shown with all three drugs, as well as increased uptake and sensitivity to DOX in MCF-7 and EMT-6 cells (mouse mammary carcinoma) (Lee and Tannock, 2006). Another study looked at the lysosomal sequestering potential of palbociclib and ultimately showed that CQ was able to lower overall accumulation of palbociclib in the lysosome. This ultimately increased the free amount of palbociclib in the cytosol, increasing sensitivity to the drug (Llanos et al., 2019). Direct contribution of V-ATPase to this phenomena was analyzed through siRNA knockdown of ATP6L, a V-ATPase subunit, resulting in a dramatic alkalinization of lysosomal pH as well as increased sensitivity/cellular relocation of DOX, 5-FU, and vincristine compared to control MCF7/ADR cells (You et al., 2009).

In some cases, MDR cells have been observed as having a higher lysosomal burden (volume * number) compared to drug-sensitive cells. Interestingly, concentration of the basic lipophilic tyrosine kinase inhibitor sunitinib was found to be 10-fold higher in resistant cell lines, which was connected with the increased expression of lysosomal-membrane protein 1 and 2 (LAMP1,2) (Azijli et al., 2015). Continuous sunitinib exposure has also been shown to cause acquired resistance in HT-29 colon

and 786-O renal tumors, with resistant tumors accumulating 1.7-2.5 times more sunitinib. This affect was associated with a significant increase in number and size of lysosomes (Gotink et al., 2011). In a separate study using a panel of seven histologically-different cell lines, sunitinib resistance showed a striking linear relationship with lysosome number per cell (Zhitomirsky and Assaraf, 2015). The role of lysosome size in resistance was shown using fluorescently-labeled sunitinib, which was shown to accumulate in lysosomes. Resistance to sunitinib and sorafenib was observed in hepatocellular carcinomas with giant lysosomes versus those with normal sized lysosomes. This group also observed ATP-binding cassette (ABC) drug efflux transporter expression on the lysosomal membrane, and were able to reverse drug resistance by treating with the ABC inhibitor verapamil (Colombo et al., 2014).

Increased lysosomal burden can also be used advantageously, as was shown by treatment of MDR cells with the cytotoxic fluorochrome imidazoacridinone (IA). IA readily accumulates in lysosomes, and was used to induce lysosome-rupture and subsequent deadly spikes in ROS by photodestruction of cells overexpressing MDR efflux transporters P-gp (ABCB1), MRP1, and BCRP. This effect was not observed in non-MDR cell lines, and was actually reversed by treatment with lysosomal alkalinizing agents NH_4Cl and BafA1 (Adar et al., 2012).

Some very recent studies have shown that the result of chemotherapeutic treatment and lysosomal disruption in cancer cells is markedly disconnected from the synergistic effects often associated with autophagy inhibition. Maycotte et. al. (Maycotte et al., 2012) observed this disconnect in the response of mouse breast cancer cells to cisplatin. They showed induction of autophagy by cisplatin DNA

damage, and by treatment with autophagy inducers rapamycin, an mTOR inhibitor, and LY290042, a PI3K inhibitor. While treatment with CQ sensitized cells to these autophagy induction treatments, knockout of the essential autophagy genes ATG12, BECN1, and treatment with BafA1 did not reproduce sensitization (Maycotte et al., 2012). A similar study was carried out in tongue squamous cell carcinoma, which are shown to have higher autophagic flux in comparison to normal tongue epithelial cells. In this case, sensitization to cisplatin was caused by BafA1, attributed to reduced lysosomal trapping and increased cisplatin-DNA binding; however, this sensitization was not observed in combination with ATG5 knockout (Chu et al., 2018). A third example investigated lysosomotropic sensitization in KRAS mutant cells, a cell-type thought to be autophagy-dependent. KRAS mutant and wild-type cells actually showed equal sensitivity to CQ and Lys01, but ATG7 depletion did not cause a decrease in cell growth *in vitro* or *in vivo* even though autophagy was thoroughly inhibited. Furthermore, cells with deleted ATG7 were equally sensitive to both CQ treatment and CQ/sunitinib or erlotinib combination as those still harboring ATG7 (Eng et al., 2016).

Specific mechanisms behind this disconnect have been investigated, although the exact cause is unclear. FGFR3-mutant bladder cancer is another reported CQ-sensitive cell type in which the mechanism of death is independent of autophagy inhibition. Knockout of ATG7, ATG13, ULK1, and VPS34 did not recapitulate CQ sensitivity, whereas cell death was actually shown to be lysosomally-mediated due to cathepsin-related caspase activation. Interestingly, cholesterol treatment prevented CQ-triggered cell death, and blocking of cholesterol metabolism enhanced CQ-triggered cell death both pharmacologically through atorvastatin treatment, or directly through

siRNA KO (King et al., 2016). Another study was able to characterize sensitivity of cell lines to CQ based on expression of the autophagy-unrelated genes alcohol dehydrogenase 1 family member A1 (ALDH1A1) and helicase like transcription factor (HLTF). Increased expression of ALDH1A1 was shown to enhance uptake of lysosomotropic drugs, but is not directly related to autophagic flux or lysosomal disruption. Increased expression of HLTF was shown to improve repair of ROS-based DNA damage. Cell lines were effectively profiled into the CQ-sensitive ($ALDH1A1_{high,low}$, $HLTF_{low}$) and CQ-insensitive ($ALDH1A1_{low}$, $HLTF_{high}$) categories (Piao et al., 2017). To recapitulate – while treatment with autophagy inhibitors has been shown as an effective method of tumor sensitization to standard treatment methods, the actual mechanism of sensitization remains unclear and may be connected to some part of the lysosomal cell death pathway rather than (or in addition to) autophagy.

Lysosomal Biogenesis in Response to Lysosomotropic Compounds

To further compound the lysosomal drug sequestering effect, lysosomal biogenesis is often triggered by lysosomal trapping and lysosomal disruption, which can exacerbate the effects of drug sequestration. More specifically, multiple studies using lysosomal-accumulating drugs have been shown to trigger the activation of transcription factor EB (TFEB), which is often regarded as the master regulator of lysosomal biogenesis. TFEB is a member of the MiT/TFE family of transcription factors, along with MITF, TFE3, and TFEC, and is a direct promoter of the coordinated lysosomal expression and regulation (CLEAR) network. TFEB is located directly on the lysosomal membrane and is bound to mTORC1. Under nutrient-rich conditions TFEB remains on the lysosomal membrane in the phosphorylated state, maintained by mTORC1 (Martina

et al., 2012). Under autophagy-inducing conditions, namely starvation, lysosomal disruption, or mTORC1 inhibition, TFEB is subsequently dephosphorylated and translocated to the nucleus where it interacts with components of the CLEAR network to activate gene transcription related to lysosomal biogenesis, synthesis of lysosomal proteins, increased autophagy, and lysosomal exocytosis (Settembre et al., 2012; Napolitano and Ballabio, 2016). This process can also be replicated by pharmacologic or genetic interventions (Roczniak-Ferguson et al., 2012; Settembre et al., 2012). The general mechanism of TFEB activation is depicted in Figure 1.3.

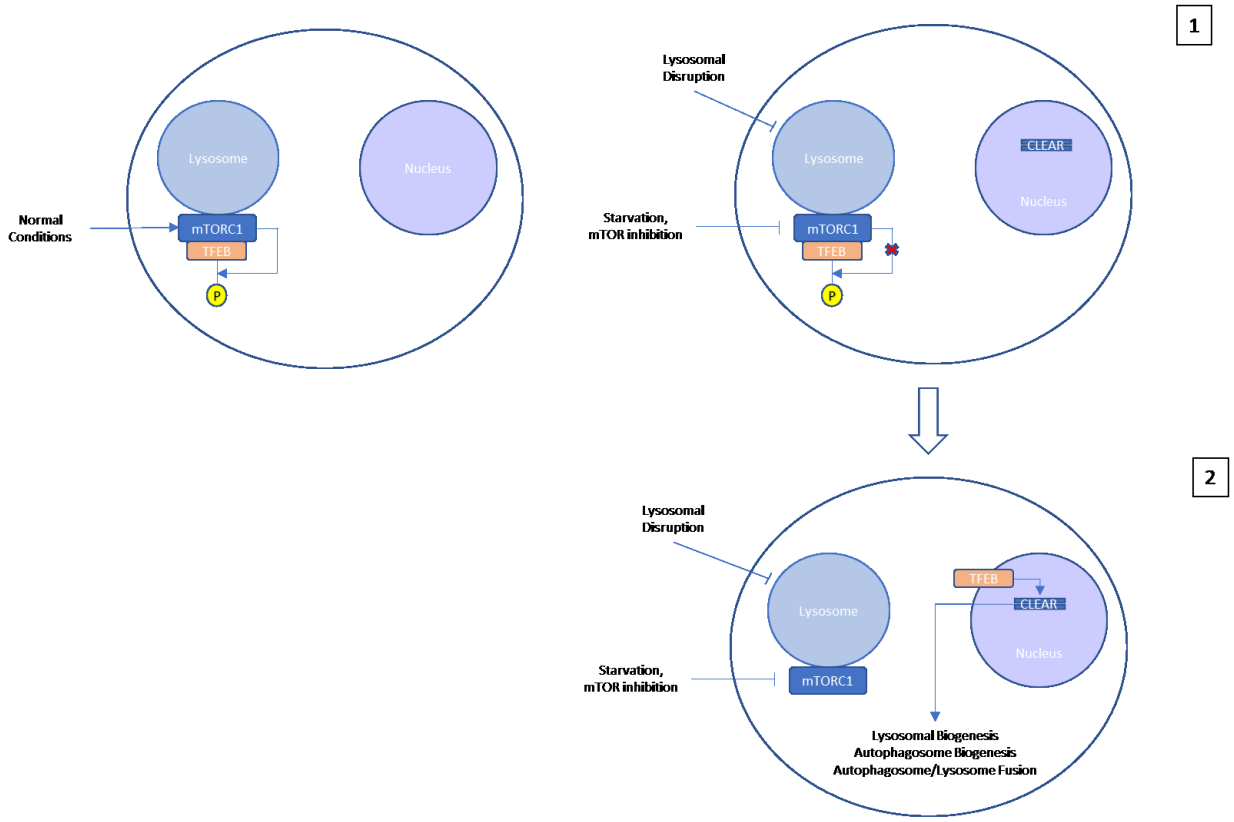

Figure 1.3. Mechanism of TFEB activation. Under normal nutrient and growth factor conditions (left) TFEB is actively phosphorylated by mTORC1 and remains bound to the lysosome. Conditions inducing autophagy, like starvation, pharmacologic mTOR inhibition, or lysosomal disruption (right) cause mTORC1 to release its hold on TFEB by stopping its active phosphorylation (1), activating TFEB. TFEB translocates to the nucleus where it activates components of the Coordinated Lysosomal Expression and

Regulation (CLEAR) network of genes, causing lysosomal biogenesis, autophagosome biogenesis, and autophagosome-lysosome fusion.

TFEB has also been shown to be phosphorylated by master growth regulator ERK2/MAPK1, but details of the interaction are much less clear (Settembre et al., 2013; Napolitano and Ballabio, 2016). Of note, components of the CLEAR network maintain a basal level of expression, meaning lysosomal turnover is always occurring – TFEB activation just works to increase this (Napolitano and Ballabio, 2016).

Another major player in TFEB activity is calcineurin. As lysosomes serve as the calcium store for mammalian cells, autophagy inducing conditions cause release of intralysosomal Ca^{2+} stores by way of the mucolipin-1 (MCOLN1) channel. This leads to activation of calcineurin, a phosphatase which also dephosphorylates TFEB (Medina et al., 2015).

The role of TFEB and the MiT/TFE family in autophagy is becoming increasingly clear. TFEB has been shown to bind promoter regions of a handful of autophagy genes (Settembre et al., 2013), which causes effects such as biogenesis of autophagosomes, promotion of autolysosome formation, and autophagy substrate degradation steps (Settembre et al., 2011). Cells overexpressing TFEB have shown increased autophagosome count and buildup of LC3, which is further enhanced by treatment with BafA1 and two other autophagy inhibitors, pepstatin and cysteine proteinase inhibitor 64 (Settembre et al., 2013). On the other hand, TFEB knockdown results in decreased LC3-II in both nutrient rich and scarce situations, an effect which was not altered by treatment with BafA1 (Settembre et al., 2013). In addition, TFEB overexpressing cells

increased autophagy gene expression matching nutrient deprivation conditions with high significance (Settembre et al., 2013). Results were recapitulated in the livers of transgenic mice (Settembre et al., 2013).

Due to the critical role of TFEB as a transcription factor, mutations or large changes in expression can have a significant impact on cellular function. Mutations to the two serines governing phosphorylation status (Ser142 and 211), specifically Ser-Ala mutations, are shown to cause constant TFEB activation and residence in the nucleus (Napolitano and Ballabio, 2016). As expected, TFEB overexpression has been shown to cause significant increase in the number of lysosomes and lysosomal enzyme activity (Napolitano and Ballabio, 2016). Increased MiT/TFE family expression or alteration has been linked to tumorigenesis. Amplification of MITF has been found to account for roughly 20% of melanomas (Stark and Hayward, 2007), as well as soft tissue tumor clear cell sarcoma survival and progression (Davis et al., 2006). TFEB amplification has been linked with non-small cell lung cancer metastasis (Giatromanolaki et al., 2015) and pancreatic ductal adenocarcinoma (PDA) (Perera et al., 2015). PDA solid tumors were noted to have roughly 15-fold higher lysosome number, significantly higher MiT/TFE gene expression (expression less than only melanoma and kidney), and autophagy dependence (Perera et al., 2015). Knockdown of MiT/TFE in PDA resulted in lysosomes of roughly 3-fold larger in diameter, mimicked by BafA1 treatment. Buildup of autolysosomes, wherein substrates have not completed digestion, elevated lysosomal pH, and lower autophagic flux were associated with TFE3 knockdown. Elevation of MITF or TFE3 expression was shown to activate lysosomal genes and autophagy, including a higher level of LC3-II which was further increased with CQ

treatment in PDA (Perera et al., 2015). TFEB and lysosomal gene overexpression was also observed in stage 1 human breast cancer. Specifically, upregulated TFEB was associated with genes like LAMP-2, cathepsin D, LC3-A, and, of particular interest, hypoxia-inducible factor 2α. Additionally, TFEB overactivation in the nucleus was shown to be linked to increased glycolysis and acidic extracellular conditions (Giatromanolaki et al., 2015).

Overall, the role of the MiT/TFE family is still being investigated for its direct role in cell progression and survival, but indirect involvement is largely apparent as the result of some drug treatments as indicated by lysosomal biogenesis and other results from MiT/TFE stimulation. Lysosomotropics primarily induce these effects that trigger lysosomal adaptation. One particular study by Lu et. al. (Lu et al., 2017) heavily examined lysosome-related treatment effects of a small panel of eight clinically and chemically-diverse drugs in the immortalized retinal pigmented epithelium cell line, ARPE-19. Drugs tested include autophagy inhibitor CQ, and autophagy inducers fluoxetine, imipramine (IMP), latrepirdine (dimebon), tamoxifen, chlorpromazine, amitriptyline, and verapamil; reporting comprehensive treatment effects as they relate to lysosome-related responses discussed previously in this chapter. Lysosomal burden was reported to increase by 50% or greater by 24 hours for all drugs/doses (CQ highly dose-dependent at 25, 50, 100μM), as indicated by both LAMP-2 staining and mRNA expression. Diminished staining of LysoTracker Red indicated pH-quenching between 30-60 minutes for all drugs except IMP, followed by recovered staining between 4 and 24 hours indicating pH-restoration. Cathepsin B activity (Magic Red staining) was markedly increased with all drugs/concentrations at both 4 and 24 hour timepoints;

Cathepsin D (Bodipy FL-pepstatin A staining) showed the same trend only at 24 hours along with increased mRNA expression. Regarding actual MiT/TFE factors, all drugs induced dose-dependent increases in TFEB, TFE3, and MITF nuclear translocation at 4 and 24 hours – with CQ being effective as soon as 1 hour after treatment. In the presence of TFEB and TFE3, but not MITF knockdowns, CQ still caused upregulation of TFEB and TFE3 mRNA expression along with increased LAMP-2 and cathepsin D. MITF knockdown and knockdown of all three was associated with reduced mRNA expression of LAMP-2 and cathepsin D. CQ and dimebon treatment in the presence of the triple knockdown further decreased expression of LAMP-2 and cathepsin D, signifying that all three transcription factors are coherently involved in lysosomal response. As it relates to autophagy inhibition, all drugs caused significant dose-dependent increase of p62 (macroautophagy), membrane phospholipid (macroautophagy), and GAPDH (chaperone-mediated autophagy) at 24 hours. Additionally, an extracellular photoreceptor that is taken up and degraded by lysosomes, opsin, showed increase signaling for all drugs relative to control. Results from these autophagy markers indicate that lysosomotropic-mediated lysosomal biogenesis does not necessarily result in a reduction of lysosomal dysfunction. Finally, the importance of calcium signaling in lysosomal function was highlighted by pretreatment with BAPTA-AM, a permeable Ca^{2+} chelator. A 1hr pretreatment with 5μM BAPTA caused 1) decreased lysosomotropic-induced nuclear translocation of TFEB/TFE3 but not MITF, 2) decreased lysosomotropic-induced lysosomal biogenesis, 3) caused greater than additive combination cytotoxicity effects (Lu et al., 2017).

While not as comprehensive, a handful of studies report similar lysosome-biogenesis and related effects as a result of treatment with lipophilic weakly basic chemotherapeutics. Vincristine treatment at 100nM over 24hr in HeLa and MCF-7 cells led to a significant increase in lysosomal burden, and massively sensitized the cells to the lysosomal destabilizer (causes cathepsin-mediated cell death) siramesine (Groth-pedersen et al., 2007). Another study in MCF-7 observed TFEB translocation in response to nM concentrations of DOX and mitoxantrone. Of particular note was that mitoxantrone was able to increase lysosomal burden by 2.7-fold at 10nM, 6% of the reported IC50, and as much as 16.4-fold at 30nM (Zhitomirsky and Assaraf, 2015). In a study previously discussed with tongue squamous cell carcinoma, cisplatin resistance was attributed to cisplatin-induced lysosomal biogenesis mediated by TFEB-activation. Interestingly, this mechanism was regulated by c-ABL – a tyrosine kinase that modulates the key tumor suppressor p53 (Chu et al., 2018). TFEB overexpression and knockdown was examined in the presence of DOX, finding that overexpression enhanced DOX autophagy activation while reducing sensitivity to DOX, whereas knockdown caused complete opposite effects. ATG5 knockdown under these circumstances had the same effect of increasing DOX potency even during TFEB overexpression (Fang, 2017). Additionally, the weakly basic MEK inhibitors trametinib and refametinib were associated with an increase in overall lysosome volume fraction of PDAC cells, which was further exacerbated the longer the cells were exposed to the drugs. The lysosomal biogenesis was shown to be caused by TFEB activation, and knockdown of TFEB was able to prevent lysosomal biogenesis associated with MEK inhibition by trametinib and refametinib (Zhao et al., 2020).

A study investigating TFEB dynamics in response to lysosomotropic drugs showed that TFEB was significantly activated in the nucleus of cells in as little as 90 minutes of exposure to agents including siramesine, sunitinib, mefloquine, and chloroquine (Zhitomirsky et al., 2018). TFEB continued to increase in nuclear activity for the duration of the experiment, 180 minutes, and, specifically with siramesine, the study observes a disassociation of mTORC1 from the membrane. This suggests that lysosomtropic agents activate TFEB through inhibition of mTORC1 (Zhitomirsky et al., 2018).

In addition to autophagy inhibition, lysosomal disruption and lysosomal-mediated cell death play a role in augmenting primary chemotherapy. Many cell lines thought to be autophagy-dependent due to their CQ/HCQ sensitivity have shown mechanistically that their sensitivity is due to other lysosomal-related pathways affected by CQ/HCQ treatment. This highlights the need to clearly characterize mechanistic autophagy dependence versus sensitivity to lysosomal disruption. To add complication, the two are highly connected as lysosomes are the primary autophagy mediator, and disrupting one tends to disrupt the other. Additionally, a possible link to elevated levels of autophagy in response to chemotherapy treatment has been found in TFEB. TFEB activation by cellular stress increases the autophagic and lysosomal burden of the cell, which promotes increased clearance of the primary chemotherapeutic from the cell, as well as increasing the effective lysosomal drug sink, pulling the chemotherapeutic away from its target within the cell. This highlights the importance of CQ/HCQ and BafA1 in neutralizing this drug sink effect, in addition to their autophagy inhibiting capabilities. Lysosomal studies have provided an important link between autophagy inhibitors and

their role in overcoming drug resistance in tumor cells, and have revealed the role of TFEB as a key player in acquisition of this resistance. Additionally, it is unclear what role TFEB activation may have in pharmacokinetic alterations of lysosomotropic agents, particularly over long periods of exposure both *in vitro* and *in vivo*.

Autophagy and the Acidic Microenvironment in Cancer

Extracellular acidification, response, and role in drug resistance – A Hallmark of Cancer

One of the emerging hallmarks of cancer, particularly solid tumors, is altered pH homeostasis within the tumor microenvironment – particularly an acidified extracellular space and alkalinized intracellular space (Hanahan and Weinberg, 2011). Due to the random organization of vasculature within the tumor microenvironment, hypoxic tumor subpopulations develop and must produce energy through glycolysis. Induction of acidity in these subpopulations is due to the Warburg effect, which is a result of significantly higher glucose consumption in cancer cells, even in normoxic conditions – termed “aerobic glycolysis” (Hanahan and Weinberg, 2011). Briefly, in cancer cells most glucose is converted to lactate through aerobic glycolysis, even in the presence of normal oxygen concentrations. Lactate is a known inflammatory agent, and elevated levels of lactate have been linked to tumorigenesis and metastatic potential in the clinic (Walenta et al., 1997; Brizel et al., 2001). Another byproduct of aerobic glycolysis is H+, which must be accounted for by the cell to avoid toxic cytosolic acidification. A primary mechanism to account for rapid proton formation is an increase in cellular proton pump expression, wherein cellular membrane proton pumps/exchangers and V-ATPase play a

role. Due to the higher metabolic demands of the cell, overexpression of proton pumps yields the characteristic tumor acidic extracellular space (pHe = 6.5-7.1) and alkaline intracellular space (pHi = 7.2-7.4) (Kato et al., 2013). Acidic extracellular pH has been linked to metastasis as well, and the relationship has been shown by increased metastatic burden of melanoma cells pretreated with acidic media *in vivo* (Rofstad et al., 2006).

Altered pH homeostasis in tumor cells is associated with several defining characteristics that pose a challenge from the treatment perspective. First of all, increased metastatic potential is known to be associated with the cell-ECM relationship, particularly through proteolytic enzymes that remodel the ECM, and angiogenic promoters that accelerate metastatic potential (Lunt et al., 2009). Additionally, chemoresistance in an acidic pHe is acquired through two mechanisms – induction of the drug efflux pump p-glycoprotein (P-gp), and reduced chemotherapeutic membrane permeability. P-glycoprotein is a cellular membrane pump associated with efflux of chemotherapeutics, so having higher activity of this molecule means more drug will be pumped out of the cytosol and back into the extracellular space. Higher levels of P-gp are associated with a multidrug resistant (MDR) phenotype (Lu et al., 2017c). Reduced chemotherapeutic membrane permeability in an acidic pHe is another issue entirely. It involves reduced fraction of drug that is able to diffuse across the membrane due to increased ionization as described by Henderson-Hasselbach fundamentals. Briefly, many chemotherapeutic drugs are weakly basic molecules, meaning that a majority of the drug will be in the most permeable, unionized form at neutral pH. As pH decreases, the fraction of unionized form of a weakly basic molecule decreases as well, meaning a

smaller fraction of that molecule can permeate the membrane – the same concept which applies to lysosomal trapping.

Another characteristic of MDR tumor cells involves higher prevalence of acidic organelles, and a larger pH gradient between them and the cytosol (You et al., 2009). The effect of this phenotype also involves reduced chemotherapeutic membrane permeability, as described above, except in the context of lysosomal trapping. To reiterate the description in the previous chapter - highly acidic organelles (pH ~4-5) exhibit an ion trap effect, meaning that once a weakly basic molecule permeates into the lumen a majority becomes ionized and cannot diffuse back into the cytosol. This results in a natural “drug sink” that pulls weakly basic molecules away from their target site elsewhere in the cell. In this case acidic pHe causes weakly basic drugs to protonate, preventing them from crossing the cell membrane. This effect was observed in MCF7 cells, where mitoxantrone, daunorubicin, and doxorubicin (all weak bases) were significantly reduced in potency by 2-8 fold as media pH was decreased from 7.4-6.8 (Mahoney et al., 2003). Alternatively, weak acids increased in potency, and the zwitterion paclitaxel was not significantly affected by pH.

Another observed effect of acidic pHe is altered lysosomal trafficking, specifically from the perinuclear region to the cell periphery. As discussed in the previous chapter, MDR and metastatic progression are associated with lysosomal relocation from the perinuclear region to the cell periphery. This observation is recapitulated as increasing degree of lysosomal relocation to the periphery with acidic pH is associated with increased metastatic potential of a panel of cell lines (Glunde et al., 2003). More so,

acidic pHe is associated with a significant decrease in lysosomal burden for poorly metastatic cells, and an increase in highly metastatic cells (Glunde et al., 2003).

In relation to altered lysosomal trafficking, several studies have shown elevated autophagy under hypoxic/acidic conditions, which acts as a protective mechanism. Exposure to acidic conditions (pH < 7.0) has been associated with increased LC3 in human melanoma cells, which is further increased with BafA1 treatment (Marino et al., 2012). Acidic media was shown to cause increased phosphorylation of AMPK and inhibition of mTOR, similar to glucose starvation. Human melanoma cells also experienced slower growth rates with decreasing pH, which was significantly exacerbated by ATG5 knockdown (Marino et al., 2012). A similar study observed two-fold increase of LC3-II and p62 buildup as well as hypoxia-induced cell death in MCF7, PC3, and LNCaP cell lines. This effect was also amplified with ATG7 and Beclin1 knockdown, or pharmacologic V-ATPase inhibition by pantoprazole, which were recapitulated in xenografts. Interestingly, this study noted increasing LC3 relative to increased hypoxia (based on distance from blood vessels), which was reduced significantly in ATG7 and BECN1 knockdown xenografts (Tan et al., 2016). While these observations of autophagy dependence in hypoxic/acidic environments may make inhibiting autophagy seem like a good treatment option, acidic pHe has actually been shown to prevent autophagy inhibition by CQ (Pellegrini et al., 2014). Acidic media completely prevented CQ-induced apoptosis and autophagy inhibition, where buffering acid-conditioned cells restored sensitivity to CQ. Interestingly, *in vivo* tumor samples showed LC3 accumulation only in normoxic areas (Pellegrini et al., 2014).

In addition to studies of acidity and hypoxia in cell lines or tumor xenografts, 3-D spheroids have shown to be a useful *in vitro* tool for mimicking these features of the tumor microenvironment. Specifically, the larger the spheroid the more pronounced the microenvironmental effect. Spheroids >500um in diameter can reflect microenvironmental factors observed in human solid tumors, particularly acidic and hypoxic gradients as well as a hypoxic core (Nath and Devi, 2016). The paper by Nunes et. al. (Nunes et al., 2019) outlines three studies in spheroids that confirm the suspected mechanism of hypoxic gradient formation in spheroids, which indicates a higher consumption of oxygen by cell proliferation at the periphery of the spheroid, leading to lower oxygen concentrations in these regions compared to surrounding media. This, coupled with the oxygen diffusion gradient, ultimately exacerbates the total oxygen gradient and leads to a hypoxic core (Mueller-Klieser and Sutherland, 1982; Mueller-Klieser, 1984; Grimes et al., 2014a; Grimes et al., 2014b). Recapitulation of hypoxic factors, particularly of proteins of the hypoxia-inducible factor (HIF) have been shown to increase in cells cultured in 3-D spheroid format versus 2-D, particularly pronounced HIF-1α in Hela cells cultured in 3-D versus 2-D (Tian et al., 2010). In MCF7 cell spheroids HIF-1α was highly expressed, associated with an increase in P-gp which caused doxorubicin resistance and ultimately a decrease in doxorubicin uptake in MCF7 spheroids relative to 2-D cultures which reproduced a known mechanism of MDR (Doublier et al., 2012).

In addition to extrinsic microenvironmental features such as hypoxia, spheroids have been observed to mimic autophagy of the *in vivo* tumor microenvironment more so than in 2-D cultures. Follo et. al. (Follo et al., 2016) investigated autophagic flux in

mesothelioma cell lines by quantitation of LC3 puncta for autophagy inhibition and ATG13 for autophagy initiation. They observed an overall increase in autophagic flux in 3-D when compared to 2-D. Furthermore, the suggest that increased ATG13, i.e. increased autophagy initiation, is linked with a more positive outcome in patients. In addition to overall autophagic flux, core autophagy transcription factors such as TFEB and FOXO3 are observed to be more highly expressed in spheroid cultures versus 2-D, and inhibition of core autophagy proteins such as BECN1, ATG5, and ATG7 or pharmacologic inhibition with CQ increases sensitivity of spheroid cultures to chemotherapeutic agents (Bingel et al., 2017). Autophagy overactivation has also been observed in 3-D ovarian cancer cultures, associated with decreased proliferation with ATG KD (Wang et al., 2016).

Due to more *in vivo* similar microenvironments, spheroids can and have been used to study cellular uptake of drugs in the tumor microenvironment. Moving further from the outer boundary towards the core, tumor spheroids have been shown to produce more lactate, which is linked to subsequent acidification of this region (Carlsson and Acker, 1988; Hirschhaeuser et al., 2010). The oxygen gradient in spheroids is also associated with a pH gradient due to the inability of lactate to diffuse out of the spheroid center. Spheroid extracellular pH has been shown to decrease proportional to depth, with large spheroids reaching acidic pH values in the range of 6.4-6.8 (Swietach et al., 2012; McIntyre et al., 2016). As might be expected, this gradient has been shown to contribute to decreased uptake of weakly basic drugs in deeper regions of the spheroid. Of interest is the weakly basic compound, doxorubicin, which

was observed to decrease in overall uptake by 1.7x towards the core of the spheroid. This was associated with a decrease in sensitivity to the drug (Swietach et al., 2012).

On the other hand, it may be possible to overcome the pH gradient observed in larger spheroids. McIntyre et. al. (McIntyre et al., 2016) showed that treating spheroids with an inhibitor of sodium bicarbonate transporters could normalize pH throughout the entire spheroid, which was associated with an increase in core apoptosis. This would be assumed to result in increased weak base drug uptake as well. Additionally, the proton pump inhibitors omeprazole and lansoprazole were shown to increase doxorubicin uptake in spheroids cultured in acidic media, but not in neutral media (Paskeviciute and Petrikaite, 2019). Multiple other studies have suggested the use of spheroids as an *in vitro* tool to more accurately investigate how drug response may look *in vivo,* specifically leveraging drug diffusion, MDR, generation of ROS, pH gradients, and cytotoxicity (Achilli et al., 2014; Mittler et al., 2017; Jove et al., 2019).

Overcoming the Acidic Microenvironment

Attempts to overcome the pharmacologic treatment roadblocks and increased malignant potential correlated with acidic pHe involve targeting the tumor extracellular space for deacidification. Proton pump inhibitors (PPIs) are the current gold standard for neutralization of the extracellular space. PPIs, such as omeprazole, esomeprazole, pantoprazole, lansoprazole, and rabeprazole, are clinically approved drugs primarily used to treat gastric ulcers by targeting the gastric H+/K+ ATPase (Shin and Sachs, 2008). PPIs are weakly-basic prodrugs that require acidic pH to activate. They have short half-lives (1hr), but a pharmacodynamic effect of roughly 48 hours due to irreversible binding with the proton pump. PPIs have characteristic high oral

bioavailability, but high interpatient variability attributed to Cyp3A4 metabolism (Shin and Sachs, 2008). While PPIs are primarily used in gastric acidity-related issues, they have recently been found to inhibit other cellular proton pumps, including V-ATPase (Fais et al., 2007; Neri and Supuran, 2011). In addition to their broader proton pump targeting, there is evidence of PPIs inhibiting P-gp, observed by altered digoxin efflux in Caco-2 cells (Pauli-Magnus et al., 2001).

The idea that PPIs may serve as valuable tools in counteracting acidity of the tumor microenvironment has been significantly investigated in preclinical studies, which have led to a few recent clinical trials involving chemocombination therapy with PPIs. Regarding preclinical studies, the ability of PPIs to inhibit the V-ATPase, neutralizing lysosomal pH, has been shown using three clinically-approved PPIs in human melanoma and adenocarcinoma (Luciani et al., 2004). 24 hour pretreatment with PPIs were nontoxic and sensitized cell lines and xenografts to cisplatin, 5-FU, and vinblastine by up to 100x. This was accompanied with notable drug relocation from the lysosome to their target site, along with increased extracellular and lysosomal pH. Within the realm of chemocombination sensitization, another study investigated combo sensitization abilities of omeprazole (OMZ) and pantoprazole (PTZ) with gemcitabine and 5-FU in pancreatic cancer cells. OMZ was effective on its own, with IC50 values between 2-120μM. To put this in perspective, highest tolerable blood C_{max} for pantoprazole was 85μM in clinical trials (Lu et al., 2017c). Omeprazole also reversed hormesis of 5-FU, and enhanced sensitivity to both 5-FU and gemcitabine dose-dependently. Lysosome-related effects of OMZ by increased LAMP-1 expression and altered cathepsin-D expression, but surprisingly not V-ATPase inhibition (Udelnow et

al., 2011). Cytotoxic effects of PPIs, specifically esomeprazole (ESOM), were also shown in melanoma cells by increase of ROS through mitochondrial dysfunction. ESOM treatment shows autophagy inhibition capabilities through LC3-II accumulation, and sensitivity to treatment was significantly amplified by ATG5 and BECN1 (Marino et al., 2010). PPI role in lysosomal targeting also causes lysosomal enzyme inhibition, specifically acid phosphatase and beta-n-acetylglucosaminidase in mouse spleen tissue. Surprisingly, this was not recapitulated in liver tissue, likely due to significant first pass metabolism, which is also the primary driver of PK variability in these drugs (Liu et al., 2013). An additional study showed both the pHe and pH_{lys} targeting ability of OMZ. Dose-dependent increase in endosomal pH with CQ, BafA1, and OMZ was observed, which directly correlated with increased cytotoxicity of DOX. This did not result in significant cellular uptake of DOX, indicating it is not displaced to the lysosome anymore. OMZ also increased penetration of DOX and mitoxantrone through multicell layers of tissue, where CQ and BafA1 did not (Lee and Tannock, 2006).

While PPIs are sort of pan-specific when it comes to targeting, their role as clinically-approved V-ATPase inhibitors can be emphasized by studies directly interrupting the V-ATPase. Knockdown of the protein TM9SF4, which is an activator of V-ATPase, showed increased sensitivity to 5-FU, reducing malignant characteristics, and acidifying the cytosol while alkalinizing the extracellular space and lysosomes (Lozupone et al., 2015). Another study knocked down the ATP6L sub-unit of V-ATPase, which was associated with similar effects – sensitization and cellular relocation of 5-FU, DOX, VCR; and neutralization of lysosomal pH (You et al., 2009).

Overall, PPIs are safe and widely used drugs whose possible application to cancer therapy is being investigated clinically. A study in human osteosarcoma observed the expected effects with 24hr pretreatment of 60μM ESOM followed by cisplatin in human osteosarcoma cells, and complete tumor regression was observed in xenografts using 24hr pretreatment of 25mg/kg ESOM followed by 5mg/kg cisplatin. This study was coupled with a prospective phase 2 clinical trial in human patients, using two-day pretreatment of 40-120mg/day ESOM before regimens involving methotrexate, cisplatin, and doxorubicin. The outcome involved increased patient response compared to historical control, and while not quite statistically significant ($p = 0.07$, $n = 61$ in chondroblastic osteosarcoma) the toxicity profiles remained unchanged by ESOM pretreatment (Ferrari et al., 2013).

The indication of PPI efficacy in preclinical studies along with no observed toxicity exacerbation in initial clinical trials have led to multiple phase I/II clinical trials evaluating the efficacy of PPIs for use in treating cancer patients, including two in companion animals. One preliminary retrospective study in breast cancer patients showed OMZ treatment augmented chemotherapy and significantly improved survival, and the trial is aimed at examining the mechanism of sensitization (NCT02595372). Three other trials are investigating optimal dosing (NCT01163903), and role of high dose PPI (NCT01748500, NCT01069081) in augmenting primary chemotherapy of patients with various solid tumor types (Koltai, 2016). Results from the two phase I/II clinical trials in companion animal patients have led to overall positive results, with tumor regression for most animals observed. To recapitulate results from the phase I/II study in animals with chemoresistant tumors (Spugnini et al., 2011): 19/28 dogs

experienced varying degrees of response (including 9/11 lymphoma dogs on the Wisconsin CHOP Protocol), whereas only 2/10 control dogs experienced partial response. 4/28 dogs experienced GI side effects (vomiting and diarrhea). 6/7 cats responded, two of which had complete remission. 2/7 cats in the control group showed partial response. Overall response in PPI patients was 68% whereas control was 17% (with no patients showing complete remission). Dosing was 5 mg/kg lansoprazole for 3 consecutive days with chemotherapy administration. Clinical trial results thus far have shown dose tolerance up to 240mg/day, giving a serum C_{max} of roughly 85μM (Lu et al., 2017c) which is similar to cytotoxic concentrations observed in vitro. This high dosing strategy is consistent with Zollinger-Ellison-Syndrome patients who are treated with OMZ as much as 120mg x 3/day, resulting in uncommon mild side effects (Frucht et al., 1991) and no reported long-term side effects (Thomson et al., 2010).

Overall PPIs appear safe to use, accompanied by good evidence showing their ability to augment chemotherapy strategies. This is being investigated in early phase clinical trials and has shown positive results thus far. Due to neutralization of the tumor extracellular environment, PPIs may serve as a useful treatment strategy to augment HCQ treatment efforts in the clinic, as a likely mechanism of HCQ nonresponse is due to hypoxic subpopulations in solid tumors (Pellegrini et al., 2014; Tan et al., 2016). Additionally, PPIs have been shown to inhibit autophagy and augment primary chemotherapy treatments in a similar manner as HCQ. The combination of increased and homogenous HCQ uptake throughout the tumor microenvironment, compounded autophagy inhibition, and additive tumor cell cytotoxicity provide solid hypothetical

grounds for further investigation of treatment regimens including a combination of these two clinically-approved drug families.

References

Achilli TM, McCalla S, Meyer J, Tripathi A and Morgan JR (2014) Multilayer spheroids to quantify drug uptake and diffusion in 3D. *Mol Pharm* 11:2071-2081.

Adar Y, Stark M, Bram EE, Bergh HVD, Szewczyk G, Sarna T, Skladanowski A and Griffioen AW (2012) Imidazoacridinone-dependent lysosomal photodestruction : a pharmacological Trojan horse approach to eradicate multidrug-resistant cancers. 3:e293-210.

Altan BN, Chen Y, Schindler M and Simon SM (1998) Defective Acidification in Human Breast Tumor Cells and Implications for Chemotherapy. 187.

Amaravadi RK (2011) Autophagy in Tumor Immunity. *Science* 334:1501 LP - 1502.

Amaravadi RK and Thompson CB (2007) The roles of therapy-induced autophagy and necrosis in cancer treatment. *Clin Cancer Res* 13:7271-7279.

Amaravadi RK and Winkler JD (2012) Lys05: a new lysosomal autophagy inhibitor. *Autophagy* 8:1383-1384.

Azijli K, Gotink KJ and Verheul HMW (2015) The Potential Role of Lysosomal Sequestration in Sunitinib Resistance of Renal Cell Cancer. 2:195-203.

Ballabio A and Gieselmann V (2009) Lysosomal disorders: from storage to cellular damage. *Biochimica et biophysica acta* 1793:684-696.

Barnard RA, Regan DP, Hansen RJ, Maycotte P, Thorburn A and Gustafson DL (2016) Autophagy Inhibition Delays Early but Not Late-Stage Metastatic Disease. *J Pharmacol Exp Ther* 358:282-293.

Barnard RA, Wittenburg LA, Amaravadi RK, Gustafson DL, Thorburn A and Thamm DH (2014) Phase I clinical trial and pharmacodynamic evaluation of combination hydroxychloroquine and doxorubicin treatment in pet dogs treated for spontaneously occurring lymphoma. *Autophagy* 10:1415-1425.

Bingel C, Koeneke E, Ridinger J, Bittmann A, Sill M, Peterziel H, Wrobel JK, Rettig I, Milde T, Fernekorn U, Weise F, Schober A, Witt O and Oehme I (2017) Three-dimensional tumor cell growth stimulates autophagic flux and recapitulates chemotherapy resistance. *Cell death & disease* 8:e3013-e3013.

Blagosklonny MV (2010) Linking calorie restriction to longevity through sirtuins and autophagy: any role for TOR., in *Cell death & disease* p e12.

Boone BA, Bahary N, Zureikat AH, Moser AJ, Normolle DP, Wu W-C, Singhi AD, Bao P, Bartlett DL, Liotta LA, Espina V, Loughran P, Lotze MT and Zeh HJ (2015) Safety

and Biologic Response of Pre-operative Autophagy Inhibition in Combination with Gemcitabine in Patients with Pancreatic Adenocarcinoma. *Annals of Surgical Oncology* 22:4402-4410.

Bray K, Mathew R, Lau A, Kamphorst JJ, Fan J, Chen J, Chen H-Y, Ghavami A, Stein M, DiPaola RS, Zhang D, Rabinowitz JD and White E (2012) Autophagy suppresses RIP kinase-dependent necrosis enabling survival to mTOR inhibition. *PloS one* 7:e41831.

Brizel DM, Schroeder T, Scher RL, Walenta S, Clough RW, Dewhirst MW and Mueller-Klieser W (2001) Elevated tumor lactate concentrations predict for an increased risk of metastases in head-and-neck cancer. *International journal of radiation oncology, biology, physics* 51:349-353.

Browning DJ (2014) Pharmacology of Chloroquine and Hydroxychloroquine, in *Hydroxychloroquine and Chloroquine Retinopathy* pp 35-63, Springer.

Carlsson J and Acker H (1988) Relations between pH, oxygen partial pressure and growth in cultured cell spheroids. *Int J Cancer* 42:715-720.

Carmichael SJ, Charles B and Tett SE (2003) Population pharmacokinetics of hydroxychloroquine in patients with rheumatoid arthritis. *Ther Drug Monit* 25:671-681.

Chu H-Y, Chen X, Jiang Y-E, Wang W, Qi X, Zhong Z-M, Zeng M-S, Zhu X-F and Sun C-Z (2018) Bafilomycin A1 increases the sensitivity of tongue squamous cell carcinoma cells to cisplatin by inhibiting the lysosomal uptake of platinum ions but not autophagy. *Cancer Letters* 423:105-112.

Chude CI and Amaravadi RK (2017) Targeting Autophagy in Cancer: Update on Clinical Trials and Novel Inhibitors. *Int J Mol Sci* 18.

Collins KP, Jackson KM and Gustafson DL (2018) Hydroxychloroquine: A Physiologically-Based Pharmacokinetic Model in the Context of Cancer-Related Autophagy Modulation. *Journal of Pharmacology and Experimental Therapeutics*:jpet.117.245639.

Colombo F, Trombetta E, Cetrangolo P and Maggioni M (2014) Giant Lysosomes as a Chemotherapy Resistance Mechanism in Hepatocellular Carcinoma Cells. *PLoS ONE*:1-20.

Cook KL, Warri A, Soto-Pantoja DR, Clarke PA, Cruz MI, Zwart A and Clarke R (2014) Hydroxychloroquine inhibits autophagy to potentiate antiestrogen responsiveness in ER+ breast cancer. *Clinical cancer research : an official journal of the American Association for Cancer Research* 20:3222-3232.

Cooper GM (2000) Lysosomes. *The Cell: A Molecular Approach 2nd edition*.

Davis IJ, Kim JJ, Ozsolak F, Widlund HR, Rozenblatt-Rosen O, Granter SR, Du J, Fletcher JA, Denny CT, Lessnick SL, Linehan WM, Kung AL and Fisher DE (2006) Oncogenic MITF dysregulation in clear cell sarcoma: Defining the MiT family of human cancers. *Cancer Cell* 9:473-484.

de Duve C (1983) Lysosomes revisited. *European Journal of Biochemistry* 137:391-397.

Degenhardt K, Mathew R, Beaudoin B, Bray K, Anderson D, Chen G, Mukherjee C, Shi Y, Gelinas C, Fan Y, Nelson DA, Jin S and White E (2006) Autophagy promotes tumor cell survival and restricts necrosis, inflammation, and tumorigenesis. *Cancer cell* 10:51-64.

Dibble CC and Cantley LC (2015) Regulation of mTORC1 by PI3K signaling. *Trends Cell Biol* 25:545-555.

Donohue E, Tovey A, Vogl AW, Arns S, Sternberg E, Young RN and Roberge M (2011) Inhibition of autophagosome formation by the benzoporphyrin derivative verteporfin. *The Journal of biological chemistry* 286:7290-7300.

Doublier S, Belisario DC, Polimeni M, Annaratone L, Riganti C, Allia E, Ghigo D, Bosia A and Sapino A (2012) HIF-1 activation induces doxorubicin resistance in MCF7 3-D spheroids via P-glycoprotein expression: a potential model of the chemo-resistance of invasive micropapillary carcinoma of the breast. *BMC Cancer* 12:4.

Dowdle WE, Nyfeler B, Nagel J, Elling RA, Liu S, Triantafellow E, Menon S, Wang Z, Honda A, Pardee G, Cantwell J, Luu C, Cornella-Taracido I, Harrington E, Fekkes P, Lei H, Fang Q, Digan ME, Burdick D, Powers AF, Helliwell SB, D'Aquin S, Bastien J, Wang H, Wiederschain D, Kuerth J, Bergman P, Schwalb D, Thomas J, Ugwonali S, Harbinski F, Tallarico J, Wilson CJ, Myer VE, Porter JA, Bussiere DE, Finan PM, Labow MA, Mao X, Hamann LG, Manning BD, Valdez Reginald A, Nicholson T, Schirle M, Knapp MS, Keaney EP and Murphy LO (2014) Selective VPS34 inhibitor blocks autophagy and uncovers a role for NCOA4 in ferritin degradation and iron homeostasis in vivo. *Nature Cell Biology* 16:1069.

Dragowska WH, Weppler SA, Wang JC, Wong LY, Kapanen AI, Rawji JS, Warburton C, Qadir MA, Donohue E, Roberge M, Gorski SM, Gelmon KA and Bally MB (2013) Induction of autophagy is an early response to gefitinib and a potential therapeutic target in breast cancer. *PloS one* 8:e76503.

Duvvuri M, Gong Y, Chatterji D and Krise JP (2004) Weak base permeability characteristics influence the intracellular sequestration site in the multidrug-resistant human leukemic cell line HL-60. *J Biol Chem* 279:32367-32372.

Duvvuri M and Krise JP (2005) A novel assay reveals that weakly basic model compounds concentrate in lysosomes to an extent greater than pH-partitioning theory would predict. *Mol Pharm* 2:440-448.

Eng CH, Wang Z, Tkach D, Toral-Barza L, Ugwonali S, Liu S, Fitzgerald SL, George E, Frias E, Cochran N, De Jesus R, McAllister G, Hoffman GR, Bray K, Lemon L, Lucas J, Fantin VR, Abraham RT, Murphy LO and Nyfeler B (2016) Macroautophagy is dispensable for growth of KRAS mutant tumors and chloroquine efficacy. *Proc Natl Acad Sci U S A* 113:182-187.

Fais S, De Milito A, You H and Qin W (2007) Targeting vacuolar H+-ATPases as a new strategy against cancer. *Cancer research* 67:10627-10630.

Fan HW, Ma ZX, Chen J, Yang XY, Cheng JL and Li YB (2015) Pharmacokinetics and Bioequivalence Study of Hydroxychloroquine Sulfate Tablets in Chinese Healthy Volunteers by LC-MS/MS. *Rheumatol Ther* 2:183-195.

Fang L-m (2017) Transcription factor EB is involved in autophagy-mediated chemoresistance to doxorubicin in human cancer cells.

Farrill JMS-o, Kleinerman ES, Hollomon MG, Wang W-l, Tsai J-w and Gordon NB (2017) Phosphorylated heat shock protein 27 as a potential biomarker to predict the role of chemotherapy-induced autophagy in osteosarcoma response to therapy.

Feng X and Yang J (2016) Lysosomal Calcium in Neurodegeneration. *Messenger (Los Angel)* 5:56-66.

Ferrari S, Perut F, Fagioli F, Brach A, Prever D, Meazza C, Parafioriti A, Picci P, Gambarotti M, Avnet S, Baldini N and Fais S (2013) Proton pump inhibitor chemosensitization in human osteosarcoma : from the bench to the patients ' bed. *Journal of Translational Medicine* 11:1-7.

Foghsgaard L, Wissing D, Mauch D, Lademann U, Bastholm L, Boes M, Elling F, Leist M and Jäättelä M (2001) Cathepsin B Acts as a Dominant Execution Protease in Tumor Cell Apoptosis Induced by Tumor Necrosis Factor. *The Journal of Cell Biology* 0599911:21-9525.

Follo C, Barbone D, Richards WG, Bueno R and Broaddus VC (2016) Autophagy initiation correlates with the autophagic flux in 3D models of mesothelioma and with patient outcome. *Autophagy* 12:1180-1194.

Frucht H, Maton PN and Jensen RT (1991) Use of omeprazole in patients with Zollinger-Ellison syndrome. *Digestive diseases and sciences* 36:394-404.

Furst DE (1996) Pharmacokinetics of hydroxychloroquine and chloroquine during treatment of rheumatic diseases. *Lupus* 5 Suppl 1:S11-15.

Gallagher LE, Radhi OA, Abdullah MO, McCluskey AG, Boyd M and Chan EYW (2017) Lysosomotropism depends on glucose: a chloroquine resistance mechanism. *Cell death & disease* 8:e3014-e3014.

Giatromanolaki A, Kalamida D, Sivridis E, Karagounis IV, Gatter KC, Harris AL and Koukourakis MI (2015a) Increased expression of transcription factor EB (TFEB) is associated with autophagy, migratory phenotype and poor prognosis in non-small cell lung cancer. *Lung Cancer* 90:98-105.

Glunde K, Guggino SE, Solaiyappan M, Pathak AP, Ichikawa Y and Bhujwalla ZM (2003) Extracellular acidification alters lysosomal trafficking in human breast cancer cells. *Neoplasia* 5:533-545.

Goodall ML, Wang T, Martin KR, Kortus MG, Kauffman AL, Trent JM, Gately S and MacKeigan JP (2014) Development of potent autophagy inhibitors that sensitize oncogenic BRAF V600E mutant melanoma tumor cells to vemurafenib. *Autophagy* 10:1120-1136.

Gotink KJ, Broxterman HJ, Labots M, de Haas RR, Dekker H, Honeywell RJ, Rudek MA, Beerepoot LV, Musters RJ, Jansen G, Griffioen AW, Assaraf YG, Pili R, Peters GJ and Verheul HMW (2011) Lysosomal Sequestration of Sunitinib: A Novel Mechanism of Drug Resistance. *Clinical Cancer Research* 17:7337-7346.

Grimes DR, Fletcher AG and Partridge M (2014a) Oxygen consumption dynamics in steady-state tumour models. *R Soc Open Sci* 1:140080.

Grimes DR, Kelly C, Bloch K and Partridge M (2014b) A method for estimating the oxygen consumption rate in multicellular tumour spheroids. *J R Soc Interface* 11:20131124.

Groth-pedersen L, Ostenfeld MS, Høyer-hansen M, Nylandsted J and Ja M (2007) Vincristine Induces Dramatic Lysosomal Changes and Sensitizes Cancer Cells to Lysosome-Destabilizing Siramesine.2217-2226.

Guillaumot P, Luquain C, Malek M, Huber A-L, Brugiere S, Garin J, Grunwald D, Regnier D, Petrilli V, Lefai E and Manie SN (2010) Pdro, a protein associated with late endosomes and lysosomes and implicated in cellular cholesterol homeostasis. *PloS one* 5:e10977.

Guo JY, Chen H-Y, Mathew R, Fan J, Strohecker AM, Karsli-Uzunbas G, Kamphorst JJ, Chen G, Lemons JMS, Karantza V, Coller HA, Dipaola RS, Gelinas C, Rabinowitz JD and White E (2011) Activated Ras requires autophagy to maintain oxidative metabolism and tumorigenesis. *Genes & development* 25:460-470.

Haas NB, Appleman LJ, Stein M, Redlinger M, Wilks M, Xu X, Onorati A, Kalavacharla A, Kim T, Zhen CJ, Kadri S, Segal JP, Gimotty PA, Davis LE and Amaravadi RK (2019) Autophagy Inhibition to Augment mTOR Inhibition: a Phase I/II Trial of Everolimus and Hydroxychloroquine in Patients with Previously Treated Renal Cell Carcinoma. *Clin Cancer Res* 25:2080-2087.

Halaby R (2015) Role of lysosomes in cancer therapy. *Research and Reports in Biology* 6:147-155.

Hanahan D and Weinberg RA (2011) Hallmarks of Cancer : The Next Generation. *Cell* 144:646-674.

Helgason GV, Mukhopadhyay A, Karvela M, Salomoni P, Calabretta B and Holyoake TL (2013) Autophagy in chronic myeloid leukaemia: stem cell survival and implication in therapy. *Current cancer drug targets* 13:724-734.

Hirschhaeuser F, Menne H, Dittfeld C, West J, Mueller-Klieser W and Kunz-Schughart LA (2010) Multicellular tumor spheroids: An underestimated tool is catching up again. *Journal of Biotechnology* 148:3-15.

Ilan N, Elkin M and Vlodavsky I (2006) Regulation, function and clinical significance of heparanase in cancer metastasis and angiogenesis. *The international journal of biochemistry & cell biology* 38:2018-2039.

Ishizaki J, Yokogawa K, Ichimura F and Ohkuma S (2000) Uptake of imipramine in rat liver lysosomes in vitro and its inhibition by basic drugs. *J Pharmacol Exp Ther* 294:1088-1098.

Jin H-O, Hong S-E, Park J-A, Chang YH, Hong YJ, Park I-C and Lee JK (2016) Inhibition of JNK-mediated autophagy enhances NSCLC cell sensitivity to mTORC1/2 inhibitors. *Scientific Reports* 6:28945.

Jove M, Spencer JA, Hubbard ME, Holden EC, O'Dea RD, Brook BS, Phillips RM, Smye SW, Loadman PM and Twelves CJ (2019) Cellular Uptake and Efflux of Palbociclib In Vitro in Single Cell and Spheroid Models. *J Pharmacol Exp Ther* 370:242-251.

Jutten B and Rouschop KMA (2014) EGFR signaling and autophagy dependence for growth, survival, and therapy resistance. *Cell cycle (Georgetown, Tex)* 13:42-51.

Kato Y, Ozawa S, Miyamoto C, Maehata Y, Suzuki A, Maeda T and Baba Y (2013) Acidic extracellular microenvironment and cancer. *Cancer Cell International* 13:1.

Kazmi F, Hensley T, Pope C, Funk RS, Loewen GJ, Buckley DB and Parkinson A (2013) Lysosomal sequestration (trapping) of lipophilic amine (cationic

amphiphilic) drugs in immortalized human hepatocytes (Fa2N-4 cells). *Drug Metabolism and Disposition* 41:897-905.

Kim KA, Park JY, Lee JS and Lim S (2003) Cytochrome P450 2C8 and CYP3A4/5 are involved in chloroquine metabolism in human liver microsomes. *Arch Pharm Res* 26:631-637.

King MA, Ganley IG and Flemington V (2016) Inhibition of cholesterol metabolism underlies synergy between mTOR pathway inhibition and chloroquine in bladder cancer cells. *Oncogene* 35:4518-4528.

Kirkegaard T and Jaattela M (2009) Lysosomal involvement in cell death and cancer. *Biochimica et biophysica acta* 1793:746-754.

Klionsky DJ, Abdelmohsen K, Abe A, Abedin MJ, Abeliovich H, Arozena AA, Adachi H, Adams CM, Adams PD, Adeli K, Adhihetty PJ, Adler SG, Agam G, Agarwal R, Aghi MK, Agnello M, Agostinis P, Aguilar PV, Aguirre-Ghiso J, Aguirre-Ghiso J, Airoldi EM, Airoldi EM, Ait-Si-Ali S, Akematsu T, Akporiaye ET, Al-Rubeai M, Albaiceta GM, Albanese C, Albani D, Albert ML, Aldudo J, Algül H, Alirezaei M, Alloza I, Alloza I, Almasan A, Almonte-Beceril M, Alnemri ES, Alonso C, Altan-Bonnet N, Altieri DC, Alvarez S, Alvarez-Erviti L, Alves S, Amadoro G, Amano A, Amantini C, Ambrosio S, Amelio I, Amer AO, Amessou M, Amon A, An Z, Anania FA, Andersen SU, Andley UP, Andreadi CK, Andrieu-Abadie N, Anel A, Ann DK, Anoopkumar-Dukie S, Antonioli M, Antonioli M, Aoki H, Apostolova N, Aquila S, Aquilano K, Araki K, Arama E, Aranda A, Araya J, Arcaro A, Arias E, Arimoto H, Ariosa AR, Armstrong JL, Arnould T, Arsov I, Asanuma K, Askanas V, Asselin E, Atarashi R, Atherton SS, Atkin JD, Attardi LD, Auberger P, Auburger G, Aurelian L, Autelli R, Avagliano L, Avagliano L, Avantaggiati ML, Avrahami L, Awale S, Azad N, Bachetti T, Backer JM, Bae DH, Bae JS, Bae ON, et al. (2016) Guidelines for the use and interpretation of assays for monitoring autophagy (3rd edition). *Autophagy* 12:1-222.

Koblinski JE, Ahram M and Sloane BF (2000) Unraveling the role of proteases in cancer. *Clinica chimica acta; international journal of clinical chemistry* 291:113-135.

Koltai T (2016) Cancer: fundamentals behind pH targeting and the double-edged approach. *Onco Targets Ther* 9:6343-6360.

Kondratskyi A, Kondratska K, Vanden Abeele F, Gordienko D, Dubois C, Toillon RA, Slomianny C, Lemière S, Delcourt P, Dewailly E, Skryma R, Biot C and Prevarskaya N (2017) Ferroquine, the next generation antimalarial drug, has antitumor activity. *Scientific Reports* 7:1-15.

Kornhuber J, Henkel AW, Groemer TW, Stadtler S, Welzel O, Tripal P, Rotter A, Bleich S and Trapp S (2010) Lipophilic cationic drugs increase the permeability of lysosomal membranes in a cell culture system. *J Cell Physiol* 224:152-164.

Kos J and Lah TT (1998) Cysteine proteinases and their endogenous inhibitors: target proteins for prognosis, diagnosis and therapy in cancer (review). *Oncology reports* 5:1349-1361.

Lawrence BP and Brown WJ (1992) Autophagic vacuoles rapidly fuse with pre-existing lysosomes in cultured hepatocytes. *Journal of cell science* 102 (Pt 3):515-526.

Lazova R, Camp RL, Klump V, Siddiqui SF, Amaravadi RK and Pawelek JM (2012) Punctate LC3B expression is a common feature of solid tumors and associated with proliferation, metastasis and poor outcome HHS Public Access. *Clin Cancer Res Clin Cancer Res January* 15:370-379.

Lee C and Tannock I (2006) Inhibition of endosomal sequestration of basic anticancer drugs : influence on cytotoxicity and tissue penetration. *British Journal of Cancer* 94:863-869.

Lee HO, Mustafa A, Hudes GR and Kruger WD (2015) Hydroxychloroquine Destabilizes Phospho-S6 in Human Renal Carcinoma Cells. *PLoS One* 10:e0131464.

Leung L-SB, Neal JW, Wakelee HA, Sequist LV and Marmor MF (2015) Rapid Onset of Retinal Toxicity From High-Dose Hydroxychloroquine Given for Cancer Therapy. *American journal of ophthalmology* 160:799-805.e791.

Levine B and Abrams J (2008) p53: The Janus of autophagy?, in *Nature cell biology* pp 637-639.

Levy JM, Thompson JC, Griesinger AM, Amani V, Donson AM, Birks DK, Morgan MJ, Mirsky DM, Handler MH, Foreman NK and Thorburn A (2014) Autophagy inhibition improves chemosensitivity in BRAF(V600E) brain tumors. *Cancer Discov* 4:773-780.

Levy JMM, Towers CG and Thorburn A (2017) Targeting autophagy in cancer. *Nat Rev Cancer* 17:528-542.

Li J, Yang B, Zhou Q, Wu Y, Shang D, Guo Y, Song Z, Zheng Q and Xiong J (2013a) Autophagy promotes hepatocellular carcinoma cell invasion through activation of epithelial-mesenchymal transition. *Carcinogenesis* 34:1343-1351.

Li X, Garrity AG and Xu H (2013b) Regulation of membrane trafficking by signalling on endosomal and lysosomal membranes. *The Journal of physiology* 591:4389-4401.

Liang XH, Jackson S, Seaman M, Brown K, Kempkes B, Hibshoosh H and Levine B (1999) Induction of autophagy and inhibition of tumorigenesis by beclin 1. *Nature* 402:672.

Lim HS, Im JS, Cho JY, Bae KS, Klein TA, Yeom JS, Kim TS, Choi JS, Jang IJ and Park JW (2009) Pharmacokinetics of hydroxychloroquine and its clinical implications in chemoprophylaxis against malaria caused by Plasmodium vivax. *Antimicrob Agents Chemother* 53:1468-1475.

Liu W, Baker SS, Trinidad J, Burlingame AL, Baker RD, Forte JG, Virtuoso LP, Egilmez NK and Zhu L (2013) Inhibition of lysosomal enzyme activities by proton pump inhibitors. *J Gastroenterol* 48:1343-1352.

Llanos S, Megias D, Blanco-Aparicio C, Hernández-Encinas E, Rovira M, Pietrocola F and Serrano M (2019) Lysosomal trapping of palbociclib and its functional implications. *Oncogene* 38:3886-3902.

Lock R, Roy S, Kenific CM, Su JS, Salas E, Ronen SM and Debnath J (2011) Autophagy facilitates glycolysis during Ras-mediated oncogenic transformation. *Mol Biol Cell* 22:165-178.

Lozupone F, Borghi M, Marzoli F, Azzarito T, Matarrese P, Iessi E, Venturi G, Meschini S, Canitano A, Bona R, Cara A and Fais S (2015) TM9SF4 is a novel V-ATPase-interacting protein that modulates tumor pH alterations associated with drug resistance and invasiveness of colon cancer cells. *Oncogene* 34:5163-5174.

Lu S, Sung T, Lin N, Abraham RT and Jessen BA (2017) Lysosomal adaptation: How cells respond to lysosomotropic compounds. *PLoS ONE* 12:1-23.

Lu ZN, Tian B and Guo XL (2017c) Repositioning of proton pump inhibitors in cancer therapy. *Cancer Chemother Pharmacol* 80:925-937.

Luciani F, Spada M, De Milito A, Molinari A, Rivoltini L, Montinaro A, Marra M, Lugini L, Logozzi M, Lozupone F, Federici C, Iessi E, Parmiani G, Arancia G, Belardelli F and Fais S (2004) Effect of proton pump inhibitor pretreatment on resistance of solid tumors to cytotoxic drugs. *J Natl Cancer Inst* 96:1702-1713.

Lunt SJ, Chaudary N and Hill RP (2009) The tumor microenvironment and metastatic disease. *Clinical & experimental metastasis* 26:19-34.

Luzio JP, Pryor PR and Bright NA (2007) Lysosomes: fusion and function. *Nat Rev Mol Cell Biol* 8:622-632.

MacIntyre AC and Cutler DJ (1988) Role of lysosomes in hepatic accumulation of chloroquine. *J Pharm Sci* 77:196-199.

Mahalingam D, Mita M, Sarantopoulos J, Wood L, Amaravadi RK, Davis LE, Mita AC, Curiel TJ, Espitia CM, Nawrocki ST, Giles FJ and Carew JS (2014) Combined autophagy and HDAC inhibition: a phase I safety, tolerability, pharmacokinetic, and pharmacodynamic analysis of hydroxychloroquine in combination with the HDAC inhibitor vorinostat in patients with advanced solid tumors. *Autophagy* 10:1403-1414.

Mahoney BP, Raghunand N, Baggett B and Gillies RJ (2003) Tumor acidity, ion trapping and chemotherapeutics. I. Acid pH affects the distribution of chemotherapeutic agents in vitro. *Biochem Pharmacol* 66:1207-1218.

Marino ML, Fais S, Djavaheri-Mergny M, Villa A, Meschini S, Lozupone F, Venturi G, Della Mina P, Pattingre S, Rivoltini L, Codogno P and De Milito A (2010) Proton pump inhibition induces autophagy as a survival mechanism following oxidative stress in human melanoma cells. *Cell Death Dis* 1:e87.

Marino ML, Pellegrini P, Di Lernia G, Djavaheri-Mergny M, Brnjic S, Zhang X, Hägg M, Linder S, Fais S, Codogno P and De Milito A (2012) Autophagy is a protective mechanism for human melanoma cells under acidic stress. *Journal of Biological Chemistry* 287:30664-30676.

Martina JA, Chen Y, Gucek M and Puertollano R (2012) MTORC1 functions as a transcriptional regulator of autophagy by preventing nuclear transport of TFEB.903-914.

Mathew R, Karp CM, Beaudoin B, Vuong N, Chen G, Chen H-Y, Bray K, Reddy A, Bhanot G, Gelinas C, Dipaola RS, Karantza-Wadsworth V and White E (2009) Autophagy suppresses tumorigenesis through elimination of p62. *Cell* 137:1062-1075.

Maycotte P, Aryal S, Cummings CT, Thorburn J, Morgan MJ and Thorburn A (2012) Chloroquine sensitizes breast cancer cells to chemotherapy independent of autophagy. *Autophagy* 8:200-212.

Maycotte P, Jones KL, Goodall ML, Thorburn J and Thorburn A (2015) Autophagy Supports Breast Cancer Stem Cell Maintenance by Regulating IL6 Secretion. *Mol Cancer Res* 13:651-658.

McAfee Q, Zhang Z, Samanta A, Levi SM, Ma XH, Piao S, Lynch JP, Uehara T, Sepulveda AR, Davis LE, Winkler JD and Amaravadi RK (2012) Autophagy inhibitor Lys05 has single-agent antitumor activity and reproduces the phenotype of a genetic autophagy deficiency. *Proc Natl Acad Sci U S A* 109:8253-8258.

McChesney EW (1983) Animal toxicity and pharmacokinetics of hydroxychloroquine sulfate. *Am J Med* 75:11-18.

McChesney EW, Banks WF, Jr. and Sullivan DJ (1965) Metabolism of chloroquine and hydroxychloroquine in albino and pigmented rats. *Toxicol Appl Pharmacol* 7:627-636.

McIntyre A, Hulikova A, Ledaki I, Snell C, Singleton D, Steers G, Seden P, Jones D, Bridges E, Wigfield S, Li JL, Russell A, Swietach P and Harris AL (2016) Disrupting Hypoxia-Induced Bicarbonate Transport Acidifies Tumor Cells and Suppresses Tumor Growth. *Cancer Res* 76:3744-3755.

Medina DL, Di Paola S, Peluso I, Armani A, De Stefani D, Venditti R, Montefusco S, Scotto-Rosato A, Prezioso C, Forrester A, Settembre C, Wang W, Gao Q, Xu H, Sandri M, Rizzuto R, De Matteis MA and Ballabio A (2015) Lysosomal calcium signalling regulates autophagy through calcineurin and TFEB. *Nat Cell Biol* 17:288-299.

Melles RB and Marmor MF (2014) The risk of toxic retinopathy in patients on long-term hydroxychloroquine therapy. *JAMA ophthalmology* 132:1453-1460.

Mellman I, Fuchs R and Helenius A (1986) Acidification of the endocytic and exocytic pathways. *Annual review of biochemistry* 55:663-700.

Mittler F, Obeid P, Rulina AV, Haguet V, Gidrol X and Balakirev MY (2017) High-Content Monitoring of Drug Effects in a 3D Spheroid Model. *Front Oncol* 7:293.

Mizushima N (2009) Methods for monitoring autophagy using GFP-LC3 transgenic mice. *Methods in enzymology* 452:13-23.

Mizushima N, Yamamoto A, Matsui M, Yoshimori T and Ohsumi Y (2004) In vivo analysis of autophagy in response to nutrient starvation using transgenic mice expressing a fluorescent autophagosome marker. *Molecular biology of the cell* 15:1101-1111.

Mohamed MM and Sloane BF (2006) Cysteine cathepsins: multifunctional enzymes in cancer. *Nature reviews Cancer* 6:764-775.

Morita S, Takahashi T, Yoshida Y and Yokota N (2016) Population Pharmacokinetics of Hydroxychloroquine in Japanese Patients With Cutaneous or Systemic Lupus Erythematosus. *Ther Drug Monit* 38:259-267.

Mueller-Klieser W (1984) Method for the determination of oxygen consumption rates and diffusion coefficients in multicellular spheroids. *Biophys J* 46:343-348.

Mueller-Klieser WF and Sutherland RM (1982) Oxygen tensions in multicell spheroids of two cell lines. *Br J Cancer* 45:256-264.

Napolitano G and Ballabio A (2016) TFEB at a glance. *J Cell Sci* 129:2475-2481.

Nath S and Devi GR (2016) Three-dimensional culture systems in cancer research: Focus on tumor spheroid model. *Pharmacol Ther* 163:94-108.

Neri D and Supuran CT (2011) Interfering with pH regulation in tumours as a therapeutic strategy. *Nature reviews Drug discovery* 10:767-777.

Nicastri MC, Rebecca VW, Amaravadi RK and Winkler JD (2018) Dimeric quinacrines as chemical tools to identify PPT1, a new regulator of autophagy in cancer cells. *Mol Cell Oncol* 5:e1395504.

Nunes AS, Barros AS, Costa EC, Moreira AF and Correia IJ (2019) 3D tumor spheroids as in vitro models to mimic in vivo human solid tumors resistance to therapeutic drugs. *Biotechnology and Bioengineering* 116:206-226.

Obach RS, Lombardo F and Waters NJ (2008) Trend Analysis of a Database of Intravenous Pharmacokinetic Parameters in Humans for 670 Drug Compounds. *Drug Metabolism and Disposition* 36:1385-1405.

Ohkuma S, Moriyama Y and Takano T (1983) Electrogenic nature of lysosomal proton pump as revealed with a cyanine dye. *Journal of biochemistry* 94:1935-1943.

Palermo C and Joyce JA (2008) Cysteine cathepsin proteases as pharmacological targets in cancer. *Trends in pharmacological sciences* 29:22-28.

Pan Y, Gao Y, Chen L, Gao G, Dong H, Yang Y, Dong B and Chen X (2011) Targeting autophagy augments in vitro and in vivo antimyeloma activity of DNA-damaging chemotherapy. *Clinical cancer research : an official journal of the American Association for Cancer Research* 17:3248-3258.

Pandya HK, Robinson M, Mandal N and Shah VA (2015) Hydroxychloroquine retinopathy: A review of imaging. *Indian J Ophthalmol* 63:570-574.

Paskeviciute M and Petrikaite V (2019) Proton Pump Inhibitors Modulate Transport Of Doxorubicin And Its Liposomal Form Into 2D And 3D Breast Cancer Cell Cultures. *Cancer Manag Res* 11:9761-9769.

Pasquier B (2015) SAR405, a PIK3C3/Vps34 inhibitor that prevents autophagy and synergizes with MTOR inhibition in tumor cells. *Autophagy* 11:725-726.

Pauli-Magnus C, Rekersbrink S, Klotz U and Fromm MF (2001) Interaction of omeprazole, lansoprazole and pantoprazole with P-glycoprotein. *Naunyn-Schmiedeberg's archives of pharmacology* 364:551-557.

Pellegrini P, Strambi A, Zipoli C, Hagg-Olofsson M, Buoncervello M, Linder S and De Milito A (2014) Acidic extracellular pH neutralizes the autophagy-inhibiting activity of chloroquine: implications for cancer therapies. *Autophagy* 10:562-571.

Perera RM, Stoykova S, Nicolay BN, Kenneth N, Fitamant J, Boukhali M, Lengrand J, Selig MK, Ferrone CR, Settleman J, Dyson NJ, Zoncu R and Ramaswamy S (2015) Transcriptional control of the autophagy-lysosome system in pancreatic cancer. *Nature* 524:361-365.

Peyret T, Poulin P and Krishnan K (2010) A unified algorithm for predicting partition coefficients for PBPK modeling of drugs and environmental chemicals. *Toxicol Appl Pharmacol* 249:197-207.

Piao S, Ojha R, Rebecca VW, Samanta A, Ma XH, McAfee Q, Nicastri MC, Buckley M, Brown E, Winkler JD, Gimotty PA and Amaravadi RK (2017) ALDH1A1 and HLTF modulate the activity of lysosomal autophagy inhibitors in cancer cells. *Autophagy* 13:2056-2071.

Qu X, Yu J, Bhagat G, Furuya N, Hibshoosh H, Troxel A, Rosen J, Eskelinen E-L, Mizushima N, Ohsumi Y, Cattoretti G and Levine B (2003) Promotion of tumorigenesis by heterozygous disruption of the beclin 1 autophagy gene. *The Journal of clinical investigation* 112:1809-1820.

Qu Y, Noe G, Breaud AR, Vidal M, Clarke WA, Zahr N, Dervieux T, Costedoat-Chalumeau N and Blanchet B (2015) Development and validation of a clinical HPLC method for the quantification of hydroxychloroquine and its metabolites in whole blood. *Future Sci OA* 1:FSO26.

Rangwala R, Chang YC, Hu J, Algazy KM, Evans TL, Fecher LA, Schuchter LM, Torigian DA, Panosian JT, Troxel AB, Tan KS, Heitjan DF, DeMichele AM, Vaughn DJ, Redlinger M, Alavi A, Kaiser J, Pontiggia L, Davis LE, O'Dwyer PJ and Amaravadi RK (2014a) Combined MTOR and autophagy inhibition: phase I trial of hydroxychloroquine and temsirolimus in patients with advanced solid tumors and melanoma. *Autophagy* 10:1391-1402.

Rangwala R, Leone R, Chang YC, Fecher LA, Schuchter LM, Kramer A, Tan KS, Heitjan DF, Rodgers G, Gallagher M, Piao S, Troxel AB, Evans TL, DeMichele AM, Nathanson KL, O'Dwyer PJ, Kaiser J, Pontiggia L, Davis LE and Amaravadi RK (2014b) Phase I trial of hydroxychloroquine with dose-intense temozolomide in patients with advanced solid tumors and melanoma. *Autophagy* 10:1369-1379.

Rebecca VW, Nicastri MC, Fennelly C, Chude CI, Barber-Rotenberg JS, Ronghe A, McAfee Q, McLaughlin NP, Zhang G, Goldman AR, Ojha R, Piao S, Noguera-Ortega E, Martorella A, Alicea GM, Lee JJ, Schuchter LM, Xu X, Herlyn M, Marmorstein R, Gimotty PA, Speicher DW, Winkler JD and Amaravadi RK (2019)

PPT1 Promotes Tumor Growth and Is the Molecular Target of Chloroquine Derivatives in Cancer. *Cancer Discov* 9:220-229.

Rebecca VW, Nicastri MC, McLaughlin N, Fennelly C, McAfee Q, Ronghe A, Nofal M, Lim CY, Witze E, Chude CI, Zhang G, Alicea GM, Piao S, Murugan S, Ojha R, Levi SM, Wei Z, Barber-Rotenberg JS, Murphy ME, Mills GB, Lu Y, Rabinowitz J, Marmorstein R, Liu Q, Liu S, Xu X, Herlyn M, Zoncu R, Brady DC, Speicher DW, Winkler JD and Amaravadi RK (2017) A unified approach to targeting the lysosome's degradative and growth signaling roles. *Cancer Discovery* 7:1266-1283.

Roczniak-Ferguson A, Petit CS, Froehlich F, Qian S, Ky J, Angarola B, Walther TC and Ferguson SM (2012) The transcription factor TFEB links mTORC1 signaling to transcriptional control of lysosome homeostasis. *Sci Signal* 5:ra42.

Rofstad EK, Mathiesen B, Kindem K and Galappathi K (2006) Acidic extracellular pH promotes experimental metastasis of human melanoma cells in athymic nude mice. *Cancer research* 66:6699-6707.

Rosenfeld MR, Ye X, Supko JG, Desideri S, Grossman SA, Brem S, Mikkelson T, Wang D, Chang YC, Hu J, McAfee Q, Fisher J, Troxel AB, Piao S, Heitjan DF, Tan KS, Pontiggia L, O'Dwyer PJ, Davis LE and Amaravadi RK (2014) A phase I/II trial of hydroxychloroquine in conjunction with radiation therapy and concurrent and adjuvant temozolomide in patients with newly diagnosed glioblastoma multiforme. *Autophagy* 10:1359-1368.

Rubinsztein DC, Codogno P and Levine B (2012) Autophagy modulation as a potential therapeutic target for diverse diseases. *Nature reviews Drug discovery* 11:709-730.

Schmitt MV, Lienau P, Fricker G and Reichel A (2019) Quantitation of lysosomal trapping of basic lipophilic compounds using in vitro assays and in silico predictions based on the determination of the full pH profile of the endo-/lysosomal system in rat hepatocytes. *Drug Metabolism and Disposition* 47:49-57.

Schmitt W (2008) General approach for the calculation of tissue to plasma partition coefficients. *Toxicol In Vitro* 22:457-467.

Schrezenmeier E and Dorner T (2020) Mechanisms of action of hydroxychloroquine and chloroquine: implications for rheumatology. *Nat Rev Rheumatol* 16:155-166.

Settembre C, Di Malta C, Polito VA, Garcia Arencibia M, Vetrini F, Erdin S, Erdin SU, Huynh T, Medina D, Colella P, Sardiello M, Rubinsztein DC and Ballabio A (2011) TFEB links autophagy to lysosomal biogenesis. *Science* 332:1429-1433.

Settembre C, Polito VA, Garcia M, Vetrini F, Erdin S, Erdin SU, Huynh T, Medina D, Colella P, Sardiello M and Rubinsztein DC (2013) TFEB Links Autophagy to Lysosomal Biogenesis. *Science* 332:1429-1433.

Settembre C, Zoncu R, Medina DL, Vetrini F, Erdin S, Erdin S, Huynh T, Ferron M, Karsenty G, Vellard MC, Facchinetti V, Sabatini DM and Ballabio A (2012) A lysosome-to-nucleus signalling mechanism senses and regulates the lysosome via mTOR and TFEB. *EMBO J* 31:1095-1108.

Shao S, Li S, Qin Y, Wang X, Yang Y, Bai H, Zhou L, Zhao C and Wang C (2014) Spautin-1, a novel autophagy inhibitor, enhances imatinib-induced apoptosis in chronic myeloid leukemia. *International journal of oncology* 44:1661-1668.

Sharma N, Thomas S, Golden EB, Hofman FM, Chen TC, Petasis NA, Schonthal AH and Louie SG (2012) Inhibition of autophagy and induction of breast cancer cell death by mefloquine, an antimalarial agent. *Cancer letters* 326:143-154.

Shi TT, Yu XX, Yan LJ and Xiao HT (2017) Research progress of hydroxychloroquine and autophagy inhibitors on cancer. *Cancer Chemother Pharmacol* 79:287-294.

Shin JM and Sachs G (2008) Pharmacology of proton pump inhibitors. *Current Gastroenterology Reports* 10:528-534.

Shree T, Olson OC, Elie BT, Kester JC, Garfall AL, Simpson K, Bell-McGuinn KM, Zabor EC, Brogi E and Joyce JA (2011) Macrophages and cathepsin proteases blunt chemotherapeutic response in breast cancer. *Genes & development* 25:2465-2479.

Spugnini EP, Baldi A, Buglioni S, Carocci F, de Bazzichini GM, Betti G, Pantaleo I, Menicagli F, Citro G and Fais S (2011) Lansoprazole as a rescue agent in chemoresistant tumors: a phase I/II study in companion animals with spontaneously occurring tumors. *J Transl Med* 9:221.

Stark M and Hayward N (2007) Genome-Wide Loss of Heterozygosity and Copy Number Analysis in Melanoma Using High-Density Single-Nucleotide Polymorphism Arrays. *Cancer Research* 67:2632 LP - 2642.

Steinberg BE, Huynh KK, Brodovitch A, Jabs S, Stauber T, Jentsch TJ and Grinstein S (2010) A cation counterflux supports lysosomal acidification. *J Cell Biol* 189:1171-1186.

Stoka V, Turk B, Schendel SL, Kim TH, Cirman T, Snipas SJ, Ellerby LM, Bredesen D, Freeze H, Abrahamson M, Bromme D, Krajewski S, Reed JC, Yin XM, Turk V and Salvesen GS (2001) Lysosomal protease pathways to apoptosis. Cleavage of bid, not pro-caspases, is the most likely route. *The Journal of biological chemistry* 276:3149-3157.

Swietach P, Hulikova A, Patiar S, Vaughan-Jones RD and Harris AL (2012) Importance of intracellular pH in determining the uptake and efficacy of the weakly basic chemotherapeutic drug, doxorubicin. *PLoS ONE* 7:1-9.

Tan Q, Wang M, Yu M, Zhang J, Bristow RG, Hill RP and Tannock IF (2016) Role of Autophagy as a Survival Mechanism for Hypoxic Cells in Tumors. *Neoplasia* 18:347-355.

Tang J, Di J, Cao H, Bai J and Zheng J (2015) p53-mediated autophagic regulation: A prospective strategy for cancer therapy. *Cancer letters* 363:101-107.

Tett S, Cutler D and Day R (1990) Antimalarials in rheumatic diseases. *Baillieres Clin Rheumatol* 4:467-489.

Tett SE, Cutler DJ, Day RO and Brown KF (1988) A dose-ranging study of the pharmacokinetics of hydroxy-chloroquine following intravenous administration to healthy volunteers. *Br J Clin Pharmacol* 26:303-313.

Tett SE, Cutler DJ, Day RO and Brown KF (1989) Bioavailability of hydroxychloroquine tablets in healthy volunteers. *Br J Clin Pharmacol* 27:771-779.

Thomson ABR, Sauve MD, Kassam N and Kamitakahara H (2010) Safety of the long-term use of proton pump inhibitors, in pp 2323-2330.

Tian X, Wang W, Zhang Q, Zhao L, Wei J, Xing H, Song Y, Wang S, Ma D, Meng L and Chen G (2010) Hypoxia-inducible factor-1alpha enhances the malignant phenotype of multicellular spheroid HeLa cells in vitro. *Oncol Lett* 1:893-897.

Trapp S and Horobin ÆRW (2005) A predictive model for the selective accumulation of chemicals in tumor cells. *European Biophysics Journal* 34:959-966.

Trapp S, Rosania G, Horobin R and Kornhuber J (2008) Quantitative Modeling of Selective Lysosome Targeting for Drug Design. *European Biophysics Journal* 18:1317-1328.

Udelnow A, Kreyes A, Ellinger S, Landfester K and Walther P (2011) Omeprazole Inhibits Proliferation and Modulates Autophagy in Pancreatic Cancer Cells. *PLoS ONE* 6.

Vogl DT, Stadtmauer EA, Tan KS, Heitjan DF, Davis LE, Pontiggia L, Rangwala R, Piao S, Chang YC, Scott EC, Paul TM, Nichols CW, Porter DL, Kaplan J, Mallon G, Bradner JE and Amaravadi RK (2014) Combined autophagy and proteasome inhibition: a phase 1 trial of hydroxychloroquine and bortezomib in patients with relapsed/refractory myeloma. *Autophagy* 10:1380-1390.

Walenta S, Salameh A, Lyng H, Evensen JF, Mitze M, Rofstad EK and Mueller-Klieser W (1997) Correlation of high lactate levels in head and neck tumors with incidence of metastasis. *The American journal of pathology* 150:409-415.

Wang Q, Xue L, Zhang X, Bu S, Zhu X and Lai D (2016) Autophagy protects ovarian cancer-associated fibroblasts against oxidative stress. *Cell Cycle* 15:1376-1385.

White E (2013) Deconvoluting the context-dependent role for autophagy in cancer. *Nature Reviews Cancer* 12:401-410.

Wolpin BM, Rubinson DA, Wang X, Chan JA, Cleary JM, Enzinger PC, Fuchs CS, McCleary NJ, Meyerhardt JA, Ng K, Schrag D, Sikora AL, Spicer BA, Killion L, Mamon H and Kimmelman AC (2014) Phase II and pharmacodynamic study of autophagy inhibition using hydroxychloroquine in patients with metastatic pancreatic adenocarcinoma. *The oncologist* 19:637-638.

Wu Y-T, Tan H-L, Shui G, Bauvy C, Huang Q, Wenk MR, Ong C-N, Codogno P and Shen H-M (2010) Dual role of 3-methyladenine in modulation of autophagy via different temporal patterns of inhibition on class I and III phosphoinositide 3-kinase. *The Journal of biological chemistry* 285:10850-10861.

Xie X, White EP and Mehnert JM (2013) Coordinate Autophagy and mTOR Pathway Inhibition Enhances Cell Death in Melanoma. *PLoS ONE* 8:1-11.

Xu H and Ren D (2015) Lysosomal Physiology. *Annual Review of Physiology* 77:57-80.

Yang S, Wang X, Contino G, Liesa M, Sahin E, Ying H, Bause A, Li Y, Stommel JM, Dell'antonio G, Mautner J, Tonon G, Haigis M, Shirihai OS, Doglioni C, Bardeesy N and Kimmelman AC (2011) Pancreatic cancers require autophagy for tumor growth. *Genes & development* 25:717-729.

Yao X, Ye F, Zhang M, Cui C, Huang B, Niu P, Liu X, Zhao L, Dong E, Song C, Zhan S, Lu R, Li H, Tan W and Liu D (2020) In Vitro Antiviral Activity and Projection of Optimized Dosing Design of Hydroxychloroquine for the Treatment of Severe Acute Respiratory Syndrome Coronavirus 2 (SARS-CoV-2). *Clin Infect Dis*.

Yin Z, Pascual C and Klionsky DJ (2016) Autophagy: machinery and regulation. *Microbial cell (Graz, Austria)* 3:588-596.

Yokogawa K, Ishizaki J, Ohkuma S and Miyamoto K (2002) Influence of lipophilicity and lysosomal accumulation on tissue distribution kinetics of basic drugs: a physiologically based pharmacokinetic model. *Methods Find Exp Clin Pharmacol* 24:81-93.

You H, Jin J, Shu H, Yu B, Milito AD, Lozupone F, Deng Y, Tang N, Yao G, Fais S, Gu J and Qin W (2009) Small interfering RNA targeting the subunit ATP6L of proton

pump V-ATPase overcomes chemoresistance of breast cancer cells. *Cancer Letters* 280:110-119.

Zhao B, Dierichs L, Gu JN, Trajkovic-Arsic M, Axel Hilger R, Savvatakis K, Vega-Rubin-de-Celis S, Liffers ST, Pena-Llopis S, Behrens D, Hahn S, Siveke JT and Lueong SS (2020) TFEB-mediated lysosomal biogenesis and lysosomal drug sequestration confer resistance to MEK inhibition in pancreatic cancer. *Cell Death Discov* 6:12.

Zhitomirsky B and Assaraf YG (2015) Lysosomal sequestration of hydrophobic weak base chemotherapeutics triggers lysosomal biogenesis and lysosome-dependent cancer multidrug resistance. *Oncotarget* 6:1143-1156.

Zhitomirsky B, Yunaev A, Kreiserman R, Kaplan A, Stark M and Assaraf YG (2018) Lysosomotropic drugs activate TFEB via lysosomal membrane fluidization and consequent inhibition of mTORC1 activity. *Cell Death and Disease* 9.

Chapter Two

Hydroxychloroquine: A Physiologically-Based Pharmacokinetic Model in the Context of Cancer-Related Autophagy Modulation

Summary

Hydroxychloroquine (HCQ) is a lysosomotropic autophagy inhibitor being used in over 50 clinical trials either alone or in combination with chemotherapy. Pharmacokinetic (PK) and pharmacodynamic (PD) studies with HCQ have shown that drug exposure in the blood does not correlate with autophagy inhibition in either peripheral blood mononuclear cells (PBMCs) or tumor tissue. To better explain this PK/PD disconnect a physiologically-based pharmacokinetic model (PBPK) was developed for HCQ describing the tissue-specific absorption, distribution, metabolism, and excretion as well as lysosome-specific sequestration. Using physiologic and biochemical parameters derived from literature or obtained experimentally the model was first developed and validated in mice, and then adapted to simulate human HCQ exposure in whole blood and urine through allometric scaling and species-specific parameter modification. The human model accurately simulated average steady-state concentrations (Css) of those observed in five different HCQ combination clinical trials across seven different doses, which was then expanded by comparison of the Css distribution in a virtual human population at this range of doses. Value of this model lies in its ability to simulate HCQ

PK in patients while accounting for PK modification by combination treatment modalities, drug concentrations at the active site in the lysosome under varying pH conditions, and exposure in tissues where toxicity is observed.

Introduction

Hydroxychloroquine (HCQ) is a 4-aminoquinoline class molecule traditionally used as an anti-malarial medication, but currently being investigated in over 50 cancer clinical trials either alone or in combination with chemotherapy (ClinicalTrials.gov). HCQ's putative mechanism of anticancer activity is through the inhibition of autophagy, a naturally occurring metabolic process that involves the digestion of a cell's own organelles, proteins, and other cellular debris in the lysosome. HCQ is the current "gold standard" for autophagy inhibition in a clinical setting as it exhibits similar potency yet less toxicity in long-term dosing compared to other clinically approved autophagy inhibitors, such as chloroquine (Shi et al., 2017). There is significant evidence that autophagy is heavily upregulated in certain tumor types, acting as a survival mechanism against both the harsh tumor environment and chemotherapy treatments (Levy et al., 2017, Yang et al., 2011). Inhibition of this process by augmenting the primary treatment method with HCQ has been shown to re-sensitize tumors to a resistant therapy regimen or enhance response to a current treatment regimen (Amaravadi et al., 2011, Barnard et al., 2014, Carew et al., 2012, Levy et al., 2014).

Mechanistically, HCQ is a weakly basic compound that alkalinizes the highly acidic lysosome, preventing the autophagosome-lysosome fusion step of autophagy (de

Duve, 1983, Lu et al., 2017). This mechanism drives its pharmacokinetics (PK), primarily through an ion-trap accumulation observed in lysosomes and other acidic compartments. Overall, HCQ PK has been well characterized in multiple species, and the PK profile appears to scale linearly with dose escalation, though exhibits a significant amount of intersubject variability (Fan et al., 2015, Furst, 1996, Lim et al., 2009, McChesney, 1983, Tett et al., 1988). Sources of variability are likely due to the fact that these studies have been done by different research groups over the course of decades as well as variance in absorption, distribution, metabolism and elimination (ADME) factors related to the physicochemical properties that drive its PK.

HCQ is typically administered as an oral tablet, in doses ranging from 100 mg to 1200 mg daily by which it is readily absorbed within 2-4 hours (Browning, 2014). The fraction absorbed is estimated to be 74 ± 13% (Browning, 2014, Tett et al., 1989). HCQ blood concentration peaks shortly after the absorption phase, and falls relatively quickly due to rapid partitioning into organs. Accumulation in lysosomes appears to drive the large volume of distribution in plasma, while binding to melanin contributes to the long terminal half-life (Tett et al., 1990). It is roughly 50% bound to plasma protein in the blood (Furst, 1996). Metabolism appears to be the primary driver of HCQ clearance. It occurs in the liver through CYP3A4 and CYP2C3 driven dealkylation to form desethylhydroxychloroquine, desethylchloroquine, and bisdesethylchloroquine, the former which exhibits therapeutic activity and PK thought to be comparable to HCQ (Browning, 2014, Kim et al., 2003, McChesney et al., 1965, Qu et al., 2015). Rate of metabolism varies tremendously across species, leading to significant cross-species differences in half-life that ranges from hours in mice to days in humans (Tett et al.,

1988). Excretion takes place primarily in the kidneys, accounting for roughly 22% of HCQ total blood clearance, with liver clearance assumed to account for the rest (Tett et al., 1988). Mean renal clearance from plasma is reported as 3 to 4 times greater than GFR corrected for protein binding, suggesting the drug is secreted in addition to filtration (Tett et al., 1988).

In the context of cancer treatment, HCQ blood exposure correlates with neither tumor exposure nor pharmacodynamic (PD) markers of autophagy inhibition in both peripheral blood mononuclear cells and tumor tissue (Barnard et al., 2014). To investigate the PK/PK and PK/PD disconnect observed in HCQ treatment, as well as the high inter-individual patient variability in PK studies, a physiologically-based pharmacokinetic model (PBPK) serves as a powerful investigative tool. This model allows for simulation of patient profiles and study of relationships between drivers. Developed around key tissues as well as physiologic and biochemical properties associated with the ADME profile, this PBPK model of HCQ can simulate exposure in tissues associated with toxicity as well as therapeutic effect. It can also investigate the variability in tumor pH that may contribute to the disconnect between exposure in the blood and autophagy inhibition in the tumor, specifically the inverse relationship between HCQ uptake and extracellular pH (Pellegrini et al., 2014).

The PBPK model described for HCQ was developed using biochemical and physiologic parameters adapted from literature or obtained experimentally, with significant focus on the pH-based aspect of PK. Tissues represented in the model are involved with absorption, metabolism, excretion, binding, or are subject to toxicity. Model output simulates single intraperitoneal dose tissue exposure in mice.

Biochemical and physiologic parameters were then adjusted accordingly to simulate whole blood exposure in humans. Simulation output across multiple dosing regimens and across different species matches well with experimental PK data, indicating that key drivers of HCQ PK are accounted for by the PBPK model.

Materials and Methods

PK Study in Mice

Protocols for the mouse studies were approved by the Institutional Animal Care and Use Committee at Colorado State University. Female BALB/c mice were treated with a single intraperitoneal dose (IP) of 20, 40, or 80 mg/kg HCQ (Sigma-Aldrich, H0915). Tissues and whole blood were collected from 3 mice for each dose at 3, 6, 12, 24, 48 and 72 hours (n = 54). Levels of HCQ and dHCQ in whole blood and tissues were determined via a previously validated liquid chromatography-tandem mass spectrometry (LC-MS/MS) assay (Barnard et al., 2014). Briefly, 100µL of tissue homogenate was added to a micro centrifuge tube along with 10µL of Milli-Q water, 10µL 50/50 acetonitrile/Milli-Q, 10µL of 2.5µg/mL CQ (internal standard), and 100µL of acetonitrile. Samples were vortexed for 5 minutes and centrifuged for 10 minutes at 13,300 RPM. 80µL of this mix was transferred to an autosampler vial and mixed with 120µL of Milli-Q water prior to mass spectrometer analysis. Standards and quality controls were prepared in an identical manner. Data points below the LLOQ of 1 ng/mL for HCQ and 10 ng/mL for dHCQ were excluded. Non-compartmental analysis (NCA)

measured exposure, as determined by area under the drug concentration versus time curve (AUC0-inf), to both HCQ and dHCQ.

HCQ Microsomal Metabolism Studies

Metabolism rate constants for the human PBPK model were obtained through microsomal incubation. Pooled mixed gender human liver microsomes at 20 mg/mL were obtained from XenoTech and were split into 100 µL aliquots prior to beginning microsomal incubations. Briefly, microsome stocks were diluted to 0.5 mg/mL in 100mM phosphate buffer and pre-incubated with an NADPH regenerating system for 5 minutes. 100x HCQ (Sigma-Aldrich H0915) was spiked in to the microsome mix and incubated for up to 3 hours. Reactions were terminated by addition of 100 µL of acetonitrile, vortexed for 5 minutes, and centrifuged at 14,000 rpm for 5 minutes to pellet the microsomal protein. Prior to analysis by HPLC the samples were mixed 50:50 with the internal standard of 500 ng/mL camptothecin dissolved in MilliQ water. Rate of metabolism was determined by rate of n-desethylhydroxychloroquine formation, the primary metabolite of HCQ (Browning, 2014). Analysis of samples was done using the liquid chromatography-tandem mass spectrometry (LC-MS/MS) assay mentioned in the previous section. Standards and quality control samples were prepared in an inactive microsomal homogenate matrix in the same way as samples and containing identical amounts of internal standard. Key structural and physicochemical properties of HCQ are outlined in Figure 2.1.

Hydroxychloroquine (HCQ)

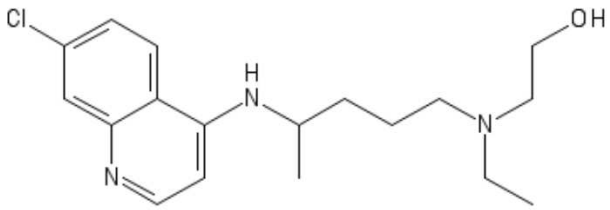

MW = 335.872 **pKa_1 = 9.67**
$Log(K_{ow})$ = 3.84 **pKa_2 = 8.27**

Figure 2.1. HCQ molecular structure with key physicochemical properties

Lysosomal Quantification in Mouse Tissue

Lysosome contents of the various tissues incorporated in the model were determined by analyzing acid phosphatase enzyme activity. It was assumed that lysosome volume fraction of the tissue was directly proportional to the acid phosphatase activity in that tissue. Tissues were extracted from BALB/c mice, diluted to 100 mg/mL in 0.2 M acetic acid buffer (pH = 5.0), and homogenized in a Bullet Blender Storm 2400 at max speed for 5 minutes. Samples were centrifuged at 5000 rpm for 10 minutes at 4°C and homogenate was collected and transferred to new tubes. Homogenate was vortexed, and 150 µL was transferred to a cuvette followed by 600 µL of acetic acid buffer to this same cuvette. The cuvette was then incubated at 37°C for 10 minutes to inactivate additional enzymes. After incubation, 250 µL of 32 mM p-nitrophenol dissolved in water was added to the cuvette. Cuvette was inverted and read immediately on a DU 800 Spectrophometer at 420 nm for 5 minutes to collect

absorbance data. Absorbance data at the 5 minute time point was normalized to the total protein content of the homogenate, as determined by comparison with a bovine serum albumin standard curve. Acid phosphatase enzyme activity was reported as moles/min/mg protein, and values for each organ were compared to a fixed fraction for kidney (Kawashima et al., 1998, Sewell et al., 1986).

PBPK Model Development

Base Model Development

The PBPK model for HCQ is represented by eight distinct, flow-limited tissue groupings that could describe HCQ PK based on physiologically-derived metabolism, renal elimination, absorption, macromolecule binding, and lysosomal sequestration. Key features that the model aimed to capture were melanin binding to investigate cases of retinal toxicity, and lysosomal uptake kinetics to model intracellular PK at the active site. Figure 2.2 depicts a schematic describing the system of these key tissues involved in HCQ PK.

Typically administered orally, HCQ absorption occurs rapidly in the gut lumen, followed by transport to the liver where it undergoes first pass metabolism. From there it is distributed to the rest of the body. Key tissues include the kidney, the site of renal excretion, as well as eyes and skin, major sites of melanin binding, and the heart, due to observed instances of cardiomyopathy. The rest of the body is lumped into the slowly perfused compartment, consisting of bone, fat, and muscle, as well as the rapidly perfused compartment which is composed of the remaining viscera. Additionally, a tumor compartment can be incorporated depending on the location of the primary

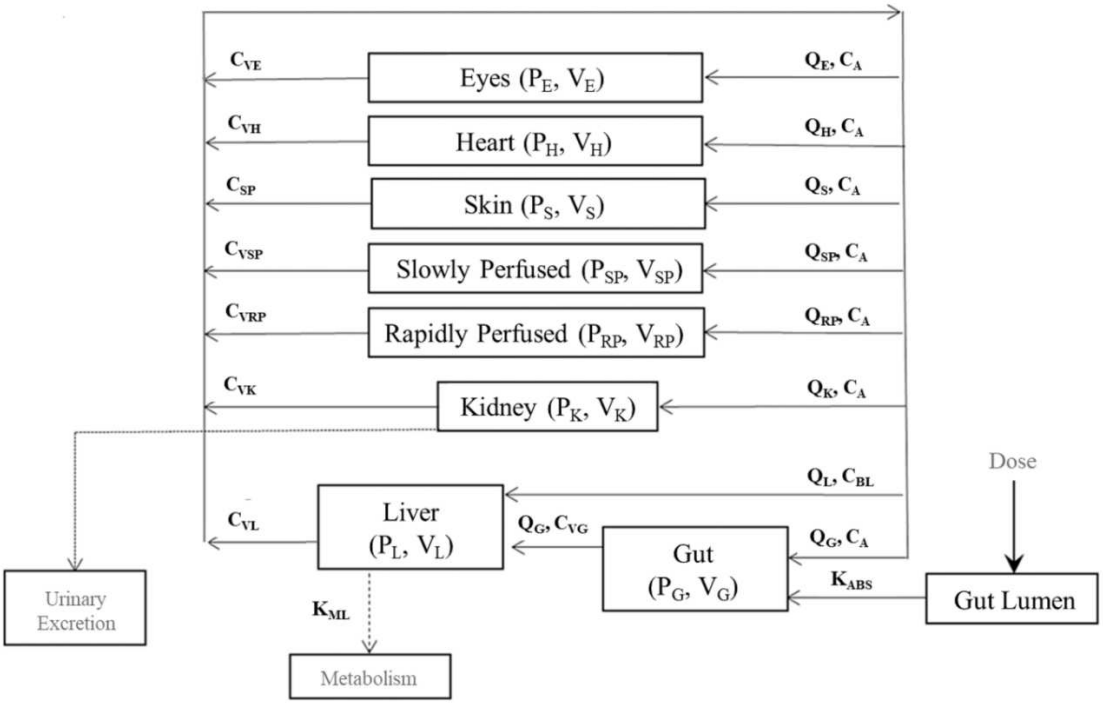

Figure 2.2. Schematic of model describing key organs involved in HCQ ADME after oral dosing. Absorption occurs in the gut, metabolism in the liver, and excretion in the kidneys. Skin and eyes exhibit unusual PK properties due to extensive binding to melanin. Heart is included due to cardiomyopathy as an observed side-effect in some cases. The rest of the organs are split into slowly perfused (muscle, fat, bone) and rapidly perfused (internal viscera).

tumor. Each compartment of the model is further described by a lysosomal sub-compartment discussed in the next sub-section .

Mass balance of a typical tissue observed in the bulk portion of the model is described by equation (1)

$$\frac{dm_t}{dt} = Q_t \cdot (C_a - \frac{C_t}{P_t}) + A_t \cdot \Delta J_{lys} \quad (1)$$

where m_t is the amount of HCQ within the tissue, Q_t is the blood flow rate to that tissue, C_a is the unbound arterial plasma concentration carried to the tissue, C_t is the free concentration within the compartment, P_t is the partition coefficient of that tissue, A_t is the lysosomal surface area, and ΔJ_{lys} is the net flux between the cytosol and lysosome. The only tissue with an exception to equation (1) is the liver, wherein arterial concentration is set to include free drug as well as bound drug due to dissociation of HCQ and protein occurring in the hepatic space (Meijer and van der Sluijs, 1989).

For tissues involved in clearance of HCQ an additional term is added to equation (1). For kidney, a renal clearance term is added and is represented by equation (2). In the case of liver, a metabolism term is added and is represented by equation (3) for mouse and equation (4) for human.

$$\frac{dm_{renal}}{dt} = GFR \cdot Q_K \cdot C_A + V_K \cdot \frac{V_{max_{sec}} \cdot C_A}{K_{m_{sec}} + C_A} \tag{2}$$

$$\frac{dm_{met}}{dt} = V_L \cdot (\frac{C_L \cdot V_{max_L}}{K_{m_L} + C_L}) \tag{3}$$

$$\frac{dm_{met}}{dt} = V_L \cdot Met \cdot C_L \tag{4}$$

The first term of equation (2) accounts for renal filtration where GFR represents glomerular filtration rate, QK¬ represents blood flow to the kidney, and CA represents arterial blood concentration. The second term represents active secretion where VK represents kidney volume, and Vmax and Km represent Michaelis-Menten constants for secretion. Equation (3) describes the amount of HCQ metabolized in mouse and is represented by VL and CL, the volume and concentration of liver, respectively. It is also

represented by Vmax and Km, Michaelis-Menten rate constants for metabolism. Equation (4) describes the amount of HCQ metabolized in human and is represented by the linear rate constant Met. Melanin binding is the other driving factor of distribution in the model, and so the amount of free HCQ unbound to melanin, applying to skin and eyes, is represented by equation (5).

$$m_{free} = \frac{m_{cyt}}{\frac{T_{mel}}{K_{mel}+C_t}} \tag{5}$$

where mfree is the amount of unbound drug in the cytosol, mcyt is the total amount in the cytoplasm, Tmel – a function of melanin/HCQ binding ratio (MelBR) and melanin concentration in the tissue (Ctmel), is the binding capacity of melanin for HCQ, Kmel is the binding affinity of HCQ to melanin, and Ct is the free concentration in the cytosol. Values for Tmel and Kmel were estimated from a previous study on HCQ binding (Schroeder and Gerber, 2014) and melanin concentrations for skin and eye have been reported (Browning, 2014, Durairaj et al., 2012). The parameters for the PBPK model can be found in Table 2.1 along with the source of each variable.

ADME Parameters

Tissue volumes and blood flows were standard, fixed values as previously described (Brown et al., 1997). The only exception was eye, which came from multiple sources (Choi et al., 2012, Zhi et al., 2012).

Absorption parameters were obtained from a prior study (Tett et al., 1989). Specifically, the absorption rate constant (KA) was modeled as linear uptake that achieved near full absorption within an average of 3 hours. Fraction absorbed was set

Table 2.1. PBPK Model Variables

Tissue Volume	**Symbol**	**Mouse**	**Human**	**Reference**
Kidney	% body weight	1.7	0.4	Brown et al., 1997
Heart		0.5	0.5	Brown et al., 1997
Eye		0.034 (g)	15 (g)	Mou – Experimental; Hum - Brittanica
Skin		16.5	3.7	Brown et al., 1997
Gut		4.2	1.4	Brown et al., 1997
Liver		5.5	2.57	Brown et al., 1997
Blood		4.9	7.9	Brown et al., 1997
Slowly Perfused		56.1	75.7	Brown et al., 1997
Rapidly Perfused		10.4	7.5	Brown et al., 1997
Tissue Blood Flow				
Kidney	% cardiac output	9.1	17.5	Brown et al., 1997
Heart		6.6	4.0	Brown et al., 1997
Eye		0.0566	0.0016	Mou – Zhi et al., 2012; Hum – Choi et al., 2012
Skin		5.8	5.8	Brown et al., 1997
Gut		14.1	18.1	Brown et al., 1997
Liver		2.0	4.6	Brown et al., 1997
Slowly Perfused		34.2	28.5	Brown et al., 1997
Rapidly Perfused		28.1	21.5	Brown et al., 1997
Tissue Partioning[a]				
Kidney	PK	50	50	Wei et al., 1995
Heart	PH	44	44	Wei et al., 1995
Eye	PE	33	33	Wei et al., 1995
Skin	PS	26	26	Wei et al., 1995
Gut	PG	35	35	McChesney et al., 1967
Liver	PL	193	193	Wei et al., 1995
Blood	PB	7.2	7.2	Tett et al., 1988
Slowly Perfused	PSP	10	10	Wei et al., 1995; McChesney et al., 1967
Rapidly Perfused	PRP	150	150	Wei et al., 1995
Metabolism[b]				
Metabolism Affinity	Km_L (μM)	357		Optimized from mouse PK
Metabolism Max Rate	$Vmax_L$ (μM/hr)	1171		Optimized from mouse PK

Metabolism Rate Constant	Met (hr^{-1})		0.154	Optimized from human liver microsomes
Clearance[c]				
Plasma Protein Binding	% bound	0.45	0.45	Browning, 2014
Glomerular Filtration Rate	GFR	0.125	0.11	Mou – Qi and Breyer, 2009
Secretion Affinity	Km_{sec} (μM)	1000	1000	optimization
Secretion Max Rate	$Vmax_{sec}$ (μM/hr)	32500	32500	optimization
Intestinal Absorption				
Absorption Rate	KA (hr^{-1})		0.5	Tett et al., 1989
Absorption Fraction	FA		0.75	Tett et al., 1989
Melanin Binding[d]				
Melanin Affinity	Km_{mel} (μM)		217	Schroeder and Gerber, 2014
Binding Ratio	HCQ_{mel}		0.178	Schroeder and Gerber, 2014
Eye Melanin Concentration	CE_{ME} (μM)		2.4E04	Durairaj et al., 2012
Skin Melanin Concentration	CS_{ME} (μM)		300	Browning, 2014

[a.] Most partition coefficients were optimized from Wei et al., 1995, McChesney et al., 1967, and Tett et al., 1998. Slowly perfused was an average value of adipose from Wei et al., 1995 and McChesney et al., 1967

[b.] Values for mouse were calculated from liver PK data; Human rate constant was calculated from human liver microsomes and optimized to meet the ratio of metabolism vs. clearance reported by Tett et al., 1988 and 1989

[c.] Total renal clearance was a function of plasma protein binding and GFR, with secretion coefficients optimized to meet total renal clearance values in tandem with metabolism reported by Tett et al., 1988 and 1989

[d.] Melanin binding parameters were taken from a bunch of sources and optimized for human. Skin melanin is for an average person of light colored skin. The value increases up to 4x based on skin color

to an average of 0.75 ± 0.13 of the dose, as described by human urine and blood data. First pass hepatic effect was deemed insignificant in this study as well, and was calculated at only 6% of the total dose. Biliary secretion was initially considered, as fecal excretion of HCQ in rat was cited as 25% of total dose (McChesney, 1983); however, ratio of metabolite vs. parent were not observed. Biliary secretion was tested in the model, assuming complete absorption, and was representative of a model lacking biliary clearance with 0.85-0.9 fraction absorbed. As this fell within the range of absorption fraction observed in humans, biliary secretion was not considered a major driving factor of HCQ PK and was omitted from the model.

Distribution of the bulk model was primarily described by partition coefficients, the concentration ratio between plasma and tissue at steady state. The partition coefficient values were derived and optimized using previously published data (McChesney et al., 1967, Tett et al., 1989, Wei et al., 1995).

Metabolism values for mouse were obtained and optimized from liver PK data by determining the Michaelis-Menten relationship that represented the compartmental clearance of this region. The human metabolism rate constant was obtained by incubating HCQ with activated human liver microsomes, as described in the microsome section of materials and methods, and optimized to best fit human PK data. Intrinsic scaling of in vitro to in vivo metabolism for CYP450 enzymes as previously described (Chiba et al., 2009) was not considered since moderate optimization of the microsome-derived metabolism rate yielded clearance that fit the clinical data well, and satisfied the hepatic clearance portion observed in human patients (Tett et al., 1988). Intestinal metabolism was considered negligible due to the significantly lower CYP3A and 2C

levels observed in intestine compared to liver as well as low first pass metabolism (Thelen and Dressman, 2009).

Excretion was modeled as filtration and secretion, since mean renal clearance was found to be 3-4x greater than GFR (Tett et al., 1990, Tett et al., 1988, Tett et al., 1989). GFR was set to 0.125 for mouse (Qi and Breyer, 2009) and 0.11 for human of the unbound plasma flow to the renal tubules. The Km and Vmax for renal secretion were optimized using the Nelder-Mead method to best fit the data, accounting for 3-4x GFR as secretion as well as the ~3:1 ratio of non-renal clearance (assumed to be liver clearance) to total renal clearance upon scaling from mouse to human (Furst, 1996, Tett et al., 1990).

Lysosomal Compartment Development

Within each tissue compartment was a lysosomal sub-compartment that was mathematically described as separate from its parent compartment. The sub-compartment was modeled to represent the ion trap effect that causes HCQ accumulation to millimolar concentrations in acidic regions, primarily the lysosome. A schematic of lysosomal sequestration is represented in Figure 2.3, which depicts HCQ and HCQ+ moving freely across membranes at physiologic pH, but upon entering the acidic lysosome a majority of HCQ is in the 2+ state where it can no longer permeate the membrane and becomes trapped.

The mass balance of the lysosomal sub-compartment for each tissue is represented by the second term in equation (1) and is described by equation (6)

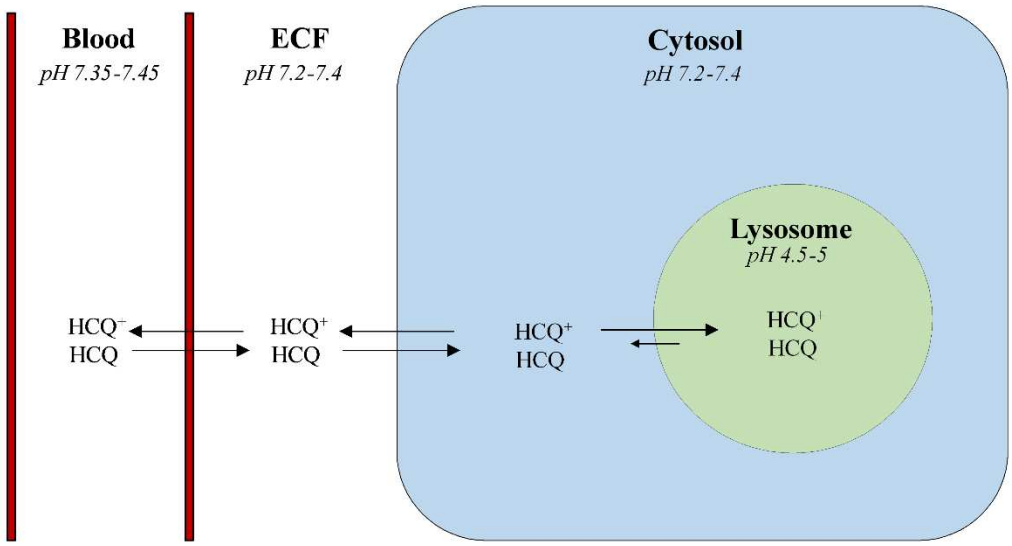

Figure 2.3. Intracellular mechanism of HCQ PK with pH dependence. HCQ crosses membranes readily, but accumulates in acidic compartments due to being non-permeable in the +2 state.

$$\frac{dm_{lys}}{dt} = A_t \cdot \Delta J_{lys} \tag{6}$$

where A_t represents the lysosomal surface area and ΔJ_{lys} represents the net flux between the cytosol and lysosome compartments. The flux portion was adapted from the cell model proposed by Trapp et al. that describes lysosomal drug uptake on a cellular pharmacokinetic level. It was validated using a select handful of drugs with a variety of pKa and lipophilicity (Kow) values, one of which was chloroquine (Trapp and Horobin, 2005, Trapp et al., 2008). The overarching principle in their cell model was application of Fick's 1st law of diffusion with the Nernst-Planck equation, which incorporates electric charge into the movement of molecules through a biological environment. Fick's 1st Law of Diffusion, which only applies to the neutral form of HCQ

(J_n), is depicted by equation (7), and the combined Fick's-Nernst-Planck version of diffusion (J_d) is equation (8). These equations are combined to yield equation (9)

$$J_n = f_n P_n C \tag{7}$$

$$J_d = f_d D_z P_d C \frac{N}{e^N - 1} \tag{8}$$

$$\Delta J_{lys} = (J_n + J_d)_{lys} - (J_n + J_d)_{cyt} \tag{9}$$

where f_n represents the fraction of freely dissolved neutral HCQ, described by equation (10) (or reference equation 6 from (Trapp et al., 2008) for a more derived description). P_n and P_d represent the permeabilities of neutral and ionic HCQ states, D_z is the Henderson-Hasselbach activity ratio, C is the total HCQ concentration in the compartment (applying to either cytosol or lysosome), and N is the Nernst equation. Equation (7) and (8) represent HCQ flux in the neutral and ionic states, and are combined to give the net flux between both compartments in equation (9). The fraction of freely dissolved HCQ in this equation is represented by f_n, and is described by equation (10):

$$f_n = \left(\frac{W + K_n}{\gamma_n} + \frac{D_1 W + D_1 K_1}{\gamma_1} + \frac{D_2 W + D_2 K_2}{\gamma_2}\right)^{-1} \tag{10}$$

which represents the fraction of HCQ in the system that is available to move. This description has been well described previously (Trapp et al., 2008), but briefly it represents the fraction available to move by taking into account lipid binding, sorption, and ionic activity. W represents water fraction in the compartment, L represents lipid

fraction in the compartment, K_n and K_z are sorption coefficients of neutral and ionic HCQ, and gammas represent the ionic activity coefficients for the compartment.

The effect of charge on lipophilicity (Kow) of a molecule, which sets the framework for the ionic sorption coefficents (K_z) and ionic permeability has been previously described (Trapp et al., 2008). The equation for charged lipophilicity is shown in equation (11)

$$Kow_z = 10^{log_{10}(Kow)-3.5z} \tag{11}$$

where z is the charge HCQ. Equation (11) is applied to the permeability equation (12) and sorption equation (13) to represent these properties of charged HCQ

$$P_z = 10^{log_{10}(Kow_z)-1.1427} \tag{12}$$

$$K_z = 1.22 \cdot L \cdot Kow_z \tag{13}$$

Additionally, equation (8) incorporates the Henderson-Hasselbach activity ratio, D_z, which represents the ratio between neutral and ionic fractions of the molecule. D_z is represented by equations (14) for the 1^+ state and equation (15) for the 2^+ state.

$$D_1 = 10^{(pKa_1-pH)} \tag{14}$$

$$D_2 = 10^{(pKa_1+pKa_2-2pH)} \tag{15}$$

All values of physicochemical properties of HCQ and lysosomal properties used in equations related to this section of the model can be found in Table 2.2 along with the source of these values (Ishizaki et al., 2000, Kawashima et al., 1998, Trapp et al., 2008, Warhurst et al., 2003).

Table 2.2. Physicochemical properties of HCQ and lysosomal properties

Drug Constants	**Symbol**	**Value**	**Reference**
Molecular Weight	MW	335.872	
Lipophilicity	$Log_{10}(Kow)$	3.84	Warhurst et al., 2003
1st Dissociation Constant	pKa_1	9.67	
2nd Dissociation Constant	pKa_2	8.27	
Lysosomal Parameters			
Lysosomal Lipid Fraction	L	0.05	Trapp et al., 2008
Lysosomal Water Fraction	W	0.95	Trapp et al., 2008
Neutral Activity Coefficient	γ_N	1.23	Trapp et al., 2008
1st Activity Coefficient	γ_1	0.74	Trapp et al., 2008
2nd Activity Coefficient	γ_2	0.3	Trapp et al., 2008
Lysosomal Radius	r_{lys} (µm)	0.275	Kawashima et al., 1998
Lysosomal Buffering Capacity	β (mM)	46	Ishizaki et al., 2000
Lysosomal pH	pH_{lys}	5.0	Trapp et al., 2008
Cytosolic pH	pH_{cyt}	7.2	Trapp et al., 2008
Lysosome Content[a]			
Kidney	%tissue volume	0.05	
Heart		0.1	
Eye		0.015	
Skin		0.1	
Gut		0.1	
Liver		0.05	
Slowly Perfused		0.1	
Rapidly Perfused		0.2	

[a.] Starting values from Kawashima et al., 1998; Sewell et al., 1986. Final values determined from acid phosphatase and optimization

An additional component to consider at the cellular scale is the effect of lysosomal HCQ accumulation on pH. Previous studies have demonstrated the pH neutralization effect of weak base accumulation in lysosomes (Ohkuma and Poole, 1978), and this has been taken into account in more recently developed cellular models

(Ishizaki et al., 2000, Kornhuber et al., 2010). Equation (16) was used to describe the dynamic pH of the lysosome compartment

$$\Delta pH = \frac{C_{lys}}{\beta} \tag{16}$$

where C_{lys} is the free lysosomal concentration and β is the buffering capacity as previously described (Ishizaki et al., 2000). Dynamic pH affects the free fraction of HCQ in each ionic state, which causes net flux to approach an equilibrium as lysosome pH becomes more neutral. Dynamic pH based on buffering capacity was not considered for the cytosolic compartment. Initial pH values for lysosome and cytosol compartments were the same for all tissues and were set to 5.0 and 7.2, respectively.

Volume of the lysosome compartment for each tissue was determined by total acid phosphatase activity in the tissue. Acid phosphatase activity was assumed to correlate directly with total lysosomal volume fraction of the tissue. Acid phosphatase activity / lysosome volume fraction was compared between tissues on a ratio basis using a set value for kidney lysosome volume fraction, and optimized to fit the mouse model (Kawashima et al., 1998, Sewell et al., 1986). Lysosome size was set to a constant spherical volume using a radius of 275nm.

Data Analysis

The ability of the model to accurately predict concentration-time profiles was analyzed by comparing PBPK simulation pharmacokinetic variables to those of actual data, as well as through calculation of the median absolute performance error (MAPE%) and the median performance error (MPE%). The performance error (PE) of the model

was calculated as the difference between the measured and simulated concentrations normalized to the simulated concentration as shown in equation (17):

$$PE = \frac{C_{measured} - C_{simulated}}{C_{simulated}} \cdot 100 \quad (17)$$

The MAPE%, which measures prediction accuracy, was calculated by equation (18):

$$MAPE\% = (|PE_1|, |PE_2|, ...|PE_N|) \quad (18)$$

where *N* represents the total number of samples for the given tissue. The MPE%, which is a measure of positive or negative prediction bias, was calculated by equation (19):

$$MPE\% = median(PE_1, PE_2, ...PE_N) \quad (19)$$

Computer Simulation and Software

PBPK model development and simulation was done in Advanced Continuous Simulation Language Xtreme (acslX) version 3.1.4.2. from Aegis Technologies Group, Inc. Pharmacokinetic evaluation of simulated and clinical data was done on Phoenix 64 build 7.0.0.2535.

Results

HCQ Model Simulations in Mice

PK data from mice was generated following a single intraperitoneal (IP) dose of 20, 40, or 80 mg/kg HCQ. Tissues and whole blood were collected from mice at 3, 6, 12, 24, 48, and 72 hours after dosing. The PBPK model was developed from the

following tissues in this study: whole blood, liver, kidney, and gut. Figure 2.4 shows the HCQ PK profile from these mice compared to PBPK generated simulation data.

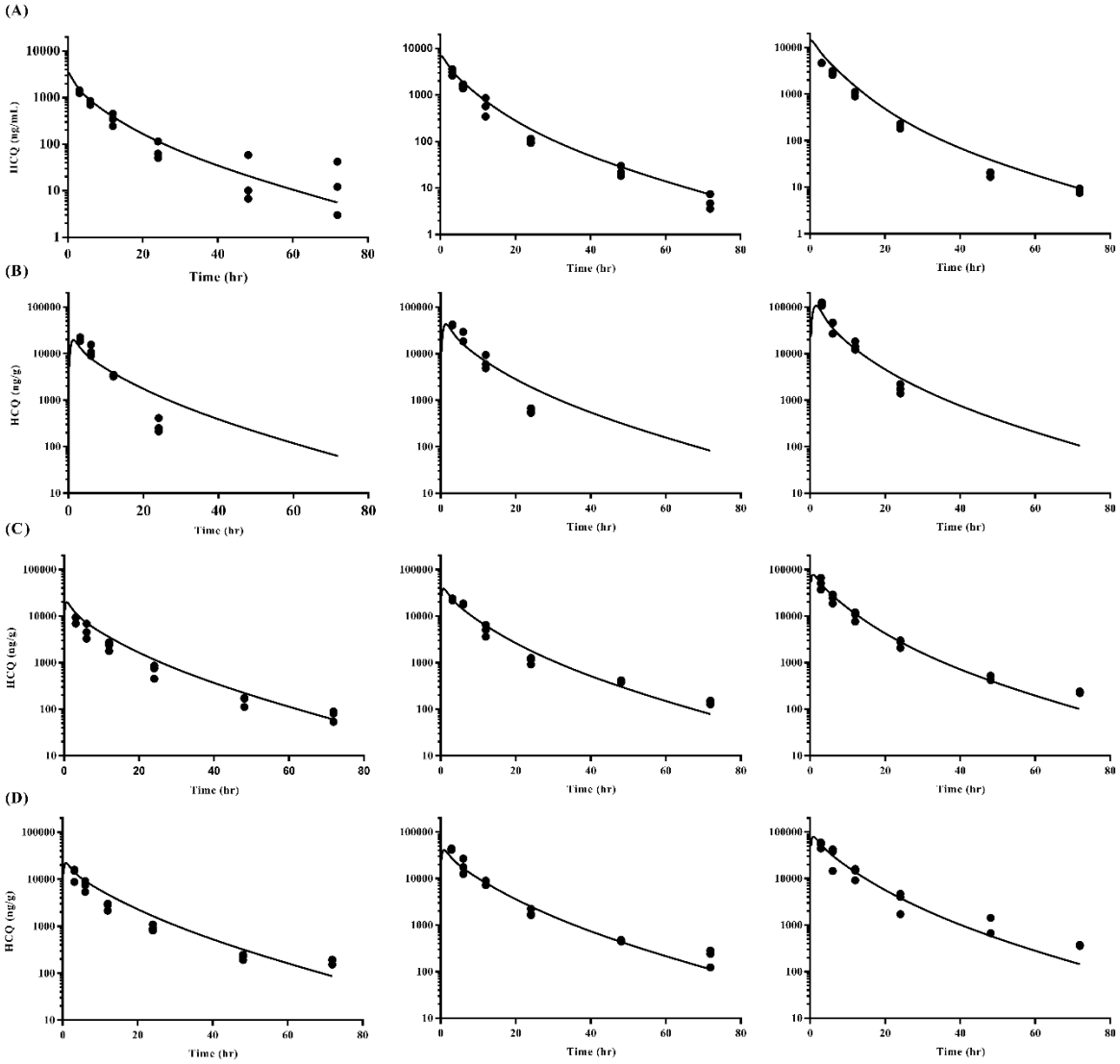

Figure 2.4. Mouse PK data compared to PBPK simulation. Mice were treated with a single IP dose of HCQ at 20, 40, and 80 mg/kg (left, middle, and right columns) and data was collected at 3, 6, 12, 24, 48, and 72 hours from whole blood (A), liver (B), kidney (C), and gut (D). Circles represent tissues from treated mice (three replicates per time point, n = 54) and lines represent simulation output.

In addition to whole tissue PK, the contributions of lysosomal sub-components were examined and are found in Supplementary Figure 2.1. Lysosomal HCQ PK profiles were similar between tissues and simulated concentrations peaked between 20-40 mM, which are consistent with lysosomal concentrations of lysosomotropic agents reported in previous studies (Browning, 2014).

The ability of the model to accurately predict the concentration-time profile of HCQ was determined through calculation of median absolute prediction error (MAPE%) and median prediction error (MPE%) presented as a percentage for tissues and whole blood, shown in Table 2.3.

Table 2.3. Measure of Predictive performance of the PBPK model

Dose	Tissue/Patient	MAPE%	MPE%
20 mg/kg	Blood	27.25	-11.06
	Liver	73.25	-41.16
	Kidney	33.89	-25.28
	Gut	39.35	-31.87
40 mg/kg	Blood	23.93	-23.93
	Liver	71.31	-46.90
	Kidney	27.48	8.17
	Gut	18.52	8.08
80 mg/kg	Blood	37.01	-37.01
	Liver	43.80	-24.80
	Kidney	24.19	5.90
	Gut	23.52	9.90
200 mg (oral)	4 (blood)	18.64	14.79
	5 (urine)	15.53	-3.34
200 mg (IV)	4 (blood)	33.51	-11.58
	5 (urine)	20.99	9.55
	1 (blood)	42.13	17.36
400 mg (IV)	1 (blood)	39.32	20.82

MAPE% is a method of determining model accuracy, while MPE% indicates under or over prediction bias (Sheiner and Beal, 1981). Overall, MAPE% for each dosing cohort were within similar ranges. The ranges were 27-73%, 19-71%, and 24-44% for 20, 40, and 80 mg/kg respectively. Upper bounds of this range were skewed by the deviation of model simulation from actual PK data for liver after 24 hours due to the concentration-time profile for HCQ PK dropping to zero after 24 hours. The model prediction follows the actual data well for the first 24 hours, after which it predicts a slower decline at these later time points. Removing the liver MAPE% drops the ranges to 27-39%, 19-27%, and 24-37%. Comparing this range of MAPE% to the variation in actual PK data, determined by the range of average coefficient of variation (CV) for each dosing cohort, is a strong indicator of whether or not model prediction is within the dispersion of the actual data. CV values for the PK cohorts are 16-43%, 9-20%, and 8-28% for 20, 40, and 80 mg/kg, respectively, which are quite similar to the MAPE% for the respective cohorts. This suggests that the model accounts for a majority of natural variation within the clinical data. Taking into account MPE%, the model tends to slightly over-predict blood and liver concentrations in each dose cohort. Kidney and gut are over-predicted in the 20 mg/kg cohort, but slightly under-predicted in the 40 and 80 mg/kg mice indicating no significant bias in over- or under-prediction of the model. An additional method of determining the model's predictive capability was through comparison of simulation vs. actual pharmacokinetic variables generated through noncompartmental analysis (NCA), which are presented in Table 2.4.

Table 2.4. NCA parameter comparison between PK and PBPK data

Mouse	**Tissue**		**$t_{1/2}$ (hr)**	**AUC (hr·µg/mL)**	**$t_{1/2}$ (ratio)**	**AUC (ratio)**
20 mg/kg	Blood	Actual	24.09 ± 8.84	10.84 ± 0.63	1.87	0.97
		Simulated	12.91	11.22		
	Liver	Actual	3.38 ± 0.37	116.93 ± 11.16	0.49	1.08
		Simulated	6.84	107.9		
	Kidney	Actual	15.12 ± 0.72	72.25 ± 2.69	1.17	0.73
		Simulated	12.96	99.01		
	Gut	Actual	20.45 ± 2.00	100.55 ± 15.03	1.58	0.76
		Simulated	12.97	131.80		
40 mg/kg	Blood	Actual	11.2 ± 1.49	19.50 ± 0.66	0.88	0.89
		Simulated	12.67	21.89		
	Liver	Actual	3.31 ± 0.17	244.87 ± 33.98	0.55	1.24
		Simulated	6.00	198.19		
	Kidney	Actual	16.24 ± 1.24	191.54 ± 12.56	1.27	1.09
		Simulated	12.74	175.82		
	Gut	Actual	15.82 ± 3.20	272.23 ± 18.75	1.24	1.22
		Simulated	12.76	222.82		
80 mg/kg	Blood	Actual	10.51 ± 0.52	33.27 ± 2.25	0.84	0.75
		Simulated	12.45	44.17		
	Liver	Actual	4.03 ± 0.88	512.92 ± 44.22	0.79	1.28
		Simulated	5.07	400.70		
	Kidney	Actual	13.77 ± 0.76	339.17 ± 4.11	1.10	1.05
		Simulated	12.53	322.20		
	Gut	Actual	16.04 ± 3.65	432.80 ± 97.44	1.29	1.12
		Simulated	12.43	385.13		
Human						
200 mg – Patient 4 (oral)	Blood	Actual	77.47	5.57	1.00	1.01
		Simulated	77.24	5.54		

200 mg – Patient 4 (IV)	Blood	Actual	84.90	5.85	1.16	0.78
		Simulated	73.45	7.51		
200 mg – Patient 1 (IV)	Blood	Actual	54.58	5.23	0.70	0.89
		Simulated	77.76	5.86		
400 mg – Patient 1 (IV)	Blood	Actual	117.50	10.01	1.72	0.80
		Simulated	68.25	12.55		

The NCA variables compared for blood and each tissue were terminal half-life (t½) and area under the curve (AUC). Values of each were determined over the 72 hour interval and compared ratiometrically (actual/simulated). Overall, the AUC ratios were very close to one, indicating a high degree of accuracy within the model. Half-lives were also relatively close except for liver 20 and 40mg/kg cohorts, which, as noted with MAPE%, is due to the lack of a terminal phase in the actual liver data. While half-life ratios were low for each dosing cohort, the ratios near one for AUC indicate that the model predicts overall liver exposure with a high degree of accuracy.

HCQ Model Simulations in Human

After validating the simulation in mice, the model was scaled to human patients by adjusting appropriate physiologic parameters, which are compared in Table 2.1. Concentration-time data for individual humans were used (Tett et al., 1988, Tett et al., 1989) and included both oral and IV infusion doses of 200mg and 400mg HCQ sulfate. Whole blood data was available for two patients (patient 1 and 4) from this study, and cumulative urinary excretion of HCQ was available for another (patient 5). The concentration-time profile between simulation and actual data were compared over a 72 hour time period, and are presented in Figure 2.5. In addition to whole blood PK, tissue

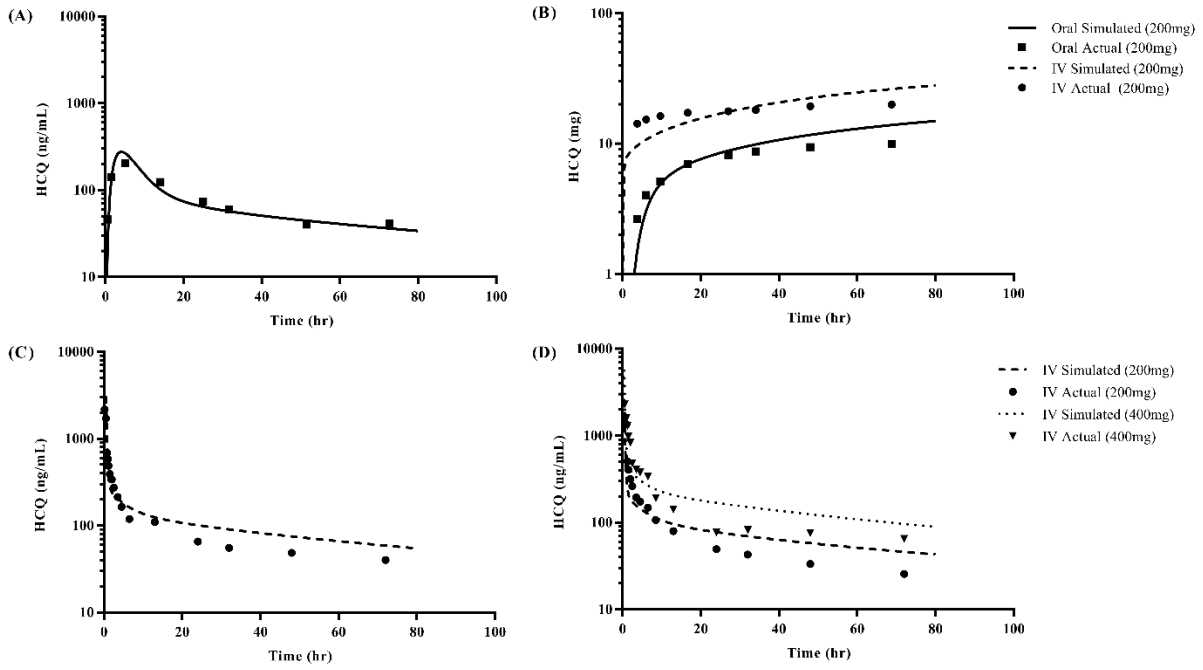

Figure 2.5. Human whole blood and urine concentrations of HCQ. Whole blood concentrations of patient 4 from the studies, was simulated after a single 200mg oral dose (A). Urinary excretion of HCQ was simulated in patient 5 from the studies following 200mg oral and IV doses (B). Whole blood concentrations of patient 4 from the studies were simulated after a single 200mg IV infusion (C) and of patient 1 after 200mg and 400mg IV infusions (D). HCQ (points) were compared to PBPK simulation (lines) (Tett et al., 1988 and 1989).

concentrations were simulated following these dosing schemes as well and can be found in Supplementary Figure 2.2. Simulated PK profiles for each of the dosing routes were notably different from each other, specifically in that liver and gut peak concentrations were roughly 2-3x higher, and kidney much lower, in patients receiving oral vs. IV infusion dosing due to the absorption phase. Lysosomal PK for these human tissues were also simulated following these dosing schemes and can be found in Supplementary Figure 2.3. Peak concentrations are similar to those in mice, at 20-30 mM in liver and gut, and as low as 6 mM in kidney following 200 mg oral dosing.

As individual physiologic data was not available for the human patients, generic human physiologic parameters were assumed (see Table 2.1) for patient 4 and patient 5 (Brown et al., 1997). After fitting the model to these patients through optimization of absorption, metabolism, and renal clearance parameters, the model was fit to patient 1 by simply increasing body weight from 70 to 85kg. For the human model the MAPE% range, presented in Table 2.3, for whole blood was between 19-42% and for urine was between 16-21%, indicating strong predictive power of the model. As this was individual patient data, the coefficient of variation was not reported for comparison with these patients. MPE% indicated a slight under prediction of the actual PK profile for all those compared except patient 4 IV infusion, which was a slight over prediction.

NCA parameters were also compared for human whole blood data, and can be found in Table 2.4. Overall the actual/simulation ratios of t½ and AUC indicated strong predictive power of the model.

To investigate the toxicity-related aspect of HCQ regarding retinopathy, HCQ exposure was simulated in human eyes at 200, 600, and 1200 mg/day of oral dosing and can be found in Supplementary Figure 2.4. Single dose HCQ at these levels generate relatively low concentrations in the eye relative to the other tissues shown in Supplementary Figure 2.2, although eyes continue to retain HCQ as blood levels decline. After 30 days of once daily dosing, it is clear that 1200 mg/day causes significantly higher accumulation of HCQ within the eyes, roughly 10-fold more than 200 mg/day. It is of note that even two months after dosing is discontinued the concentration of HCQ in the eyes decreases only slightly, indicating an extremely long half-life. 60 days of once daily dosing show a similar trend as 30 days, although

concentration buildup begins to taper off. Concentrations in the human eyes at 1200 mg/day are close to those observed in the eyes of hooded rats dosed at 40 mg/kg for 6 days/week over the same timeframe (McChesney, 1983).

Simulated Steady State Concentration and Clinical Trial Comparison

After the model was validated for single dose HCQ in human patients, the dosing interval was extended out to investigate predictive capability over a much longer period of time. Using generic human PBPK parameters as listed in Table 2.1, the model was used to simulate once-daily oral dosing of 100, 200, 400, 600, 800, 1000, and 1200mg HCQ for a 30 day period. The steady state concentration (Css) was taken as the average whole blood concentration occurring after 20 days. Simulated Css for each dosing regimen was compared to the patient Css distribution of the corresponding dosing regimen in five different cancer clinical trials using HCQ in combination with another treatment in Figure 2.6 (Mahalingam et al., 2014, Rangwala et al., 2014$_a$, Rangwala et al., 2014$_b$, Rosenfeld et al., 2014, Vogl et al., 2014).

The trials reported reaching the concentration distribution depicted by the following days: Temsirolimus at 15 days, Vorinostat at 20 days, Bortezomib at 21 days, Temozolomide Glioblastoma did “not distinctly represent steady state” and the time was not reported, and Temozolomide Solid Tumor/Melanoma was at 16 days. The depicted range in all trials represents concentrations falling within the second and third quartile of patient data, except for Vorinostat which represents the mean ± standard deviation. Of all trials examined, only the Temozolomide Glioblastoma patient population had a regression line statistically significant from the PBPK simulation. The regression line for this trial had a mean slope of 3.3 with 95% confidence interval bounds of 2.3 to 4.3,

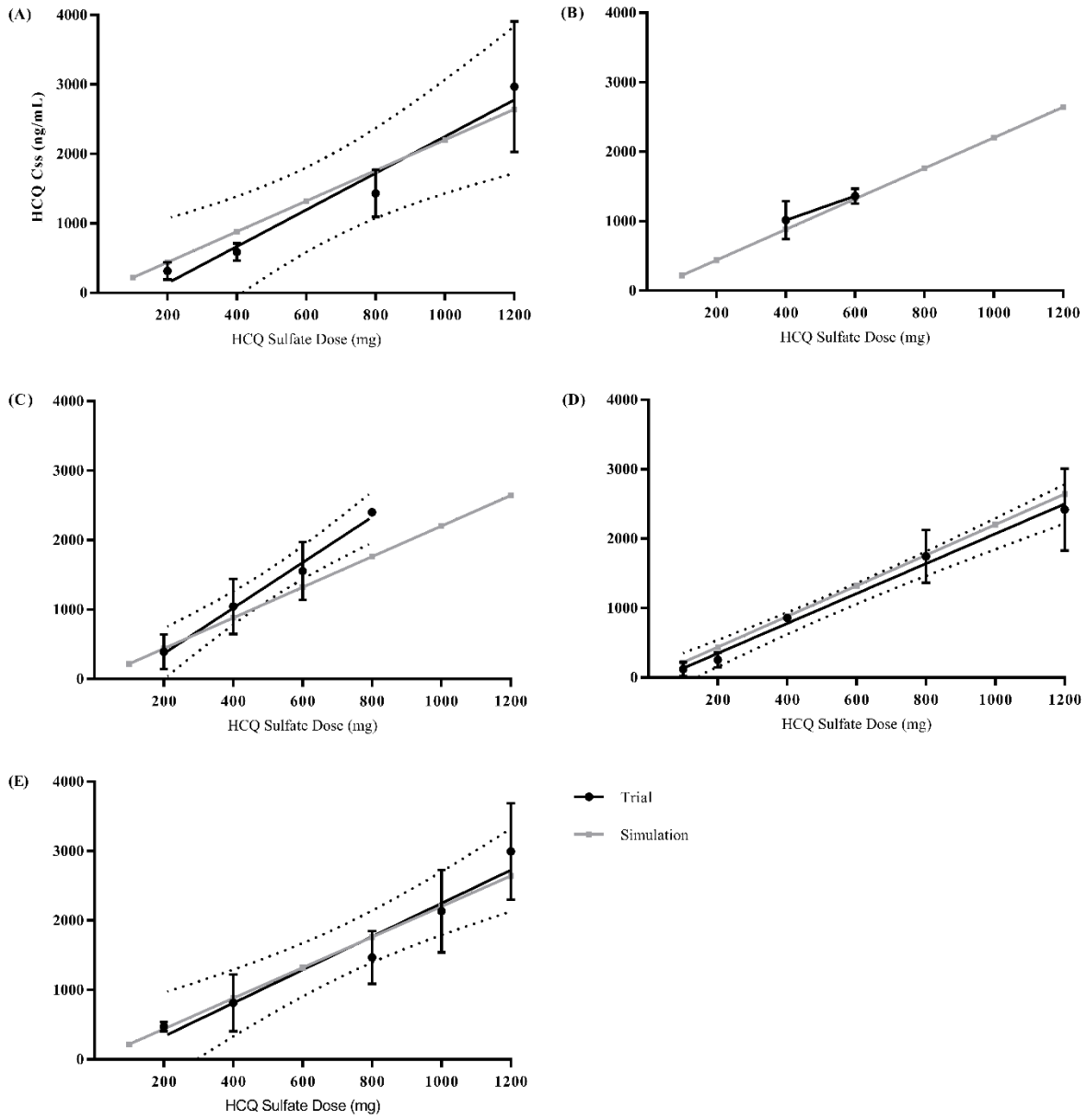

Figure 2.6. Whole blood concentrations of HCQ at steady state. Data comparison between five different human cancer clinical trials and PBPK model output at varying doses. The combination trials represented include (A) Temsirolimus (Rangwala et al., 2014$_a$), (B) Vorinostat (Mahalingam et al., 2014), (C) Temozolomide in glioblastoma patients (Rosenfeld et al., 2014), (D) Bortezomib (Vogl et al., 2014), and (E) Temozolomide in advanced solid tumor and melanoma patients (Rangwala et al., 2014$_b$). Clinical trial data represents steady state concentrations between the second and third quartile of patients, except for the Vorinostat trial (B) which represents the mean ± standard deviation. Steady state concentrations from the PBPK model were taken as the average concentration occurring at 20 days of once daily oral dosing. Black lines represent the regression lines for clinical trial data, dotted black lines

represent the 95% confidence interval, and grey lines represent the regression line for PBPK simulated data. The only trial that had a regression slope statistically different from the PBPK simulation was the Temozolomide glioblastoma trial (C).

compared to the regression line of the PBPK simulation which had a mean slope of 2.2. The Vorinostat patient population did not undergo regression analysis due to only two daily doses of HCQ (400 and 600mg) used in the trial, but the slope of this line was 1.7 compared to the PBPK simulation of 2.2. Of all trials tested against the PBPK simulation average Css from the model human fell within the bounds of the 2nd and 3rd quartile for all dosing regimens except for the Temozolomide Glioblastoma 800mg and Temsirolimus 400mg.

Simulation of HCQ in a Virtual Population

Once model simulated Css was found to be in good agreement with clinical trial Css distributions, the model was tested in a virtual population of humans. 250 males and 250 females were generated from the physiological parameters for PBPK modeling (P3M) database using PopGen (McNally et al., 2015). Briefly, P3M is a massive database of U.S. patient records containing their associated physiologic data, and was developed by The Lifeline Group. Using PopGen to extract from this database, a virtual population of individuals was generated using available demographic data from the Bortezomib/HCQ combination phase I clinical trial (Vogl et al., 2014). This was assumed to generate a population representative of a general cancer clinical trial. Css was then simulated for this population at each dosing regimen, and the simulated distribution was compared to the actual distribution observed in the clinical trials referenced. Each dose from 100-1200mg dosed once-daily was simulated in each of

the 500 total patients to generate a realistic range of steady state concentrations. The results of this simulated patients compared to the actual distribution from each trial are shown in Figure 2.7.

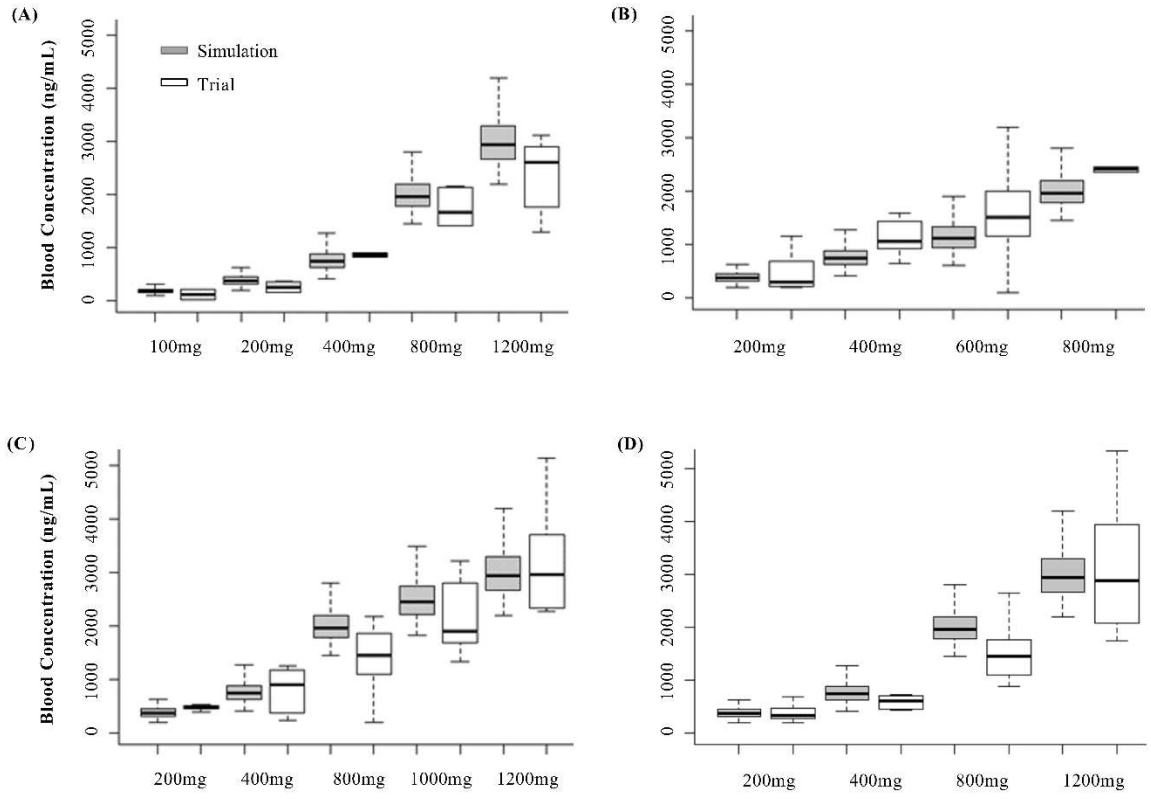

Figure 2.7. Distribution of steady state whole blood concentrations of HCQ. Css (at 20 days) for patients in different dosing cohorts was compared as simulated data vs. actual patient data from four clinical trials. Plots in grey represent the PBPK model simulation of HCQ in a virtual population of 500 patients (half male and half female) randomly generated using demographic data from the Bortezomib Trial. Plots in white represent the whole blood HCQ concentration distribution for patients in one of the four clinical trials, including (A) Bortezomib (Vogl et al., 2014), (B) Temozolomide in glioblastoma patients (Rosenfeld et al., 2014), (C) Temozolomide in patients with solid tumors or melanoma (Rangwala et al., 2014_b), and (D) Temsirolimus (Rangwala et al., 2014_a). Virtual Population was generated for 250 males and 250 females using the PopGen web software and pulling patient data from the P3M patient database.

The model captured the distribution of steady state whole blood concentrations in the simulated patient population extremely well at low doses. The higher doses in the clinical trial population exhibited much more distributional variability between trials. This was expected due to the more prominent effect that variability in physiologic parameters will have at higher doses. Additionally, the clinical trial patient populations were relatively small, especially in comparison to the 500 virtual patients simulated by the model, which is another likely contributor to the distributional variability between trials.

Discussion

PBPK modeling is a relatively well-established concept, dating back to the first modern model of methotrexate in 1971 (Bischoff et al., 1971). Cancer therapy is a major field for development of these models due to the ability to simulate multiple dosing regimens in a relatively short period of time with the purpose of maintaining therapeutic efficacy while minimizing toxicity. This includes PBPK models for some drugs that have been used in clinical trials in combination with HCQ, including three of those discussed in this paper (Ballesta et al., 2014, Gustafson et al., 2002, Zhang and Mager, 2015). Although the utility of PBPK models appears increasingly clear, their use in a clinical setting is not well established. With treatment including, but not limited to malaria, lupus, rheumatoid arthritis, and now cancer, HCQ is a prime candidate for use of PBPK models in a personalized-medicine setting. Due to the widespread use of this drug, accounting for sources of PK variability from easily monitored driving parameters, such as GI absorption, CYP3A4 and CYP2C3 metabolism, and renal clearance could be a quick method of accounting for the broad range of patient PK profiles observed in a

clinical setting. This would concurrently improve prediction of exposure in areas that are more difficult to monitor, such as melanin binding in the eye or variation in lysosomal content of a target site.

The described PBPK model for HCQ successfully predicts blood and tissue disposition in both mice and humans in single dose oral, IP, and IV scenarios. More so, it is capable of establishing a population distribution at doses ranging from 100-1200mg for long-term daily oral dosing in a human population representative of a general cancer clinical trial. This model was developed based on flow-limited uptake for the bulk compartments with perfusion-based uptake for the lysosomal compartment, and accounts for specific binding to melanin and non-specific binding to plasma protein. It is built based off of physiological and biochemically relevant parameters for eight compartments, three of which are validated by clinical PK data. These validated compartments consist of gut, liver, and kidney, along with whole blood. Gut and liver were included due to absorption and metabolism, respectively. Kidney is involved in renal clearance through filtration and secretion. There is evidence of reabsorption, but that mechanism was not considered in this model due to the lack of clinical data available relating urine pH to renal clearance of HCQ. Melanin binding was the primary reason for including eyes, specifically with regards to retinopathy observed in higher doses of HCQ used in cancer clinical trials. Accumulation of HCQ in the eyes was simulated to investigate the difference dosing levels may have on retinal exposure to this drug. While actual concentrations associated with retinopathy are unknown, patients classified as high risk are categorized as those receiving >6.5 mg/kg/day for >5 years (Pandya et al., 2015). The model can be used to simulate and avoid HCQ retinal

accumulation thresholds observed within these high risk dosing levels. Heart was included due to rare incidence of irreversible cardiomyopathy that could possibly be exacerbated during long term dosing of combination therapies that also exhibit some level of cardiovascular toxicity (Al-Bari, 2015). Treatments associated with cardiomyopathy are extremely rare, with only 42 known cases as of 2014 and reported mean cumulative doses of 1843 g (Yogasundaram et al., 2014). Remaining tissues were grouped into the rapidly perfused compartment, consisting of remaining viscera, and the slowly perfused compartment which consists of bone, muscle, and adipose.

The model was initially developed in mice and began with gathering of relevant biochemical and physiological parameters. After this step, parameter effect on model fit to actual data was assessed. This was followed by optimization to maximize model accuracy across dosing regimens. Scaling to humans involved modifying relevant physiological parameters and biochemical parameters as seen in Table 2.1, and optimizing the model to fit human data. Validating against multiple types of human PK data offers the predictive power to simulate HCQ PK in patients while accounting for PK modification by combination treatment modalities, drug concentrations at the active site in the lysosome under varying pH conditions, and exposure in tissues where toxicity is observed. Interindividual variability in response is one of the primary concerns in treatments with HCQ. From a PK perspective, of all parameters the ones that the blood portion of the model are most dependent on are body weight, rate of metabolism, and blood partitioning and protein binding. Contribution of these factors to model performance are not dose dependent, i.e. linear with dose escalation. Patients with

impaired liver or kidney function would likely be exposed to higher concentrations of HCQ, which would need to be accounted for in application of this model.

Primary value of this model is found through accurate simulation of HCQ PK in mice and humans while taking into account exposure in tissues, especially those where toxicity or clinical efficacy may be observed. Mice were the species chosen to begin model development due to the option of PK/PD investigation in whole organs. Between the mouse PK data, PD data (not yet published), and the likelihood that mice will be used in future preclinical studies with HCQ or next generation analogues, this model will prove a valuable tool to make connections between exposure and response in a preclinical setting. This is especially relevant in the context of lysosomal uptake and the effect of these various factors on the PK/PD of HCQ and next generation lysosomotropic autophagy inhibitors. Being a major driver of HCQ PK, it is important to note that lysosomes are a dynamic system undergoing effects such as swelling, biogenesis, pH modulation, and turnover that is not well characterized from a quantitative perspective in the presence of HCQ (Lu et al., 2017, Zhitomirsky and Assaraf, 2015). As pH is the driver for lysosomal accumulation it plays an important role, especially in a tumor context where acidic conditions can dramatically affect HCQ uptake (Pellegrini et al., 2014, Zhitomirsky and Assaraf, 2015). The cellular model of lysosomal uptake applied in our PBPK model (Kornhuber et al., 2010, Trapp and Horobin, 2005, Trapp et al., 2008) serves as a strong base of modification to begin describing whole tissue PK based on the pH-lysosome relationship. Further advancement of this PBPK model will require stronger prediction power in a tumor setting. Achieving this involves further characterization of these natural and HCQ-

influenced lysosomal dynamics, and how they are related to intra and extracellular pH in a tumor setting.

In addition to its use as a tool for further characterization of autophagy-dependence and preclinical study, this model has proven its utility in predicting exposure in human patients as well. The model was validated in humans by accurately simulating blood exposure and urinary clearance of HCQ over a 72 hour period following oral and IV administration of two different doses. Additionally, it captured the distribution of steady state concentrations at seven different dosing levels in a larger population of patients. Overall, it is able to simulate both early time points and steady state values of patients at all concentrations used in a cancer clinical trial setting. This validation, in conjunction with the physiologic nature of the model, makes it a powerful tool in predicting patient exposure in the 50+ clinical trials currently administering HCQ.

References

Al-Bari MA (2015) Chloroquine analogues in drug discovery: New directions of uses, mechanisms of actions and toxic manifestations from malaria to multifarious diseases. *J Antimcrob Chemother* 70:1608-1621.

Amaravadi RK, Lippincott-Schwartz J, Yin XM, Weiss WA, Takebe N, Timmer W, DiPaola RS, Lotze MT, and White E (2011) Principles and current strategies for targeting autophagy for cancer treatment. *Clin Cancer Res* 17:654-666.

Ballesta A, Zhou Q, Zhang X, Lv H, and Gallo JM (2014) Multiscale design of cell-type–specific pharmacokinetic/pharmacodynamic models for personalized medicine: Application to temozolomide in brain tumors. *CPT Pharmacometrics Syst Pharmacol* 3:e112.

Barnard RA, Wittenburg LA, Amaravadi RK, Gustafson DL, Thorburn A, and Thamm DH (2014) Phase I clinical trial and pharmacodynamic evaluation of combination hydroxychloroquine and doxorubicin treatment in pet dogs treated for spontaneously occurring lymphoma *Autophagy* 10:1415-1425.

Bischoff KB, Dedrick RL, Zaharko DS, and Longstreth JA (1971) Methotrexate pharmacokinetics. *J Pharm Sci* 60:1128-1133.

Brown RP, Delp MD, Lindstedt SL, Rhomberg LR, and Beliles RP (1997) Physiological parameter values for physiologically based pharmacokinetic models. *Toxicol Ind Health* 13:407-484.

Browning DJ (2014) Pharmacology of chloroquine and hydroxychloroquine, in *Hydroxychloroquine and Chloroquine Retinopathy* (Browning DJ ed) pp 35-63, Springer-Verlag, New York.

Carew JS, Kelly KR, and Nawrocki ST (2012) Autophagy as a target for cancer therapy: New developments. *Cancer Manag Res* 4:357-365.

Chiba M, Ishii Y, and Sugiyama Y (2009) Prediction of hepatic clearance in human from *in vitro* data for successful drug development. *AAPS J* 11:262-276.

Choi W, Baumann B, Liu JJ, Clermont AC, Feener EP, Duker JS, and Fujimoto JG (2012) Measurement of pulsatile total blood flow in the human and rat retina with ultrahigh speed spectral/Fourier domain OCT. *Biomed Opt Express* 3:1047-1061.

de Duve C (1983) Lysosomes revisited. *Eur J Biochem* 137:391-397.

Durairaj C, Chastain JE, and Kompella UB (2012) Intraocular distribution of melanin in human, monkey, rabbit, minipig, and dog eyes. *Exp Eye Res* 98:23-27.

Fan HW, Ma ZX, Chen J, Xang XY, Cheng JL, and Li YB (2015) Pharmacokinetics and bioequivalence study of hydroxychloroquine sulfate tablets in Chinese healthy volunteers by LC–MS/MS. *Rheumatol Ther* 2:183-195.

Furst DE (1996) Pharmacokinetics of hydroxychloroquine and chloroquine during treatment of rheumatic diseases. *Lupus* 5 Suppl 1:S11-S15.

Gustafson DL, Rastatter JC, Colombo T, and Long ME (2002) Doxorubicin pharmacokinetics: Macromolecule binding, metabolism, and excretion in the context of a physiologic model. *J Pharm Sci* 91:1488-1501.

Ishizaki J, Yokogawa K, Ichimura F, and Ohkuma S (2000) Uptake of imipramine in rat liver lysosomes *in vitro* and its inhibition by basic drugs. *J Pharmacol Exp Ther* 294:1088-1098.

Kawashima A, Sato A, Kawashima M, Nitta K, Yumura W, Sugino N, Nihei H, and Natori Y (1998) A simple procedure for the isolation of rat kidney lysosomes. *Kidney Int* 54:275-278.

Kim KA, Park JY, Lee JS, and Lim S (2003) Cytochrome P450 2C8 and CYP3A4/5 are involved in chloroquine metabolism in human liver microsomes. *Arch Pharm Res* 26:631-637.

Kornhuber J, Henkel AW, Groemer TW, Stadtler S, Welzel O, Tripal P, Rotter A, Bleich S, and Trapp S (2010) Lipophilic cationic drugs increase the permeability of lysosomal membranes in a cell culture system. *J Cell Physiol* 224:152-164.

Levy JM, Thompson JC, Griesinger AM, Amani V, Donson AM, Birks DK, Morgan MJ, Mirsky DM, Handler MH, Foreman NK, and Thorburn A (2014) Autophagy inhibition improves chemosensitivity in BRAF(V600E) brain tumors. *Cancer Discov* 4:773-780.

Levy JMM, Towers CG, and Thorburn A (2017) Targeting autophagy in cancer. *Nat Rev Cancer* 17:528-542.

Lim HS, Im JS, Cho JY, Bae KS, Klein TA, Yeom JS, Kim TS, Choi JS, Jang IJ, and Park JW (2009) Pharmacokinetics of hydroxychloroquine and its clinical implications in chemoprophylaxis against malaria caused by *Plasmodium vivax*. *Antimicrob Agents Chemother* 53:1468-1475.

Lu S, Sung T, Lin N, Abraham RT, and Jessen BA (2017) Lysosomal adaptation: How cells respond to lysosomotropic compounds. *PLoS ONE* 12:e0173771.

Lu ZN, Tian B, and Guo XL (2017) Repositioning of proton pump inhibitors in cancer therapy. *Cancer Chemother Pharmacol* 80:925-937.

Mahalingam D, Mita M, Sarantopoulos J, Wood L, Amaravadi RK, Davis LE, Mita AC, Curiel TJ, Espitia CM, Nawrocki ST, Giles FJ, and Carew JS (2014) A Phase I safety , tolerability , pharmacokinetic , and pharmacodynamic analysis of hydroxychloroquine in combination with the HDAC inhibitor vorinostat in patients with advanced solid tumors. *Autophagy* 10:1403-1414.

McChesney EW (1983) Animal toxicity and pharmacokinetics of hydroxychloroquine sulfate. *Am J Med* 75:11-18.

McChesney EW, Banks WF, and Fabian RJ (1967) Tissue distribution of chloroquine, hydroxychloroquine, and desethylchloroquine in the rat. *Toxicol Appl Pharmacol* 10:501-513.

McChesney EW, Conway WD, Banks WF, Rogers JE, and Shekosky JM (1965) Studies of the metabolism of some compounds of the 4-amino-7-chloroquinoline series. *J Pharmacol Exp Ther* 151:482-493.

McNally K, Cotton R, Hogg A, and Loizou G (2015) Reprint of PopGen: A virtual human population generator. *Toxicology* 332:77-93.

Meijer DK, and van der Sluijs P (1989) Covalent and noncovalent protein binding of drugs: Implications for hepatic clearance, storage, and cell-specific drug delivery. *Pharm Res* 6:105-118.

Ohkuma S, and Poole B (1978) Fluorescence probe measurement of the intralysosomal pH in living cells and the perturbation of pH by various agents. *Proc Natl Acad Sci U S A* 75:3327-3331.

Pandya HK, Robinson M, Mandal N, and Shah VA (2015) Hydroxychloroquine retinopathy: A review of imaging. *Indian J Opthalmol* 63:570-574.

Pellegrini P, Strambi A, Zipoli C, Hagg-Olofsson M, Buoncervello M, Linder S, and De Milito A (2014) Acidic extracellular pH neutralizes the autophagy-inhibiting activity of chloroquine: Implications for cancer therapies. *Autophagy* 10:562-571.

Qi Z, and Breyer MD (2009) Measurement of glomerular filtration rate in conscious mice. *Methods Mol Biol* 466:61-72.

Qu Y, Noe G, Breaud AR, Vidal M, Clarke WA, Zahr N, Dervieux T, Costedoat-Chalumeau N, and Blanchet B (2015) Development and validation of a clinical HPLC method for the quantification of hydroxychloroquine and its metabolites in whole blood. *Future Sci OA* 1:FSO26.

Rangwala R, Chang YC, Hu J, Algazy KM, Evans TL, Fecher LA, Schuchter LM, Torigian DA, Panosian JT, Troxel AB, Tan KS, Heitjan DF, DeMichele A, M., Vaughn DJ, Redlinger M, Alavi A, Kaiser J, Pontiggia L, Davis LE, O'Dwyer PJ,

and Amaravadi RK (2014$_a$) Combined mtor and autophagy inhibition Phase I trial of hydroxychloroquine and temsirolimus in patients with advanced solid tumors and melanoma. *Autopahgy* 10:1391-1402.

Rangwala R, Leone R, Chang YC, Fecher LA, Schuchter LM, Kramer A, Tan KS, Heitjan DF, Rodgers G, Gallagher M, Piao S, Troxel AB, Evans TL, DeMichele AM, Nathanson KL, O'Dwyer PJ, Kaiser J, Pontiggia L, Davis LE, and Amaravadi RK (2014$_b$) Phase I trial of hydroxychloroquine with dose-intense temozolomide in patients with advanced solid tumors and melanoma. *Autophagy* 10:1369-1379.

Rosenfeld MR, Ye X, Supko JG, Desideri S, Grossman SA, Brem S, Mikkelson T, Wang D, Chang YC, Hu J, McAfee Q, Fisher J, Troxel AB, Piao S, Heitjan DF, Tan KS, Pontiggia L, O'Dwyer PJ, Davis LE, and Amaravadi RK (2014) A Phase I/II trial of hydroxychloroquine in conjunction with radiation therapy and concurrent and adjuvant temozolomide in patients with newly diagnosed glioblastoma multiforme. *Autophagy* 10:1359-1368.

Schroeder RL, and Gerber JP (2014) Chloroquine and hydroxychloroquine binding to melanin: Some possible consequences for pathologies. *Toxicol Rep* 1:963-968.

Sewell RB, Dillon C, Grinpukel S, Yeomans ND, and Smallwood RA (1986) Pericanalicular location of hepatocyte lysosomes and effects of fasting: A morphometric analysis. *Hepatology* 6:305-311.

Sheiner LB, and Beal SL (1981) Some suggestions for measuring predictive performance. *J Pharmacokinet Biopharm* 9:503-512.

Shi TT, Yu XX, Yan LJ, and Xiao HT (2017) Research progress of hydroxychloroquine and autophagy inhibitors on cancer. *Cancer Chemother Pharmacol* 79:287-294.

Tett S, Cutler D, and Day R (1990) Antimalarials in rheumatic diseases. *Baillieres Clin Rheumatol* 4:467-489.

Tett SE, Cutler DJ, Day RO, and Brown KF (1988) A dose-ranging study of the pharmacokinetics of hydroxy-chloroquine following intravenous administration to healthy volunteers. *Br J Clin Pharmacol* 26:303-313.

Tett SE, Cutler DJ, Day RO, and Brown KF (1989) Bioavailability of hydroxychloroquine tablets in healthy volunteers. *Br J Clin Pharmacol* 27:771-779.

Thelen K, and Dressman JB (2009) Cytochrome P450-mediated metabolism in the human gut wall. *J Pharm Pharmacol* 61:541-558.

Trapp S, and Horobin RW (2005) A predictive model for the selective accumulation of chemicals in tumor cells. *Eur Biophys J* 34:959-966.

Trapp S, Rosania GR, Horobin RW, and Kornhuber J (2008) Quantitative modeling of selective lysosomal targeting for drug design. *Eur Biophys J* 37:1317-1328.

Vogl DT, Stadtmauer EA, Tan KS, Heitjan DF, Davis LE, Pontiggia L, Rangwala R, Piao S, Chang YC, Scott EC, Paul TM, Nichols CW, Porter DL, Kaplan J, Mallon G, Bradner JE, and Amaravadi RK (2014) Combined autophagy and proteasome inhibition: A Phase I trial of hydroxychloroquine and bortezomib in patients with relapsed/refractory myeloma. *Autophagy* 10:1380-1390.

Warhurst DC, Steele JC, Adagu IS, Craig JC, and Cullander C (2003) Hydroxychloroquine is much less active than chloroquine against chloroquine-resistant *Plasmodium falciparum*, in agreement with its physicochemical properties. *J Antimicrob Chemother* 52:188-193.

Wei Y, Nygard GA, Ellertson SL, and Khalil SK (1995) Stereoselective disposition of hydroxychloroquine and its metabolites in rats. *Chirality* 7:598-604.

Yang ZJ, Chee CE, Huang S, and Sinicrope FA (2011) The role of autophagy in cancer: Therapeutic implications. *Mol Cancer Ther* 10:1533-1541.

Yogasundaram H, Putko BN, Tien J, Paterson DI, Cujec B, Ringrose J, and Oudit GY (2014) Hydroxychloroquine-induced cardiomyopathy: Case report, pathophysiology, diagnosis, and treatment. *Can J Cardiol* 30:1706-1715.

Zhang L, and Mager DE (2015) Physiologically-based pharmacokinetic modeling of target-mediated drug disposition of bortezomib in mice. *J Pharmacokinet Pharmacodyn* 42:541-552.

Zhi Z, Yin X, Dziennis S, Wietecha T, Hudkins KL, Alpers CE, and Wang RK (2012) Optical microangiography of retina and choroid and measurement of total retinal blood flow in mice. *Biomed Opt Express* 3:2976-2986.

Zhitomirsky B, and Assaraf YG (2015) Lysosomal sequestration of hydrophobic weak base chemotherapeutics triggers lysosomal biogenesis and lysosome-dependent cancer multidrug resistance. *Oncotarget* 6:1143-1156.

Zhitomirsky B, and Assaraf YG (2015) The role of cytoplasmic-to-lysosomal pH gradient in hydrophobic weak base drug sequestration in lysosomes. *Cancer Cell Microenviron* 2:e807.

Chapter Three

Lysosomal Biogenesis and Implications for Hydroxychloroquine Disposition

Summary

Lysosomes act as a cellular drug sink for weakly basic, lipophilic (lysosomotropic) xenobiotics, with many instances of lysosomal trapping associated with MDR. Lysosomotropic agents have also been shown to activate master lysosomal biogenesis transcription factor EB (TFEB), and ultimately lysosomal biogenesis. We investigated the role of lysosomal biogenesis in the disposition of hydroxychloroquine (HCQ), a hallmark lysosomotropic agent, and observed that modulating the lysosomal volume of human breast cancer cell lines can account for differences in disposition of HCQ. Through use of an *in vitro* pharmacokinetic (PK) model we characterized total cellular uptake of HCQ within the duration of static equilibrium (1 hour), as well as extended exposure to HCQ that are subject to dynamic equilibrium (>1 hour) wherein HCQ increases the size of the lysosomal compartment through swelling and TFEB-induced lysosomal biogenesis. In addition, we observe that pretreatment of cell lines with TFEB-activating agent Torin 1 contributed to an increase of whole cell HCQ concentrations by 1.4 to 1.6-fold, which were also characterized by the *in vitro* PK model. This

investigation into the role of lysosomal volume dynamics in lysosomotropic drug disposition, including the ability of HCQ to modify its own disposition, advances our understanding of how chemically-similar agents may distribute on the cellular level, and examines a key area of lysosomal-mediated MDR and DDI.

Introduction

Hydroxychloroquine (HCQ) has been investigated in over 50 cancer clinical trials and countless preclinical studies through the past decade as an additive compound to primary chemotherapy treatment. Mechanistically, HCQ acts to inhibit autophagy, which has been identified as a mechanism of tumor cell resistance to chemotherapy and a key pathway to survival within the tumor microenvironment. While next generation autophagy inhibitors are in preclinical stages of development, HCQ remains the only clinically approved autophagy inhibitor. Overall HCQ is generally effective and safe as a treatment but suffers from various pitfalls within the pharmacologic space – specifically in terms of predictability of patient likelihood of response and reliable pharmacokinetic (PK) and pharmacodynamic (PD) metrics. There is a general disconnect between HCQ PK in the tumor and blood; creating a challenge when optimizing dosing strategies to be confident that target concentrations of HCQ are achieved within the tumor (Barnard et al., 2014). Characterization of HCQ PK properties on a cellular level may provide insight towards tumor-specific factors that would promote this disconnect.

Cellular uptake of HCQ is driven primarily through lysosomal ion-trapping due to its weakly basic and lipophilic properties that characterize it as a hallmark

lysosomotropic agent. HCQ readily diffuses through neutral spaces, but becomes diprotonated in the lysosome, whose acidic environment facilitates accumulation. This results in concentrations significantly higher than other compartments within the cell (Duvvuri and Krise, 2005). Key mechanisms contributing to pharmacokinetics have been considered and consolidated into *in vitro* mathematical models to describe cellular uptake of compounds with similar physicochemical properties to HCQ, namely weakly basic and lipophilic (Ishizaki et al., 2000; Trapp et al., 2008; Kornhuber et al., 2010; Schmitt et al., 2019). These models assume the cell behaves as a static system of compartments, but recent evidence suggests that lysosomotropic compounds induce changes in the lysosome itself.

Lysosomes swell in response to chloroquine (CQ) exposure, which is mechanistically and pharmacokinetically similar to HCQ. Near clinically-relevant doses of CQ have been observed to cause a 3-fold increase in relative lysosomal volume after multiple days of exposure to the drug (King et al., 2016), and recruitment of galectin-3 to sites on these swollen lysosomes, indicating membrane damage (Gallagher et al., 2017). In addition to an increase in lysosomal size, an increase in lysosomal number has also been reported in response to a panel of lysosomotropic agents, including CQ, over the course of 4 and 24 hours (Lu et al., 2017). This increase in lysosomal number was linked to an increase in nuclear translocation of master lysosomal biogenesis transcription factors, TFEB, TFE3, and MITF. TFEB activation of the CLEAR network of genes has been described as the master regulation system of lysosomal biogenesis (Settembre et al., 2012; Settembre et al., 2013). Lysosomotropic agents cause activation of this network by inducing lysosomal stress, and has been shown to activate

as early as 90 minutes of exposure to CQ (Zhitomirsky et al., 2018). The results of lysosomal swelling and TFEB activation by lysosomotropic agents may be linked to their long-term tissue PK. Extended dosing of HCQ is characterized by a consistent increase in HCQ concentrations in rat tissue over the course of 3 months of daily dosing. In some tissues (spleen, kidney, liver, heart) HCQ concentrations continued to increase out to the latest timepoint measured at 7 months (McChesney, 1983). This long-term PK profile is noted by McChesney to be similar to other lysosomotropic drugs such as chlorpromazine.

Due to the frequent, high doses of HCQ used in cancer clinical trials we characterized this lysosomal adaptation response on a cellular level and investigated the extent to which it may influence cellular disposition of the drug. The data described herein suggests that baseline cell uptake of HCQ is associated with different baseline lysosomal profiles between cell lines, which were integrated into a lysosome cellular PK mathematical model (Trapp et al., 2008; Kornhuber et al., 2010) to accurately model whole cell HCQ PK to chemical kinetic equilibrium. Small, but consistent increases in whole cell uptake of HCQ over an extended time period were also observed, and attributed to an increasing volume of the lysosomal compartment. The *in vitro* PK profile of HCQ was thus broken up into a short-term kinetic equilibrium portion, within 1 hour of exposure, and a long-term dynamic portion, out to 24 hours of exposure for all cell lines. This data was used, in conjunction with observed differences in baseline lysosomal profiles, to further characterize the cellular PK of HCQ by accounting for a dynamic lysosomal compartment.

Materials and Methods

Cell Lines

Human breast cancer cell lines including MDA-MB-231, MDA-MB-468, T47D, and MCF7 human breast cancer cell lines were purchased from Cell Culture Services at University of Colorado Anschutz Medical Campus (Aurora, CO). For cell pharmacokinetic experiments, all cell lines were stably transfected with Incucyte NucLight Red Lentivirus (Sartorius, Cat. 4476) prior to experimentation.

Cell lines were cultured in Dulbecco's Modified Essential Medium (Corning, 10-017-CV) supplemented with 10% fetal bovine serum (Peak Serum, PS-FB3), 1% penicillin/streptomycin (Fisher, 30-002-CI), and 1% sodium pyruvate (Fisher, 25-000-CI) at 37°C and 5% CO2 in a humidified incubator.

Chemicals and Reagents

Hydroxychloroquine (HCQ) sulfate was purchased from SigmaAldrich (St. Louis, MO). Monensin (MN) was purchased from VWR (Radnor, PA). Torin1 (T1) was purchased from Fisher (Hampton, NH). Hoechst 33342 20mM solution (62249) and CellLight Lysosomes-GFP, BacMam 2.0 (C10507) were purchased from ThermoFisher (Waltham, MA). ETP, a pH-insensitive lysosomal lumen dye applicable for live and fixed cell imaging, was received as a gift from Dr. Yi Pang at the University of Akron (Abeywickrama et al., 2019).

Cell Uptake Experiments

4 human breast cancer cell lines were used to perform experiments. The first 2, MBA-MB-231 and MDA-MB-468, are mechanistically sensitive to autophagy inhibition through gene knockdown (Maycotte et al., 2014; Towers et al., 2019) and pharmacologically sensitive to hydroxychloroquine. The second 2, MCF7 and T47D, are insensitive to both methods (Maycotte et al., 2014).

Cell lines were cultured in standard DMEM supplemented with 10% FBS, 1% PS, and 1% sodium pyruvate in an incubator at 37°C and 5% CO2. T47D and MCF7 cell lines required supplementation of 8µg/mL of insulin to maintain growth. For acidic media experiments with MDA-MB-231 cells, DMEM without sodium bicarbonate was purchased, and bicarbonate was added to achieve an incubator-conditioned media pH. Culture media buffers other than sodium bicarbonate, such as HEPES, were purposely omitted as HEPES has been shown to activate the MiT/TFE network, resulting in lysosomal biogenesis (Tol et al., 2018).

Cell lines were plated, allowed to adhere overnight, and treated at roughly 70% confluence. All cell lines stably expressed NucLight Red, and cell counts were measured by counting red fluorescent nuclei on an Incucyte ZOOM (Sartorius; Gottingen, Germany) prior to treatment with drug. For 4 hour and 24-hour timepoints cells were counted immediately prior to harvesting, as the doubling time for these cell lines is between 16-20 hours. Experiments were not extended past 24 hours to avoid cell line growth inhibition in response to HCQ. For treatment, culture media was aspirated and replaced with fresh, incubator-conditioned media containing 10µM HCQ and placed in a 37° C incubator until the designated timepoint. At the timepoint cell

media containing HCQ was aspirated and cells were washed with HBSS, then trypsinized for 5 minutes. Trypsinized cells were washed off the plate with additional culture media at a ratio of 4:1 media:trypsin. Cells were then pelleted at 1600 rpm for 5 minutes, media was carefully aspirated, and the cell pellet reconstituted in MilliQ-water and frozen until LCMS extraction and analysis.

LC/MS-MS analysis follows methods described in (Barnard et al., 2014), but briefly – cell pellets were vortexed and lysed for 10 minutes in a sonication water bath. Acetonitrile (ACN) was then added to the cell pellets to yield a final solution of 50% ACN + 50% MilliQ-H2O. Cells were vortexed for 10 minutes, then centrifuged at 13,300 rpm for 10 minutes. Supernatant was transferred to polypropylene inserts. Chloroquine (CQ) was used as an internal standard. Concentrations of supernatant obtained on LC/MS-MS were normalized to the cell counts obtained for each sample from an Incucyte ZOOM, and samples were then normalized to cell volume, obtained for each cell line from suspended cell diameter measured on a Countess system (n=4), to obtain HCQ concentration (μM) in each cell.

For experiments with monensin (MN), cells were pretreated with 25μM MN for 30 minutes prior to adding HCQ. After 30 minutes 10μM HCQ was added for the duration for of the 1hr exposure. For experiments with Torin1 (T1), cells were pretreated with 250nM Torin1 for 16 hours prior to adding HCQ. All cell uptake experiments were performed in at least triplicate.

Lysosomal Imaging

For all imaging experiments cells were plated at 10,000 cells/well on an 8-well glass chamber slide (Cellvis, C8-1.5H-N) and allowed to adhere overnight.

To determine lysosomal volume, live cells were treated with 1μM of ETP (Abeywickrama et al., 2019), and incubated for 30 minutes. Excess dye was removed by washing twice with warm media, and incubated with 10μM of Hoescht 33342 for 10 minutes. Cells were then washed twice with PBS and fixed for 10 minutes in 2% PFA. PFA was washed off twice with PBS and cells were imaged on an Olympus IX83 microscope with a Plapon 60x Objective, NA = 1.42 on Cy3 and DAPI confocal channels. 43 z-stacks of 0.24μm step-size were captured on Cy3 and DAPI channels. Lysosomal volume fraction of cells was determined using an in-house image processing pipeline which is described briefly as follows: Raw confocal image stacks were converted to .tif files and imported into Python version 3.7.6. A reference image was created by compressing the stack by its maximum pixel intensity. Each slice of each image stack was analyzed to determine the peak signal to noise ratio (PSNR) relative to the reference image using the sewar module (https://pypi.org/project/sewar/). A .csv file containing the top 10 PSNR slices for each image stack was generated and imported into a FIJI macro that calculated the Cy3 (lysosome) area for each raw .vsi image slice based on an algebraic threshold of mean intensity. The area for each slice was multiplied by the step size (0.24μm) to generate a volume, and then volumes from the 10 slices per image stack were summed to generate a lysosomal volume for the image. The lysosomal volume was normalized to the cell count of each image, and the cell count was normalized to the experimentally determined cell volume for each cell line to

generate a lysosomal volume fraction per cell. 5-10 images were obtained for each experimental replicate, and lysosomal volume fraction is presented as the mean ± standard deviation of each replicate (n=3) for each cell line. Imaging of cell lines for GFP-LAMP-1 expression followed the same imaging process, except cells were incubated with 1μL of the baculovirus overnight prior to treatment with HCQ.

For drug treated conditions, single plane images were captured at 20x using the same microscope, but an Uplsapo 20x objective, NA = 0.75 on Cy3 and DAPI LED channels. To determine a change in lysosome content of the cell, cells were treated with the same drug treatment conditions as described in the cell uptake experiments section. Chamber slides were prepared in the same way as described above. Images were quantitated using a FIJI macro with an algebraic threshold of the mean intensity, and data was calculated as Cy3 area / DAPI area. Roughly 10 images were obtained for each experimental replicate, and data is reported as the mean ± standard deviation of each replicate (n=4). Statistical significance was calculated as a one-way ANOVA with Dunnett's multiple comparisons test relative to the control, where $P < 0.05$ was significant.

TFEB Activation

TFEB activation by HCQ was determined with 2 different kinds of methods including gene set enrichment analysis (GSEA) of the TFEB-regulated CLEAR network, and through a TFEB transcription factor activity assay (RayBiotech, TFEH-TFEB). Gene expression microarray data was prepared for all 4 hBC lines following cell culture preparation steps as outlined in the cell uptake experiments section. Cell lines were treated with 20μM HCQ, for 24 hours prior to harvesting for gene expression

preparation in triplicate. Prepared cell extraction homogenate was run on an HG_U133_Plus_2 chip. CEL file data was extracted and prepared for GSEA using the Affymetrix Bioconductor package in R, and normalized using RMA. Expression data was then analyzed using the GSEA 4.0.3 software provided by the BROAD Institute. Gene sets from the 4 cell lines, treated with HCQ or vehicle, were analyzed in GSEA using a gene set representative of TFEB lysosome targets (Palmieri et al., 2011) and run in tandem with the Hallmarks of Cancer gene set database version 7.1 provided in the GSEA software. The run was set for 1000 permutations following a “gene_set” permutation type. Data is reported as the NES value and significance determined by FDR q-value generated in the run. Raw .CEL files are available in the supplement. TFEB nuclear activation was performed in duplicate and was determined using the human TFEB transcription factor activity assay following manufacturer’s instructions. TFEB activity data is expressed as mean ± standard deviation, and was analyzed by one-way ANOVA with Dunnett’s multiple comparison test relative to control with significance as $P < 0.05$.

Cell Pharmacokinetic Mathematical Modeling and Simulation

To simulate the lysosomal uptake of HCQ into cells a previously published base model of lysosomal uptake was used (Trapp et al., 2008; Kornhuber et al., 2010). Lysosomal volume fraction for each cell line was determined by imaging methods described above. Extracellular pH was determined by measuring the pH of incubator-equilibrated media in a pH meter (7.6), and then testing the change in cellular uptake of HCQ at the 1hr timepoints in a media of decreased pH (7.0). The influence of the lysosome and cytosolic pH were determined experimentally by pretreating MDA-MB-

231 cells with monensin (MN), a lysosome-selective ionophore (Grinde, 1983), and simulating the experimental uptake of HCQ in cells after pre-treatment. The model values of cytosolic pH of roughly 7.0 and lysosomal pH of 5.0 worked well with the cell lines used, which are similar to what has been previously reported for MCF7 cytosolic pH (Belhoussine et al., 1999), and MCF7 and MDA-MB-231 lysosomal pH values (Montcourrier et al., 1994). It is noted that the range of the pH values from different literature reports is quite broad, with lysosomal pH values reported around 4.2 for MDA-MB-231 cells (Ndolo et al., 2012), 4.5 for MCF7 and MDA-MB-231 cells (Wang et al., 2019), and 5.1 for MCF7 and MDA-MB231 cells (Montcourrier et al., 1994). Cytosolic pH exhibited a similar trend from literature, with reported values around 6.9 for MCF7 (Belhoussine et al., 1999), 7.3 for MCF7 (Persi et al., 2018), and 7.4 for MDA-MB-231 and MCF7 (Wang et al., 2012). From the studies using multiple human breast cancer lines, that were also used in this work, the lysosomal and cytosolic pH were not very different between each cell line and so we chose to use fixed values for these parameters across all 4 cell line models.

Evaluation of Model Fit

Model fit versus experimental data was evaluated by comparing the experimental $AUC_{0\text{-}1hr}$ or $AUC_{0\text{-}24hr}$ to the simulated value for each cell line. Additionally, model accuracy was analyzed by calculating the performance error (PE), median performance error (MPE%) to investigate positive/negative bias, and mean absolute performance error (MAPE%) to determine overall model fit (Gustafsson et al., 1992). These calculations included all timepoints relevant to the parent figure.

Computer Simulation and Software

Intracellular PK model simulation was done in MATLAB, version R2020a (Mathworks; Natick, MA) and the intracellular compartmental system was solved using the ode45 package. Image selection was done in Python, version 3.7.6, using sewar and tqdm packages. Image analysis was done in ImageJ, version 1.52p using methods described above.

Results

Whole Cell Uptake of HCQ is Proportional to Basal Lysosomal Volume Fraction

The *in vitro* PK of HCQ was assessed in 4 human breast cancer cell lines (hBC), MDA-MB-231, MDA-MB-468, T47D, and MCF7 by collecting total cell homogenate at 1, 5, 15, 30, 60, 240, and 1440 minutes after incubating with 10μM HCQ. This concentration of HCQ was chosen as it is clinically achievable. HCQ concentration within the whole cell was determined by normalizing total HCQ in the homogenate to the total cell volume in the homogenate outlined in Supplementary Figure 3.1. We observed different concentration levels of HCQ for each cell line, which mostly followed the ranking of MDA-MB-231 > MDA-MB-468 > T47D > MCF7 (Fig. 3.1A). For all 4 hBC lines the HCQ total cellular concentrations increased the longer the cell lines were exposed to the drug up to total cellular concentrations peaking between 0.58-2.67mM, which were 58-267x the extracellular concentration of HCQ, and are consistent with steady-state partition coefficients of HCQ tissue:plasma from previous *in vivo* studies (McChesney et al., 1967; McChesney, 1983; Wei et al., 1995).

As acidic organelles are suggested to account for a majority of cellular distribution of diprotic lipophilic compounds, we investigated the total lysosomal volume fraction of each cell line using microscope imaging methods outlined in Supplement Fig. 3.2. We observed lysosomal percent volume of total cellular volume ranging from 0.50

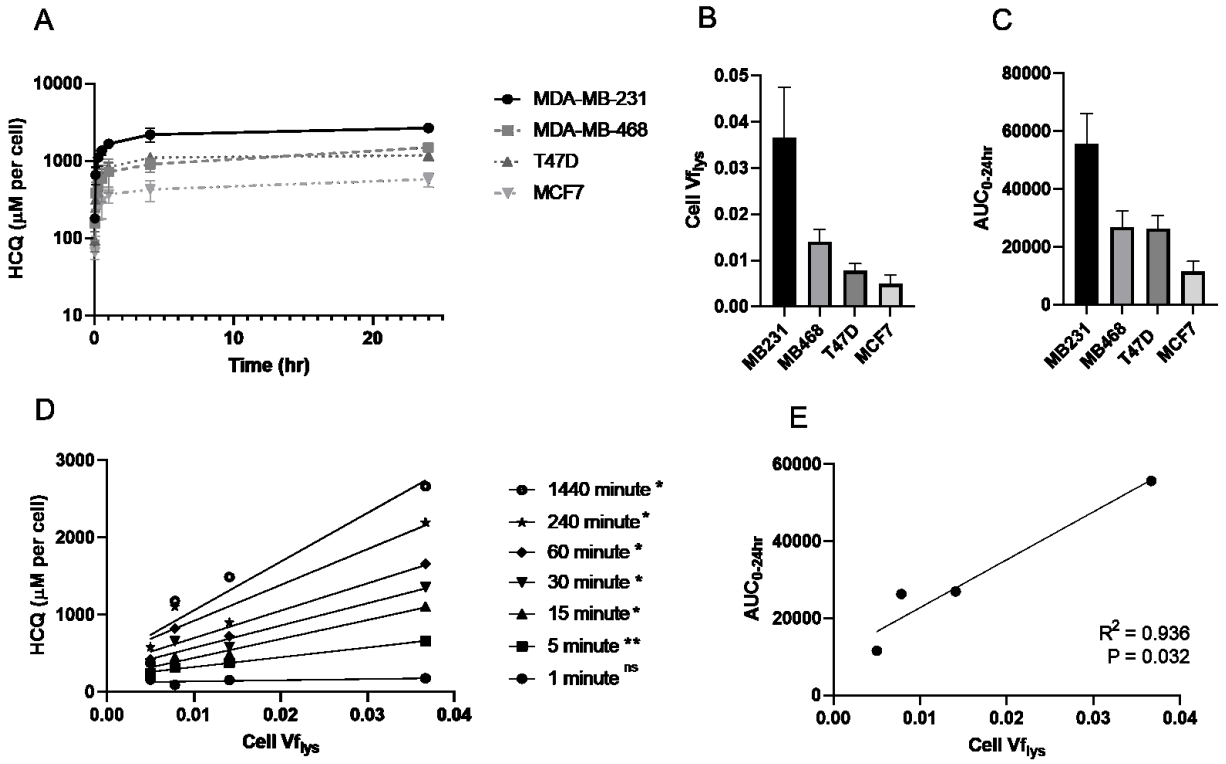

Figure 3.1. Whole cell uptake of HCQ is proportional to basal lysosomal volume fraction. The *in vitro* whole cell PK of HCQ was assessed in 4 human breast cancer cell lines (hBC), MDA-MB-231, MDA-MB-468, T47D, and MCF7 at 1, 5, 15, 30, 60, 240, and 1440 minutes after incubating with 10µM HCQ (A). Cell lysosomal volume fraction was calculated as outlined in Supplementary Figure 2 (B). Lysosomal volume fraction closely followed the ranking of $AUC_{0\text{-}24hr}$ of the whole cell PK data (C). Mean whole cell HCQ concentrations at each timepoint, except 1 minute, was significantly correlated with cellular lysosome volume fraction (D). This correlation was also significant when comparing the mean $AUC_{0\text{-}24hr}$ of each cell line to the cellular lysosome volume fraction (E). Applicable data is shown as mean ± sd, and significance is defined as $P < 0.05$.

± 0.19% in MCF7 cells to roughly 3.67 ± 1.09% in MDA-MB-231 cells (Fig. 3.1B), which followed roughly the same trend as total cellular uptake of HCQ based on $AUC_{0\text{-}24hr}$

(Fig. 3.1C). Overall, mean total cell uptake concentrations of HCQ showed a significant Pearson correlation with lysosomal volume fraction for timepoints 5, 15, 30, 60, 240, and 1440 minutes (Fig. 3.1D). The 1 minute timepoint was not significant, likely due to insufficient time for HCQ to diffuse into the lysosomal compartment. Total exposure to HCQ, as calculated by $AUC_{0\text{-}24hr}$, also had a strong correlation ($P=0.032$, $R^2=0.936$) with cellular lysosomal volume fraction (Fig. 3.1E).

Basal Lysosomal PK Model of HCQ Accounts for Uptake by Adjusting Lysosomal Volume Fraction

To further investigate the *in vitro* PK of HCQ in the 4 hBC lines we used a base pharmacokinetic (PK) model of lysosomotropic drug uptake (Trapp et al., 2008; Kornhuber et al., 2010), and modified it to be specific to the 4 cell lines in the study with experimentally determined lysosomal volume fractions. HCQ *in vitro* PK was modeled as a diffusion-based 3-D system where net flux of HCQ across membranes is driven by the permeability of each ionization state, and ionization state (0, 1^+, 2^+) is a function of pH described by the Henderson-Hasselbach activity ratio. The model consisted of 3 compartments representative of *in vitro* settings, which include culture media, cytosol, and lysosomes (Fig. 3.2A). Trafficking between compartments was driven by net flux. The lysosomal compartment had a dynamic pH (ΔpH) term that was a function of lysosomal HCQ concentration, as HCQ is suggested to neutralize the acidic lysosomal pH. Model parameters are listed in Supplementary Table 3.1.

By adjusting the lysosomal volume fractions for each cell line, we simulated the *in vitro* PK experiment of HCQ administered at 10μM for each cell line out to 1 hour (Fig. 3.2B). For all cell lines except T47D, the experimentally-derived mean lysosomal

volume fraction allowed the simulation to capture the mean concentration of HCQ with a strong fit. The simulation was also run using the 95% CI bounds for the experimentally-derived lysosomal volume fractions to investigate variability due to this parameter. The simulation suggested that the system reaches equilibrium around 30 minutes; however,

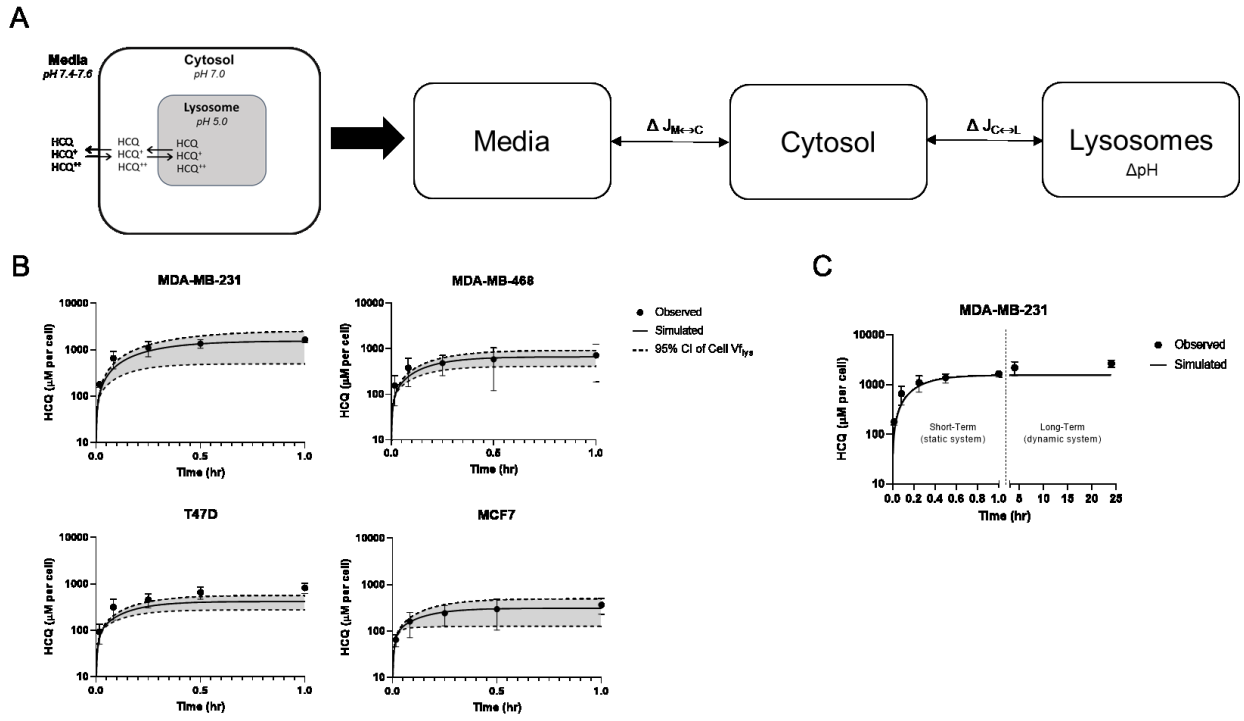

Figure 3.2. Basal Lysosome PK Model of HCQ Accounts for Uptake by Adjusting Lysosomal Volume Fraction. To further investigate the *in vitro* PK of HCQ in the 4 hBC lines we used a previously published base model of lysosomotropic drug uptake into cells. The compartmental model is outlined, where compartments considered are culture media, cytosol, and lysosome, with the lysosome contained within the cytosolic compartment (A). Mathematically, the 3 compartments are separate, where HCQ diffuses freely from Media ←→ Cytosol ←→ Lysosomes, and diffusion is represented by a net flux term (∆J) that is the sum of permeability of each HCQ ionization state (neutral, 1+, 2+). The lysosomal compartment has a dynamic pH feedback term that was representative of the proposed mechanism of HCQ to increase the pH of the lysosome based on free drug concentration. The model was used to simulate HCQ uptake in each cell line based on lysosomal volume fractions and other parameters in Table 1. The output of the model simulation for each cell line is shown as the observed mean ± 95% CI bounds in conjunction with the simulated mean ± 95% CI bounds of the cellular lysosomal volume fraction (B). The model only considered timepoints out to the first hour, which were labeled as short-term static equilibrium. In the experimental data

it is observed that concentrations continue to increase after 1 hour, which is characterized as the long-term dynamic system (C), and investigated in later figures.

the experimental PK data for all 4 cell lines suggests that HCQ concentrations in the cell continue to increase steadily at 1, 4, and 24 hours (Fig. 3.2C). Early timepoints were characterized by chemical kinetic equilibrium, where the cellular physiologic parameters are static, followed by later timepoints where the system physiologic parameters are dynamic. The dynamic system is investigated further in later figures. The model fit for each of the cell lines out to 1 hour is characterized by the ratios of simulated/observed AUC (Table 3.1), as well as measures of predictive performance PE, MAPE%, and MPE% (Supplementary Table 3.2).

Table 3.1. Static Model Metrics (AUC)

AUC Summary (0-1hr)	Experimental	Simulated	Ratio
Cell line	Mean	Mean	Mean Sim / Exp
MDA-MB-231	1239	1160	0.936
MDA-MB-468	551	549	0.995
T47D	588	354	0.602
MCF7	276	270	0.980

Using a previously determined range of 0.5-2.0 as acceptable ratios for AUC of simulated/experimental, the model captured MDA-MB-231, MDA-MB-468, and MCF7 very closely (0.936, 0.995, 0.980). T47D was underpredicted, but still fell within the acceptable range (0.602). In comparing the model performance error (PE), the model underpredicted early timepoints (1, 5 minutes) for all cell lines except MCF7. Timepoints between 15-60 minutes were predicted with good accuracy, aside from T47D. MAPE%, a metric of model accuracy, suggests that the model predicts individual timepoints in MDA-MB cell lines with about 30% error, T47D around 60%, and MCF7 about 6.5%.

Overall, the model underpredicts concentrations (MPE%) by 18.4 and 8.6% in the MDA-MB cell lines, although this is biased by early timepoints error, 64% in T47D, and overpredicts by only 1.3% in MCF7. Observations from these metrics suggest that T47D cell uptake of HCQ may be better explained by the upper CI bound of its lysosomal volume fraction (1.16%), rather than its mean (0.78%). Model metrics also suggest that early timepoints (1, 5 minutes) in MDA-MB cell lines were either underpredicted based on uptake kinetics, or there was time-based experimental error exacerbated by early timepoint sampling.

We also investigated the influence of the pH parameters on total cellular uptake of HCQ in MDA-MB-231 cells. We measured the pH of incubator-conditioned culture media (5% CO2, 37°C) used in the previous experiments at 7.6, and made acidic culture media at an incubator-conditioned pH of 7.0. As stated in the methods section, we opted out of using culture media buffers other than sodium bicarbonate, such as HEPES, as it has been suggested to activate the MiT/TFE pathway which ultimately results in lysosomal biogenesis (Tol et al., 2018). As the model accurately captured MDA-MB-231 cell lines under neutral conditions, they were exposed to 1 or 10μM HCQ in the conditioned culture media for 1 hour, and the resulting decrease in total cellular uptake of HCQ associated with decreasing media pH was quite dramatic. We observed a 6.4-fold decrease in HCQ uptake at the treated concentrations when switching the media pH from 7.6 to 7.0, such that in most cases the 10μM HCQ uptake at pH of 7.0 was nearly equivalent to the 1μM HCQ uptake at pH of 7.6 (Supplementary Figure 3.3A). The shape of the simulated kinetics uptake curve was not visibly modified by extracellular pH out to the 1 hour timepoint tested (Supplementary Figure 3.3B).

Interestingly, lysosomotropic drug partition into cells and tissues has been suggested to be significantly reduced by acidic extracellular pH (Wojtkowiak et al., 2011), causing a subsequent resistance of cells to growth inhibition by HCQ. We tested the effect of acidic culture media in blunting HCQ growth inhibition in MDA-MB-231 cells and observed an almost complete reduction in growth inhibition (Supplementary Fig. 3.3C), similar to the trend described by with CQ (Pellegrini et al., 2014). In addition to testing the influence of extracellular pH directly, we also investigated the contribution of lysosome and cytosol pH gradient indirectly by treating cells with MN prior to HCQ in order to eliminate the gradient. In MDA-MB-231 cells pretreatment with 25μM MN for 30 minutes prior to HCQ caused a reduction in total cellular uptake of HCQ by 93.2% at 1 hour. We simulated this experiment using the model by changing the lysosomal pH to 7.0 and comparing to the model with lysosomal pH of 5.0 (Supplementary Fig 3.3D). Overall, the model captured the decrease in total cellular uptake well, with simulated MN (+) / MN (-) concentration ratio of 0.078 versus observed MN (+) / MN (-) concentration ratio of 0.068.

HCQ Increases the Size of the Lysosomal Compartment

While the model captures early timepoint *in vitro* PK (<1hr) of HCQ, as well as variabilities in influential model parameters along the pH gradient, it fails to capture later timepoints as the simulation suggests the system reaches equilibrium when the observed concentrations actually continue to gradually increase out to 24 hours (Fig. 3.2C). Recent reports suggest that many weakly basic lipophilic compounds, including CQ, activate lysosomal biogenesis by activating the transcription factor EB (TFEB) (Lu et al., 2017; Zhitomirsky et al., 2018; Zhao et al., 2020), which ultimately increases the

lysosomal volume fraction of treated cells and should allow them to sequester even more drug than their original baseline (Ruzickova et al., 2019). CQ has been observed to activate TFEB and increase lysosomal content of the cell, so we investigated the capability of HCQ to do the same. Treatment of all 4 hBCs with either HCQ for 24 hours or TFEB-activator Torin1 for 16 hours, caused a significant increase in TFEB activity in the nucleus (Fig. 3.3A), suggesting it is released from the lysosome and translocated to the nucleus after HCQ treatment. In addition, gene microarray data on all 4 cell lines treated with HCQ or vehicle for 24 hours showed a significant enrichment in expression of the TFEB-associated direct targets in lysosomal function (Fig. 3.3B) as characterized by the Ballabio group (Palmieri et al., 2011). Treatment of all 4 cell lines with HCQ or Torin1 caused an increase in the relative volume of the lysosome compartment. MCF7 cells had the most visually-distinct increase in lysosomal burden with both drugs (Fig. 3.3D). Quantitation of the increase in lysosome-positive area per nuclei suggests a relative increase in 1.59 to 14.93-fold (average 5.90-fold) in the cell lines with 24 hour treatment with HCQ, or Torin1 caused a 2.25 to 10.7-fold (average 5.55-fold) (Fig. 3.3C). This increase in lysosomal burden by HCQ may have some contribution independent of TFEB as well, as CQ has been shown to induce swelling in lysosomes at higher doses, which is visually apparent in images comparing Torin1 increase in lysosomal burden versus HCQ increase in lysosomal burden in MCF7 (Fig. 3.3D), and the other 3 cell lines (Supplemental Figure 3.4). To further investigate lysosomal swelling by HCQ we transfected MDA-MB-468, T47D, and MCF7 cells with a GFP baculovirus for lysosomal associated membrane protein 1, LAMP-1, as it more clearly defines the membranes of individual lysosomes, and imaged cells after treatment with

10μM HCQ for 24 hours. MDA-MB-231 cells would not express the virus and were omitted from this experiment. In the 3 cell lines we observed a dramatic increase in size of some lysosomes after HCQ exposure (Supplemental Figure 3.5).

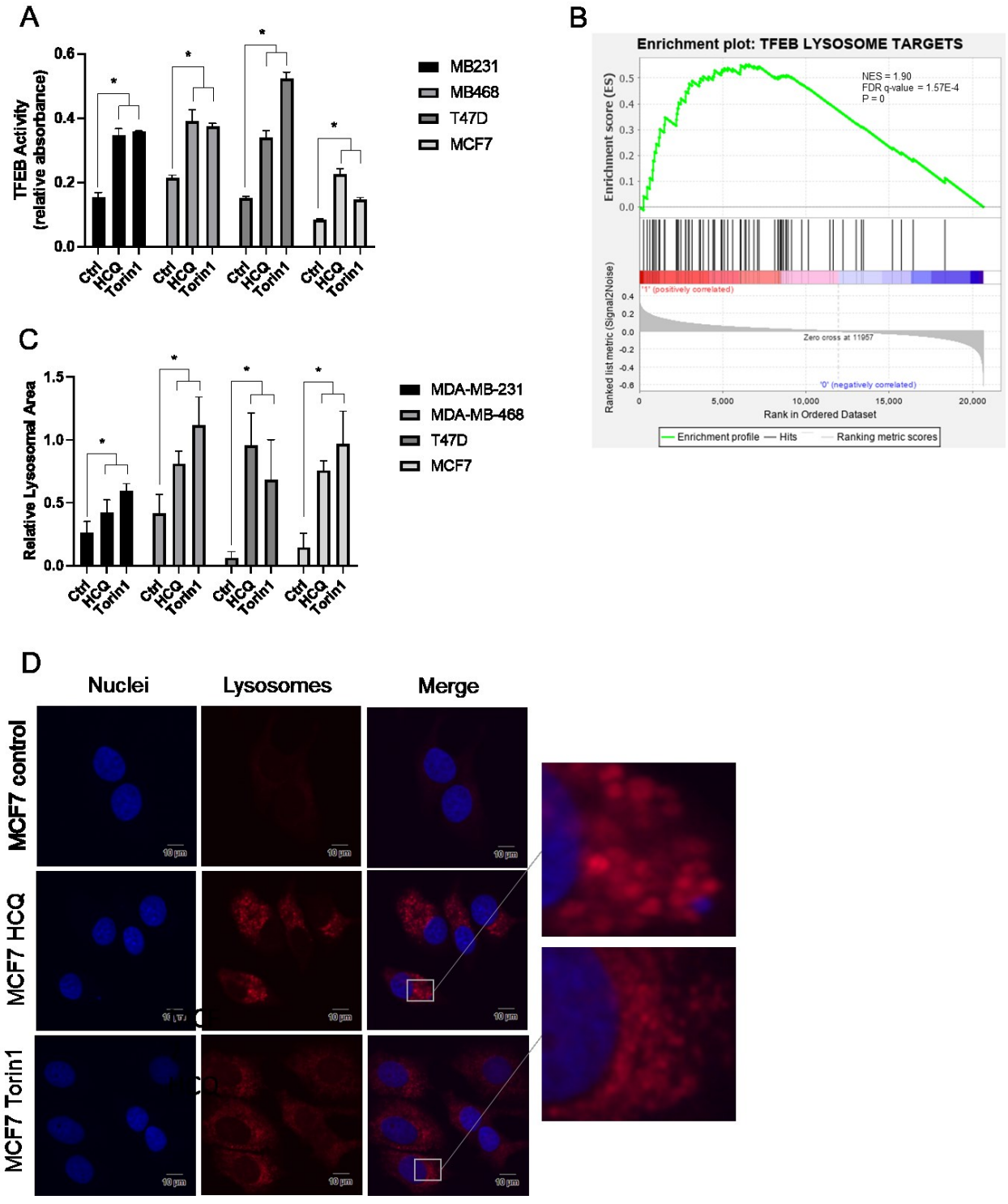

Figure 3.3. HCQ Increases the Size of the Lysosomal Compartment. We investigated the ability of HCQ to change the size of the lysosomal compartment. TFEB activity in the nucleus was significantly increased in all cell lines treated with 10μM HCQ for 24 hours, and with 250nM Torin1, a molecular TFEB activating agent, for 16 hours (A). Gene set enrichment analysis (GSEA) of all four cell lines treated with 20μM HCQ

for 24 hours also caused a significant enrichment of TFEB lysosome targets (B). Fluorescence microscopy imaging of all 4 cell lines with ETP showed a significant increase in lysosome accumulation within all cell lines treated with 10μM HCQ for 24 hours, or 250nM Torin1 for 16 hours (C). Representative images of MCF7 cells imaged with ETP under the treatment conditions are shown in in (D). Zooming in on MCF7 cells treated with HCQ shows a visual increase in lysosomal size in comparison with the Torin1 treatment. To prepare figures for publication the raw image threshold was adjusted to the same upper and lower bounds across the entire image for all images shown.

Dynamic Lysosomal Volume Accounts for Simulation Error

The original model with a static lysosomal volume compartment was able to capture total cell uptake of HCQ out to 1 hour, but significantly underpredicted 4 and 24 hour timepoints. To account for this error, we incorporated lysosomal biogenesis into the model by adding a dynamically-growing lysosomal volume fraction represented by the proposed mechanism outlined in Figure 3.4. The growing compartment is represented as a linear increase in lysosomal volume fraction as a function of time: $Vf_{lys}(t) = Vf_{lys\_0}*(1+x*t)$. We found that a 1.5 to 3-fold total increase in lysosomal volume fraction by 24 hours in the dynamic lysosomal model accounted for the underprediction of 4 and 24 hour timepoints predicted by the static lysosomal model (Fig 3.5A). The simulated 1.5-3 fold increase in lysosomal volume fraction over 24 hours of HCQ exposure was within the 95% CI of the experimentally observed increase due to HCQ in the 4 cell lines shown in Figure 3.3C, except for T47D. As such, for T47D, we tested an increase of 2.5-fold in lysosomal volume starting from the upper bound of the 95% CI (1.155%), which resulted in a better model fit to 24 hours. Incorporation of this time-based linear increase did not significantly affect timepoints before 1 hour (Fig. 3.5B).

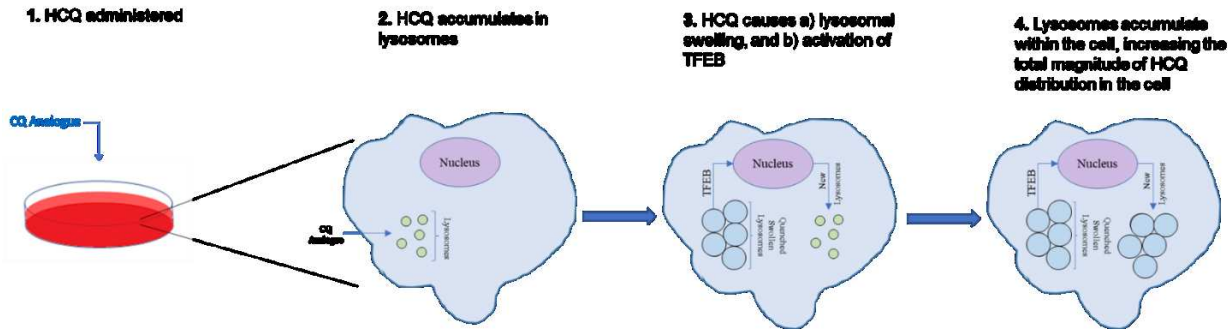

Figure 3.4. Proposed Mechanism of HCQ Altered Uptake. This figure outlines the process by which HCQ increases its volume of distribution within the cell. HCQ is initially added to the cell culture (1), after which it immediately begins to accumulate within the lysosomes of the cells until it reaches chemical equilibrium between 30 to 60 minutes (2). After reaching chemical equilibrium, the lysosomes begin to swell and simultaneously activate TFEB (3). TFEB triggers the formation of new lysosomes, which undergo the same swelling process under static extracellular concentrations of HCQ (4). This hypothesized mechanism describes the rapid chemical equilibrium of HCQ within the cell, until it starts causing a dynamic increase in the size of the lysosome compartment, ultimately leading to this positive feedback loop where HCQ increases its own cellular volume of distribution.

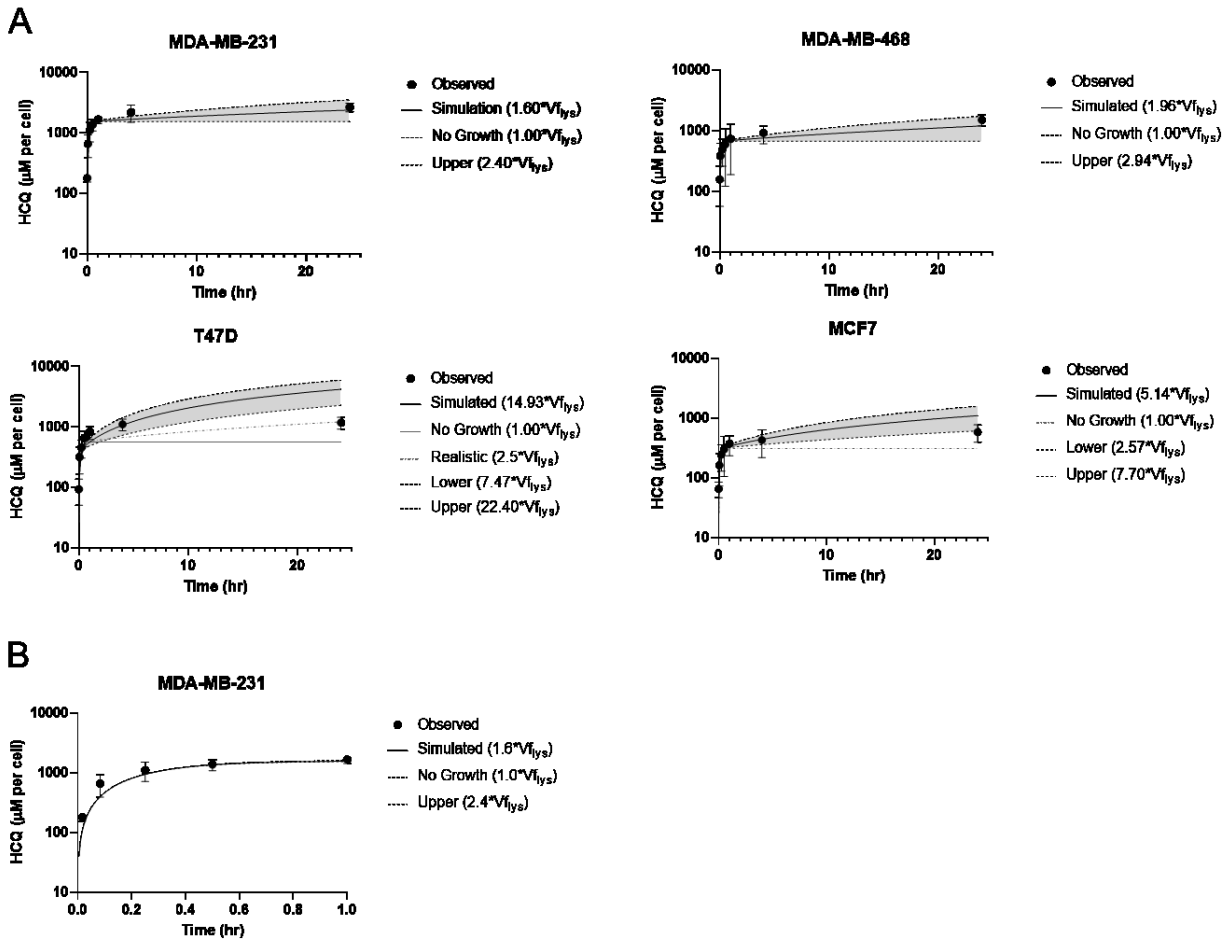

Figure 3.5. Dynamic Lysosome Volume Accounts for Simulation Error in Long-Term HCQ Uptake

To investigate HCQ whole cell uptake past 1 hour, we incorporated a growing lysosomal component into the model for all cell lines. Lysosomal growth is represented by a linear increase as a function of time, out to a maximum lysosomal volume of the fold-increase observed with HCQ treatment for each cell line in Figure 3C. The dynamic system model is shown (A) for MDA-MB-231, MDA-MB-468, T47D, and MCF7, respectively. MDA-MB-231 and MDA-MB-468 simulated uptake are shown as the mean increase in experimental lysosomal volume after HCQ treatment, the upper value of the lysosomal volume, and with no growth incorporated. T47D is shown as the mean, upper, and lower increase in lysosomal volume as well as the value we would expect based on the PK data (*realistic*) and no growth. MCF7 is shown as the mean, upper, lower, and no growth. It should be noted that the time-based increase in lysosomal volume in the dynamic model does not affect earlier timepoints, and thus would not affect model fit versus the static model out to 1 hour (B).

The model fit, as characterized by the ratios of simulated/observed $AUC_{0\text{-}24hr}$, is shown in Table 3.2, and measures of predictive performance PE, MAPE%, and MPE% are shown in Supplementary Table 3.3. Overall, the model captured the early

Table 3.2. Dynamic Model Metrics (AUC)

AUC Summary (0-24hr)	Experimental	Simulated	
Cell Line	Mean	Mean	Mean Sim / Exp
MDA-MB-231	55660	46753	0.84
MDA-MB-468	26922	22085	0.82
T47D	26340	56178	2.13
T47D (*realistic*)		21198	0.80
MCF7	11553	16823	1.46
MCF7 (*lower*)		10975	0.95

early timepoints of the cell lines with good performance, as the AUC and ratios were close to 1. PE followed the same trend to the static model for timepoints 0-1hr, with 4-24 hour timepoints being slightly underpredicted for all cell lines except MCF7 and T47D at 24hr. MAPE% suggests the model fits overall timepoints for all cell lines between 7.53-45.21%, and MPE% suggests a slight underprediction bias for the model. Overall, this experimental data and model simulation suggests that HCQ creates a positive feedback-loop within the cell-lysosomal compartment causing it to increase its own distribution within the cell over time.

Torin1 Increases Size of Lysosomal Compartment Which Increases Cell Uptake of HCQ

While HCQ appears to be able to modify its own distribution, we investigated the capability of direct modification of the cell lysosomal volume fraction to increase HCQ uptake capacity. In Figure 3.4D we observed that Torin1 increased the relative lysosomal burden by 2.25-10.7 fold. In this experiment we repeated the HCQ cell

uptake experiments out to 24 hours, but first pretreated cells with Torin1 (+) or (-) for 16 hours prior to administering HCQ. Pretreatment with Torin1 resulted in a mean increase in cellular uptake of HCQ at all timepoints in all cell lines of 1.4-1.6 fold (Figure 3.6A).

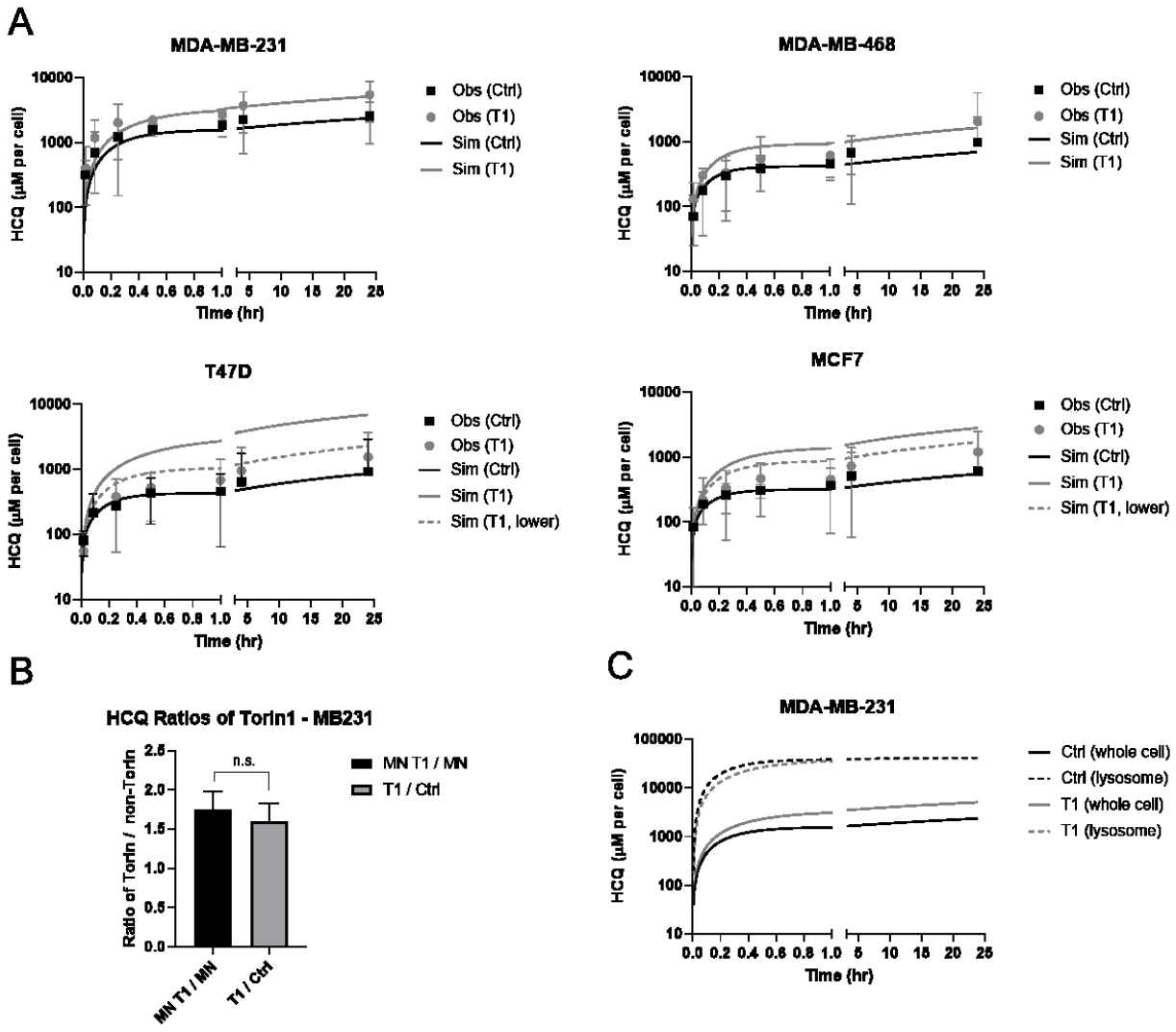

Figure 3.6. Torin1 Increases Size of Lysosomal Compartment, Increasing Whole Cell Uptake of HCQ. Cell lines were pretreated with Torin1 (T1) using the same concentration and time as in Figure 3. After Torin1 pretreatment HCQ, the PK studies from 1min-24hr were repeated in Torin1 (+) vs. Torin1 (-) cells. Torin1 pretreatment resulted in an average increase of HCQ whole cell concentrations at all timepoints by an average of 1.4 to 1.6-fold. The mathematical PK model of HCQ was tested at basal lysosomal volume fractions versus Torin1-modified starting lysosomal volume fractions by multiplying the basal lysosomal volume fraction in each cell line by the mean increase by Torin1 treatment from Figure 4D (A). MDA-MB-231 (A, top-left) fit the data

well using mean values of Torin1. MDA-MB-468 used the starting lysosomal volume fraction value of the lower 95% CI (0.753%) and mean value of Torin1 i6ncrease (A, top-right). T47D used the mean starting Vf_{lys} (0.783%), and was tested against the mean Torin1 increase in lysosomes (10.5x) as well as the lowest observed ratio within the replicates (3x) (A, bottom-left). MCF7 was tested against the mean lysosomal increase by Torin1, and the lowest observed ratio within the replicates (3.8x) (A, bottom-right). To test if the increase in uptake by Torin1 was only due to the increase in lysosomes MDA-MB-231 HCQ uptake was tested at 1 hour with no pretreatment, Torin1 pretreatment, monensin pretreatment, or Torin 1 and monensin pretreatment. No significant change in the ratio between T1/ctrl and MN+T1/MN HCQ uptake was observed (B) with a two-tailed unpaired t test ($p = 0.573$). Comparing the simulated lysosomal concentrations versus the whole cell uptake concentrations in MDA-MB-231 cells with T1 (+) or (-) show a minimal difference in lysosomal concentration in both scenarios (C).

To test this in the context of the *in vitro* PK model, we changed the cell line base lysosomal volume fraction at time 0 based on the mean fold increase of lysosomal fraction by Torin1 from Figure 3.3, and simulated the dynamic lysosome PK model (Figure 3.6A). The dynamic lysosome PK simulation suggested that this change in initial lysosome starting fraction accounts for the increased uptake of HCQ in the cells. For the new data set, the MDA-MB-468 T1 (-) uptake data was simulated against the lower CI basal Vf_{lys} (0.835%) and the T47D against the mean starting Vf_{lys} (0.783%) from Figure 3.1B. In MDA-MB-231 and 468 cells the mean increase of lysosomes by Torin1 accounted for the increased cell uptake of HCQ in the simulation. In T47D and MCF7, the experimental mean increase in lysosomes by Torin1 from Figure 3.3C was very high, and so the ratio from the lowest replicate was used to show the increase the model would account for. Comparison of observed versus simulated $AUC_{0\text{-}24hr}$ are shown in Table 3.3. All simulation/experimental ratios except the T47D and MCF7 mean T1 were within the range of 0.5-2.0; however, T47D and MCF7 simulations using the lowest T1/ctrl lysosome ratio from a replicate did fall within this range. Model

performance metrics are shown in Supplementary Table 3.4. The model for each cell line followed similar performance error (PE) trends to the earlier versions of the models. MAPE% for all cell lines suggests that the model fits overall timepoints between 15.48-61.69%, and MPE% suggests an even spread of over and underprediction of the model across the cell lines.

Table 3.3. Torin1 Dynamic Model Metrics (AUC)

AUC Summary (0-24hr)	Experimental	Simulated	
Cell Line	Mean	Mean	Mean Sim / Exp
MDA-MB-231 (Ctrl)	56214	46753	0.83
MDA-MB-231 (T1)	104084	99813	0.96
MDA-MB-468 (Ctrl)	18490	13141	0.71
MDA-MB-468 (T1)	29517	30276	1.03
T47D (Ctrl)	17692	15304	0.87
T47D (T1)	28044	119838	4.27
T47D (T1 - *lower*)		39299	1.40
MCF7 (Ctrl)	12849	10284	0.80
MCF7 (T1)	21471	49679	2.31
MCF7 (T1 - *lower*)		30585	1.42

In addition, we ran the same experiment in MDA-MB-231 cells, except pretreated cells with T1, T1 + MN, or MN alone prior to treatment with HCQ for 1 hour. We observed that the ratio of T1/ctrl was not statistically significant from the ratio of MN-T1/ MN-ctrl (1.6), suggesting that this increase in cell uptake of HCQ is due to only the increase in lysosomal volume fraction induced by T1 (Fig. 3.6C). In MDA-MB-231, model simulation of the T1 (+) vs. T1 (-) scenarios represented an increase in total cellular uptake of HCQ, but also showed that the lysosomal concentrations in both conditions was roughly the same (Fig. 3.6D). This suggests that even though the

quantifiable concentration of HCQ from a PK study, whole cell or tissue homogenate, may change, the concentration in the lysosome may be the same. This observation could have implications for PK:PD correlations as the lysosome is the target site of HCQ for autophagy-inhibition.

Discussion

Lysosomes have been observed as a drug sink for many lysosomotropic agents, including many prescribed drugs like doxorubicin, vinblastine, imipramine, and a variety of TKIs, like gefitinib (Skoupa et al., 2020), imatinib (Burger et al., 2015), and sunitinib (Ruzickova et al., 2019). In a recent study by Ruzickova et. al. the lysosomotropic agent sunitinib was shown to be capable of increasing overall lysosomal sequestration of the TKIs tested, although this effect was insufficient in reducing sensitivity to the TKIs by the hypothesized mechanism of sequestering them away from their mechanistic target sites as the concentrations tested in culture maintained a static extracellular concentration. The *in vitro* PK model of HCQ supports this finding, and would suggest the same observation as the direct increase of lysosomal volume fraction by pretreating with Torin1 (Fig. 3.6C) barely increases HCQ concentration in the lysosome even though the whole cell concentration is higher. This observation sheds light onto one commonly suggested hypothesis for HCQ growth-inhibition synergism with other lysosomotropic agents in cell culture, which is that HCQ displaces drugs from the lysosome, reducing overall sequestration, and increasing concentration at target sites elsewhere within the cell. This work in conjunction with other recent findings would suggest that under static extracellular concentrations this hypothesized mechanism is

unlikely, as an overall reduced cellular uptake of lysosomotropic drugs may be due to displacement by HCQ, but would not result in a subsequent increase in concentration at the drug's mechanistic target. This does not eliminate this hypothesized mechanism *in vivo* though, as extracellular concentrations are not constant.

Many drugs have been shown to activate TFEB *in vitro* in recent publications (Lu et al., 2017; Zhitomirsky et al., 2018; Zhao et al., 2020), most of which are weakly basic lipophilic agents that would be physicochemically characterized as lysosomotropic. If lysosomotropism is a major factor in the PK of these drugs, as it is for HCQ, then the distribution of these drugs might be altered by their effect on the lysosome as we have observed for HCQ. Our findings emphasize care in cell-level PK studies of drugs with weakly-basic lipophilic structures, especially when attempting to correlate concentration with response. This is especially important when using multiple lysosomotropic agents in combination.

Regardless, the possibility of occurrence of this lysosome-altered distribution is supported by *in vitro* studies in other lysosomotropic agents, whether it be through the activation of lysosomal biogenesis or through lysosomal fusion that is independent of biogenesis (Skoupa et al., 2020), but with limited data to suggest it may occur *in vivo*. HCQ is somewhat unique in this context because of its long half-life combined with often prolonged dosing regimens, which means that tissue will be exposed to relatively high concentrations of the drug for an extended duration. Extended duration of exposure to tissues might exacerbate the lysosomotropic effects due to HCQ, that may not necessarily be prevalent with other drugs that are dosed more short term. We are unaware of any long term preclinical PK studies involving HCQ that investigate multiple

timepoints aside from the work by McChesney, EW (McChesney, 1983). This study looked at a variety of different tissues in rats that were treated with HCQ 6 days/week for months, with timepoints at 1, 2, 3, and 7 months. The key observation from this study is that HCQ concentrations continually increase up to 3 months, where dosing is discontinued in the first study. In the 7 month study, HCQ only starts to reach tissue steady-state between 3-7 months in lung, eye, and muscle, but continues to gradually increase in concentration for other tissue. This is particularly interesting as the plasma half-life of HCQ in rats has been observed at around 10.6 hours (Moore et al., 2011), suggesting a disconnect between plasma and tissue steady-state values. The study by Wei et. al. also investigated HCQ dosing in rats, sampled multiple timepoints of blood over the course of 10 weeks, but only sampled tissue at the 10 week mark (Wei et al., 1995). Interestingly, of the 3 dosing regimens applied to both male and female rats (6 conditions total), only the 8mg/kg regimen in male rats appeared to increase in blood concentration after the first timepoint at 3 weeks, but remained steady after that. For the rest of the dosing regimens, HCQ appeared to remain constant which would suggest that steadily increasing tissue concentrations of HCQ would be undetected by the traditional PK sampling of blood in clinical studies.

This work has implications in HCQ PK, both *in vitro* and *in vivo*, particularly in the context of the cancer clinical trial in solid tumors by Barnard et al., where there was no correlation between HCQ concentrations in the tumor and plasma (Barnard et al., 2014). Further data is needed to investigate the concentration/time relationship of this effect and possible maximum values of lysosome volume fractions that are achievable *in vitro*. For this study we modeled the lysosomal compartment as increasing linearly

with time, although it is more likely that this effect follows a hyperbolic trend – increasing rapidly, and leveling off to eventually reach a pseudo-maximum. It is also likely that this effect is due to overall exposure to HCQ (AUC) rather than time or concentration alone, but to investigate that a significant number of timepoints and concentrations are necessary in conjunction with subsequent PK analysis to maintain a connection between the lysosomal biogenesis mechanism and PK outcome. In addition, a comprehensive PK/PD study connecting increasing tissue concentrations over the long term with an increase in lysosomal volume of tissues is warranted to truly confirm whether this phenomenon is important to consider *in vivo*.

References

Abeywickrama CS, Wijesinghe KJ, Stahelin RV and Pang Y (2019) Lysosome imaging in cancer cells by pyrene-benzothiazolium dyes: An alternative imaging approach for LAMP-1 expression based visualization methods to avoid background interference. *Bioorganic Chemistry* 91:103144-103144.

Barnard RA, Wittenburg LA, Amaravadi RK, Gustafson DL, Thorburn A and Thamm DH (2014) Phase I clinical trial and pharmacodynamic evaluation of combination hydroxychloroquine and doxorubicin treatment in pet dogs treated for spontaneously occurring lymphoma. *Autophagy* 10:1415-1425.

Belhoussine R, Morjani H, Sharonov S, Ploton D and Manfait M (1999) Characterization of intracellular pH gradients in human multidrug-resistant tumor cells by means of scanning microspectrofluorometry and dual-emission-ratio probes. *Int J Cancer* 81:81-89.

Burger H, den Dekker AT, Segeletz S, Boersma AW, de Bruijn P, Debiec-Rychter M, Taguchi T, Sleijfer S, Sparreboom A, Mathijssen RH and Wiemer EA (2015) Lysosomal Sequestration Determines Intracellular Imatinib Levels. *Mol Pharmacol* 88:477-487.

Duvvuri M and Krise JP (2005) A novel assay reveals that weakly basic model compounds concentrate in lysosomes to an extent greater than pH-partitioning theory would predict. *Molecular Pharmaceutics* 2:440-448.

Gallagher LE, Radhi OA, Abdullah MO, McCluskey AG, Boyd M and Chan EYW (2017) Lysosomotropism depends on glucose: a chloroquine resistance mechanism. *Cell death & disease* 8:e3014-e3014.

Grinde B (1983) Effect of Carboxylic Ionophores on Lysosomal Protein-Degradation in Rat Hepatocytes. *Experimental Cell Research* 149:27-35.

Gustafsson LL, Ebling WF, Osaki E, Harapat S, Stanski DR and Shafer SL (1992) Plasma concentration clamping in the rat using a computer-controlled infusion pump. *Pharm Res* 9:800-807.

Ishizaki J, Yokogawa K, Ichimura F and Ohkuma S (2000) Uptake of imipramine in rat liver lysosomes in vitro and its inhibition by basic drugs. *The Journal of pharmacology and experimental therapeutics* 294:1088-1098.

King MA, Ganley IG and Flemington V (2016) Inhibition of cholesterol metabolism underlies synergy between mTOR pathway inhibition and chloroquine in bladder cancer cells. *Oncogene*:1-11.

Kornhuber J, Henkel AW, Groemer TW, Stadtler S, Welzel O, Tripal P, Rotter A, Bleich S and Trapp S (2010) Lipophilic cationic drugs increase the permeability of lysosomal membranes in a cell culture system. *Journal of Cellular Physiology* 224:152-164.

Lu S, Sung T, Lin N, Abraham RT and Jessen BA (2017) Lysosomal adaptation: How cells respond to lysosomotropic compounds. *PLoS ONE* 12:1-23.

Maycotte P, Gearheart CM, Barnard R, Maycotte P, Gearheart CM, Barnard R, Aryal S and Levy JMM (2014) STAT3-Mediated Autophagy Dependence Identifies Subtypes of Breast Cancer where Autophagy Inhibition can be Efficacious. *Cancer Research* 74:2579-2590.

McChesney EW (1983) Animal toxicity and pharmacokinetics of hydroxychloroquine sulfate. *The American Journal of Medicine* 75:11-18.

McChesney EW, Banks WF and Fabian RJ (1967) Tissue distribution of chloroquine, hydroxychloroquine, and desethylchloroquine in the rat. *Toxicology and applied pharmacology* 10:501-513.

Montcourrier P, Mangeat PH, Valembois C, Salazar G, Sahuquet A, Duperray C and Rochefort H (1994) Characterization of very acidic phagosomes in breast cancer cells and their association with invasion. *Journal of Cell Science* 107:2381-2391.

Moore BR, Page-sharp M, Stoney JR, Ilett KF, Jago JD, Batty KT and Al MET (2011) Pharmacokinetics , Pharmacodynamics , and Allometric Scaling of Chloroquine in a Murine Malaria Model □. 55:3899-3907.

Ndolo RA, Luan Y, Duan S, Forrest ML and Krise JP (2012) Lysosomotropic Properties of Weakly Basic Anticancer Agents Promote Cancer Cell Selectivity In Vitro. *PLoS ONE* 7:1-9.

Palmieri M, Impey S, Kang H, di Ronza A, Pelz C, Sardiello M and Ballabio A (2011) Characterization of the CLEAR network reveals an integrated control of cellular clearance pathways. *Hum Mol Genet* 20:3852-3866.

Pellegrini P, Strambi A, Zipoli C, Hägg-olofsson M, Buoncervello M, Linder S and Milito AD (2014) Acidic extracellular pH neutralizes the autophagy-inhibiting activity of chloroquine Implications for cancer therapies. *Autophagy* 10:562-571.

Persi E, Duran-Frigola M, Damaghi M, Roush WR, Aloy P, Cleveland JL, Gillies RJ and Ruppin E (2018) Systems analysis of intracellular pH vulnerabilities for cancer therapy. *Nature Communications* 9.

Ruzickova E, Skoupa N, Dolezel P, Smith DA and Mlejnek P (2019) The Lysosomal Sequestration of Tyrosine Kinase Inhibitors and Drug Resistance. *Biomolecules* 9.

Schmitt MV, Lienau P, Fricker G and Reichel A (2019) Quantitation of lysosomal trapping of basic lipophilic compounds using in vitro assays and in silico predictions based on the determination of the full pH profile of the endo-/lysosomal system in rat hepatocytes. *Drug Metabolism and Disposition* 47:49-57.

Settembre C, Polito VA, Garcia M, Vetrini F, Erdin S, Erdin SU, Huynh T, Medina D, Colella P, Sardiello M and Rubinsztein DC (2013) TFEB Links Autophagy to Lysosomal Biogenesis. *Science* 332:1429-1433.

Settembre C, Zoncu R, Medina DL, Vetrini F, Erdin S, Erdin S, Huynh T, Ferron M, Karsenty G, Vellard MC, Facchinetti V, Sabatini DM and Ballabio A (2012) A lysosome-to-nucleus signalling mechanism senses and regulates the lysosome via mTOR and TFEB. *EMBO J* 31:1095-1108.

Skoupa N, Dolezel P and Mlejnek P (2020) Lysosomal Fusion: An Efficient Mechanism Increasing Their Sequestration Capacity for Weak Base Drugs without Apparent Lysosomal Biogenesis. *Biomolecules* 10:1-37.

Tol MJ, van der Lienden MJC, Gabriel TL, Hagen JJ, Scheij S, Veenendaal T, Klumperman J, Donker-Koopman WE, Verhoeven AJ, Overkleeft H, Aerts JM, Argmann CA and van Eijk M (2018) HEPES activates a MiT/TFE-dependent lysosomal-autophagic gene network in cultured cells: A call for caution. *Autophagy* 14:437-449.

Towers CG, Fitzwalter BE, Regan D, Goodspeed A, Morgan MJ, Liu CW, Gustafson DL and Thorburn A (2019) Cancer Cells Upregulate NRF2 Signaling to Adapt to Autophagy Inhibition. *Dev Cell* 50:690-703 e696.

Trapp S, Rosania GR, Horobin RW and Kornhuber J (2008) Quantitative Modeling of Selective Lysosome Targeting for Drug Design. *European Biophysics Journal* 18:1317-1328.

Wang K, Tu Y, Wan J-B, Chen M and He C (2019) Synergistic anti-breast cancer effect of pulsatilla saponin D and camptothecin through interrupting autophagic–lysosomal function and promoting p62-mediated ubiquitinated protein aggregation. *Carcinogenesis*:1-13.

Wang L, Niu Z, Zhang L, Liu X, Wang X, Li F and Wang Y (2012) Clinicopathological significance of mesothelin expression in invasive breast cancer. *J Int Med Res* 40:909-916.

Warhurst DC, Steele JCP, Adagu IS, Craig JC and Cullander C (2003) Hydroxychloroquine is much less active than chloroquine against chloroquine-resistant Plasmodium falciparum, in agreement with its physicochemical properties. *Journal of Antimicrobial Chemotherapy* 52:188-193.

Wei Y, Nygard GA, Ellertson SL and Khalil SKW (1995) Stereoselective Disposition of Hydroxychloroquine and Its Metabolites in Rats. *Chirality* 7(8);598-604.

Wojtkowiak JW, Verduzco D, Schramm KJ and Gillies RJ (2011) Drug resistance and cellular adaptation to tumor acidic pH microenvironment. *Molecular Pharmaceutics* 8:2032-2038.

Zhao B, Dierichs L, Gu JN, Trajkovic-Arsic M, Axel Hilger R, Savvatakis K, Vega-Rubin-de-Celis S, Liffers ST, Pena-Llopis S, Behrens D, Hahn S, Siveke JT and Lueong SS (2020) TFEB-mediated lysosomal biogenesis and lysosomal drug sequestration confer resistance to MEK inhibition in pancreatic cancer. *Cell Death Discov* 6:12.

Zhitomirsky B, Yunaev A, Kreiserman R, Kaplan A, Stark M and Assaraf YG (2018) Lysosomotropic drugs activate TFEB via lysosomal membrane fluidization and consequent inhibition of mTORC1 activity. *Cell Death Dis* 9:1191.

Chapter Four

Comparative Pharmacologic Assessment of Chloroquine Analogues

Summary

HCQ, while the only clinically-approved autophagy inhibitor used in cancer clinical trials, suffers from clinical shortcomings revolving around pharmacokinetic predictability and contextual efficacy. As discussed earlier, there is a significant disconnect between blood and tumor concentrations of HCQ, creating a challenge in predicting if target concentrations are reached within the tumor in clinical settings. This is likely due to a combination of tumor intrinsic and extrinsic factors specific to lysosomotropic agents. Intrinsic factors are focused around the lysosomal sequestering capacity of specific cells, and the ability of HCQ to modulate this sequestering capacity, creating a dynamic volume of distribution within the cell. Extrinsic factors are primarily attributed to pH variability. Solid tumors are associated with a non-homogenous acidic microenvironment, which blunts HCQ permeability into cells, and creates acidic niche populations of cells which will not be affected by HCQ due to decreased cell uptake. These intrinsic and extrinsic factors together contribute to alterations in HCQ PK *in vitro*, and are likely involved in *in vivo* variabilities in overall tumor exposure to the drug. As

no solution to address these variabilities has been effective when in conjunction with HCQ, the logical next step is to investigate next generation CQ-like autophagy inhibitors that may overcome them. Lys05 (DC221) and DC661 were investigated in a comparative study with HCQ, to determine their susceptibility to such intrinsic and extrinsic factors. Lys05 and DC661 were found to modulate their own cellular volume of distribution by induction of lysosomal biogenesis, similar to HCQ; however, were shown to be less dependent on the lysosomal:cytosolic pH gradient than HCQ. Lys05 and DC661 total cell uptake were less affected by acidified extracellular pH (<2-fold) relative to HCQ (6-fold), which was associated with less of a reduction in cellular growth inhibition. The *in vivo* PK of Lys05 and DC661 suggest higher exposure relative to dose, and maintained concentrations for a longer duration relative to HCQ. Overall, Lys05 and DC661 have advantages over HCQ regarding intrinsic and extrinsic factors related to drug exposure, but still suffer from the same shortcomings, albeit to a lesser degree.

Introduction

In the past two decades many compounds have been discovered that function as autophagy inhibitors, generally categorized by the different steps within the macroautophagic pathway in which they exert activity. Most drugs that have been applied *in vitro* to study stream-points in mechanistic autophagy inhibition have been largely unsuccessful *in vivo* in the context of cancer treatment (Onorati et al., 2018). Currently, inhibition of the endpoint of autophagy, where the lysosome fuses with the autophagosome, has shown the most promise *in vivo*. Along those lines, the only FDA

approved inhibitor of autophagy for clinical cancer treatment is hydroxychloroquine (HCQ), which inhibits the fusion of the lysosome and autophagosome by alkalinizing the lysosomal pH. HCQ has shown moderate success in cancer clinical trials, with positive outcomes including improved patient response rate (Barnard et al., 2014; Mahalingam et al., 2014; Rangwala et al., 2014a; Rangwala et al., 2014b; Boone et al., 2015) and overcoming acquired resistance when used in combination with other therapies (Levy et al., 2014), but has not been successful in monotherapy treatment (Wolpin et al., 2014).

HCQ as an anti-cancer treatment suffers from various pharmacologic shortcomings both *in vitro* and *in vivo*. In clinical trials, HCQ has been observed to cause only a small increase in autophagy inhibition at the highest doses (600 mg b.i.d.), as observed in peripheral blood mononuclear cells (PBMCs), but has also not been observed to have any marker of pharmacokinetic (PK) accumulation within the tumor (Barnard et al., 2014). HCQ (and mechanistically-similar chloroquine (CQ)) concentrations in tissue are dramatically decreased in cells if the extracellular pH is physiologically-acidic (pH < 7.0), which is a hallmark of solid tumors (Hanahan and Weinberg, 2011). This is associated with a loss in the ability of the drug to inhibit autophagy *in vivo* (Pellegrini et al., 2014). In addition, HCQ lacks potency in terms of single agent growth inhibition as well as autophagy inhibition. Typical concentrations of HCQ used in autophagy inhibition assays are 10μM or higher for an extended duration (4-24hr) (Klionsky et al., 2016). As a single agent for inhibiting cancer cells *in vitro* it has a broad range of IC_{50} values generally falling between 1-40μM. For context, clinically-achievable concentrations of HCQ reach a maximum around 10μM (Collins et al., 2018), so to have single agent efficacy it would only affect a population of cancer

cells if one assumes that partitions between the 10μM concentrations correlate directly to *in vivo* concentrations. Unfortunately, this is unlikely as extracellular pH in cell culture assays tends to be much higher (7.4-7.6) than what is observed in solid tumors *in vivo* (6.3-7.0).

As lysosomal inhibition is, so far, the most promising method of inhibiting autophagy *in vivo*, we have focused on investigating drug properties of HCQ further, and comparing directly to dimeric CQ analogues, Lys05 and DC661, that would make them more potent in terms of autophagy inhibition and single agent growth inhibiting potential. Lys05 (DC221) and DC661 are dimeric versions of CQ that contain the same 4-aminoquinoline nucleus, and are connected through a tertiary amine linker of varying carbon chain lengths (DC221 = length 2, DC661 = length 6). Both drugs are shown to be significantly more potent than CQ/HCQ in inhibiting autophagy and growth inhibition. These drugs also have single agent antitumor activity when administered to mice (McAfee et al., 2012; Rebecca et al., 2019). Lys05 is also shown to overcome decreased activity in the presence of acidic extracellular pH in comparison to HCQ (Pellegrini et al., 2014). While these drugs, along with CQ/HCQ, have recently been shown to molecularly target PPT1 (Nicastri et al., 2018; Rebecca et al., 2019), their accumulation at the active site in the lysosome is likely due to extracellular: cytosolic: lysosome pH gradient, as they share similar physicochemical properties to CQ. Lys05 and DC661 are likely to accumulate more preferentially in the lysosome due to a more dramatic shift in membrane permeability between neutral and ionized states. This is driven by the presence of 3 weakly basic amine subgroups, compared to HCQ which only has 2, resulting in increased potency. We do not know if PPT1 plays a role in drug

localization and uptake within the lysosome, but observations discussed herein suggest it likely does.

In this work we investigate how Lys05 and DC661 interact with intrinsic and extrinsic aspects of the *in vitro* system in comparison to HCQ. We observe that Lys05 and DC661 are more potent than HCQ in a panel of 8 cell lines, with correlations between sensitivity across cell lines that suggest they inhibit growth in the same way. Lys05 and DC661 *in vitro* PK are similar to HCQ in that they are driven by lysosomal uptake, modulate their own PK similar to HCQ, and can be manipulated by altering the lysosomal volume of the cell. Lys05 and DC661 are much less affected by acidic extracellular pH in comparison to HCQ, which can be characterized primarily by physicochemical differences, and suggests they would be more viable alternatives to HCQ in overcoming the acidic tumor microenvironment. Furthermore, we characterize Lys05 and DC661 *in vivo* PK in mice in liver, kidney, intestine, brain, and blood. Both drugs are retained in tissue for a significantly longer duration than HCQ and neither were observed in brain tissue, which have significant considerations for drug use in preclinical testing. We investigate the ability of these drugs to inhibit autophagy in 2-D microenvironments, and how autophagy inhibiting potential is affected by acidic extracellular pH. Overall, this work highlights important features of Lys05 and DC661 pharmacologic characterization, which will be important in predicting their use *in vivo* as well as predicting which clinical considerations they may share with HCQ.

Materials and Methods

Cell Lines

Human breast cancer cell lines including MDA-MB-231, MDA-MB-468, and MCF7 were used in experiments. For cell pharmacokinetic experiments all cell lines were stably transfected with Essen NucLight Red Lentivirus prior to experimentation. For autophagic flux experiments cell lines were stably transfected with the mCherry-GFP-LC3 reporter construct, received as a gift from Dr. Andrew Thorburn at Colorado University Anschutz Medical Campus.

Cell lines were cultured in Dulbecco's Modified Essential Medium (DMEM; Corning, 10-017-CV) supplemented with 10% fetal bovine serum (FBS; Peak Serum), 1% penicillin/streptomycin (PS; Fisher), and 1% sodium pyruvate (Fisher) at 37°C and 5% CO_2 in a humidified incubator.

Chemicals and Reagents

Hydroxychloroquine (HCQ) sulfate was purchased from Sigma Aldrich. Monensin (MN) was purchased from VWR. Torin 1 (T1) was purchased from Fisher. Hoechst 33342 20mM solution was purchased from ThermoFisher. Lysosome Dye 1 (*ETP*), a pH-insensitive lysosomal lumen stain applicable for live and fixed cell imaging, was a received as a gift from Dr. Yi Pang at the University of Akron (Abeywickrama et al., 2019). Lys05 and DC661 were gifts from Drs. Jeffrey Winkler and Ravi Amaravadi at University of Pennsylvania. Drug structures of CQ, HCQ, Lys05, and DC661 along with computationally-derived lipophilicities and pKa values are shown in Figure 4.1.

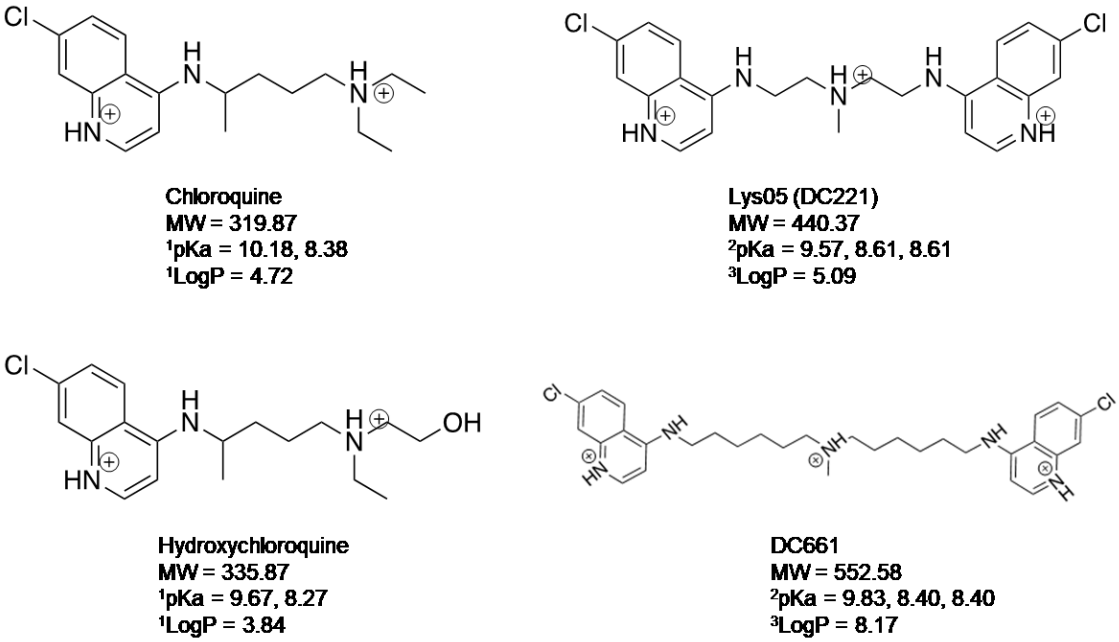

Figure 4.1. Structures of chloroquine analogues.

Cell Growth Inhibition Experiments

Cells were plated in 96-well plates at 5,000 cells/well and allowed to adhere overnight. Drug was dissolved in fresh, warm media and then added to cells for the duration of the experiment (96 hr). For acidic media experiments, cells were plated in culture media and culture media was replaced with acidic media containing the drug. Immediately after adding drug the cells were imaged on an Incucyte ZOOM every 3 hours for the duration of the experiment to count red fluorescent nuclei. Cell growth inhibition was calculated using a concentration survival curve following the Chou-Talalay method (Chou, 2010).

Cell Uptake Experiments

3 human breast cancer cell lines were chosen to perform experiments. The first 2, MBA-MB-231 and MDA-MB-468, are mechanistically sensitive to autophagy inhibition through gene knockdown (Maycotte et al., 2014; Towers et al., 2019) and pharmacologically sensitive to hydroxychloroquine. The third, MCF7, is insensitive to both methods (Maycotte et al., 2014). Cell drug uptake experiments were conducted using the same methods as those described in Chapter 3.

Lysosomal Imaging

Experiments involving the change in relative lysosomal volume of cells used the same dye and imaging methods described in Chapter 3.

Cell Pharmacokinetic Mathematical Modeling and Simulation

Modeling exercises followed the same methods as those described in Chapter 3. Cell starting parameters were identical to those in Chapter 3 for MDA-MB-231, MDA-MB-468, and MCF7. The model developed by Trapp and colleagues (Trapp et al., 2008; Kornhuber et al., 2010) was only designed to characterize mono and dibasic compounds. To account for tribasic compounds a third Henderson-Hasselbach activity radio (D_3) was added to account for fraction of drug in the third ionization state. In addition, the activity coefficient of the 3rd ionization state, gamma 3, was derived using the same methods described (Trapp et al., 2008). Briefly, the third activity coefficient (γ_3) was estimated from the Davies approximation of the modified Debye-Huckel equation at a concentration of 0.1M, which value of $\gamma_3 = 0.07$ for triprotic ions. The base lysosomal PK model developed by Trapp et. al. was only validated against molecules of

0, +1, and +2 ionic states. In testing the model with the derived γ_3, it was found that the model overpredicted cell uptake for Lys05 under neutral conditions as the predicted acid-phospholipid binding free fraction of Lys05 was only 7.38% as opposed to 31.58% for HCQ. This allowed Lys05 to build up to a much higher extent in the lysosome without neutralizing the pH (as only the free fraction is assumed to neutralize lysosomal pH). This allowed Lys05 to accumulate to dramatically high concentrations as the pH-feedback loop in the lysosome was minimally-impactful. In addition, using the derived value of γ_3 did not characterize cellular uptake of Lys05 due to perturbations in media pH very well. Thus, the model for triprotic molecules that incorporated the derived γ_3 did not capture cell uptake of Lys05 very well based on the physicochemistry of the molecule as it did for HCQ. To bypass this mathematical modeling road-block I assumed that γ_3 was similar to a diprotic molecule, and used the same value as γ_2, 0.3 instead of 0.07. This assumption allowed the model to capture *in vitro* PK of Lys05 with much better accuracy.

Mouse Pharmacokinetic Study

Mice were dosed intraperitoneally with 5 or 10 mg/kg Lys05 or 3 mg/kg DC661. Mice were grouped by timepoint with n=3 mice per timepoint. Timepoints included 4, 10, 24 hr, and 2, 3, 4, 8, and 12 days. At the designated timepoint, mice were anaesthetized and sacked. Tissues were immediately harvested, and flash frozen in liquid nitrogen. Tissues included liver, kidney, intestine, and brain. Whole blood was also harvested by cardiac stick, and kept on ice until freezing fully. For LC-MC/MS analysis, tissue was homogenized and diluted 1:10 in Milli-Q water. For Lys05 in tissue, drug was extracted by adding 50µL of tissue homogenate to 150µL of acetonitrile

(ACN). This mixture was vortexed on high for 10 minutes, centrifuged for 10 minutes at 13,300 rpm, and supernatant transferred to polypropylene inserts for analysis. For DC661 in tissue and blood, and Lys05 in blood, drug was extracted by adding 50µL of blood and 5µL of 20% NH_4OH to a tube and vortexed on high for 5 minutes. Then 1000µL of MTBE/EtOAc was added to the tube and vortexed on high for another 5 minutes. Samples were spun at 13,300 rpm for 20 minutes, and then 900µL of supernatant was transferred to a 2mL tube. Samples were dried down on a speed vacuum for 45 minutes on medium speed. Samples were reconstituted in 100µL of 90:10 ACN w/ 0.5% Formic Acid, vortexed for 20 minutes, and transferred to polypropylene inserts for analysis. DQ661 was used as an internal standard and the LLOQ of the method was 10ng/mL. Quantitative chemical analysis was done on a Shimadzu HPLC system coupled to a 3200 Q-TRAP triple quadrupole mass spectrometer (Applied Biosystems, Inc., Foster City, CA) with an Atlantis HILIC Silica 5µm, 4.6 x 150mm column (Part No. 186002028). Noncompartmental analysis of the data was done on Phoenix WinNonlin.

Autophagy Pharmacodynamic Studies

To investigate the role of HCQ, Lys05, and DC661 in endpoint autophagy inhibition in MB231, MB468, and MCF7 cell lines, cells were stably transfected with a GFP-mCherry-LC3 reporter construct. The GFP part of the probe is pH-sensitive, and so under normal conditions will be quenched in the acidic lysosome. Endpoint autophagy inhibition by preventing the autophagosome, where LC3 is located, from fusing with the lysosome should therefore prevent GFP from being quenched and ultimately result in higher GFP/mCherry fluorescence in autophagy inhibited cells. All 3

cell lines were tested for endpoint autophagy inhibition of the drugs, under both neutral and acidic conditions. Cells were treated with the indicated drug condition for 24 hours, and then live cells were imaged on GFP and Cy3 channels at 40x magnification on an LED microscope described in Chapter 3. To compare treatment conditions, the image fluorescence per area was presented as a ratio of GFP/Cy3 and statistical significance was determined using one-way ANOVA with Dunnett's multiple comparison test relative to the control.

Computer Simulation and Software

Intracellular PK model was done in MATLAB, version R2020a (MathWorks, Inc.) and solved using the ode45 package. Image analysis was done in ImageJ, version 1.52p using methods described above. Noncompartmental analysis was done in Phoenix WinNonlin.

Results

Growth Inhibition Trends Between HCQ, Lys05, DC661, and BafA1

Lys05, DC661, and Bafilomycin A1 growth inhibition was tested in a panel of 8 cell lines which included MDA-MB-231 (human breast cancer), MDA-MB-468 (human breast cancer), SK-BR-3 (human breast cancer), H292 (human lung cancer), U2OS (human osteosarcoma), SJSA-1 (human osteosarcoma), Gracie (canine osteosarcoma), and Moresco (canine osteosarcoma). The Dm_{96hr} is reported for all 3 drugs for all cell lines, except SK-BR-3 for DC661.

Cell Dm_{96hr} for Lys05 and DC661 had a significant Pearson correlation across cell lines (P = 0.034) (Fig 4.2A.). HCQ Dm_{96hr} values for the cell lines were not readily available, but all cell lines had been previously characterized as HCQ sensitive (S) or resistant (R). Cell lines Dm_{96hr} for Lys05 fell within the range of 0.5-2μM, where HCQ (S) cell lines were more sensitive to Lys05 and HCQ (R) cell lines were less sensitive (Fig. 4.2B). DC661 followed a similar pattern, although the range of Dm_{96hr} was narrower (0.2-0.5μM) which made it difficult to tell if cell lines followed the same grouping, though it appeared they did (Fig. 4.2B-C).

Cell Dm_{96} of Bafilomycin A1 was also tested in all cell lines except SK-BR-3. The range of BafA1 Dm_{96hr} values fell between 2-15nM, but did not show any correlation when compared to cell sensitivities of Lys05 and DC661 (Fig. 4.2D, E). BafA1 sensitivities also did not appear to follow the same ranking as HCQ (S) vs. (R) cell lines (Fig. 4.2F). Taken together, this data would suggest Lys05, DC661, and HCQ cause growth inhibition in cells in a similar manner. BafA1, which is a V-ATPase inhibitor, deacidifies the lysosome as the three CQ drugs are suggested too, however the manner through which it causes growth inhibition is likely different.

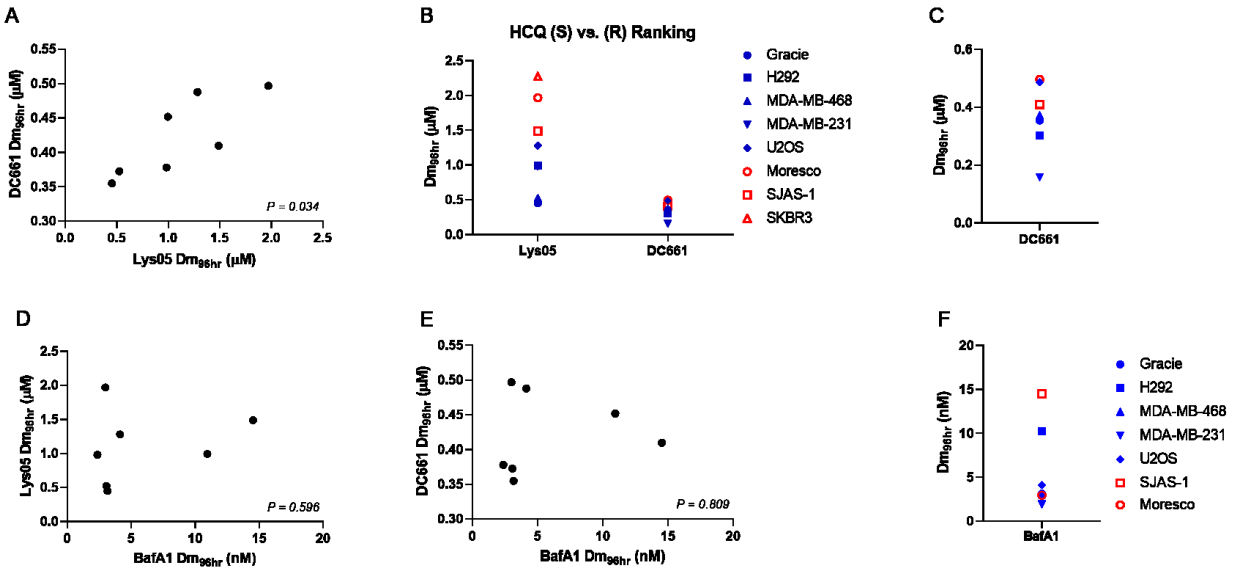

Figure 4.2. Growth inhibition between CQ analogues follows a similar trend across cell lines. Cell lines Dm_{96hr} values are shown for Lys05 vs. DC661 (A). Distribution of Lys05 and DC661 cell Dm_{96hr} values is shown for cells classified as HCQ sensitive (S – blue) or resistant (R – red) (B, C). Lys05 (D) and DC661 (E) Dm_{96hr} compared to Bafilomycin A1 Dm_{96hr}. Distribution of Bafilomycin A1 cell Dm_{96hr} values is shown for cell lines (F).

Intracellular PK of Lys05 and DC661 Exhibits Similar Behavior to HCQ

The intracellular PK of Lys05 and DC661 were determined in MDA-MB-231 cells at 1μM and 0.5μM, respectively, following experimental methods described in Chapter 3. Lys05 was observed to have a similar trend to HCQ, with rapid equilibrium uptake out to 1 hour, followed by consistent steady uptake at 4 and 24 hours (Fig. 4.3A). Total whole cell concentration of Lys05 was increased by a mean of 1.90x at each timepoint when cells were pretreated with 250nM Torin1 for 16hr, suggesting that its PK is lysosomally-driven. By 1hr, 1μM Lys05 treated whole cell concentrations reached 587μM, which compared to 10μM treated HCQ of 2670μM (Fig. 4.3C). DC661 whole cell PK was also similar to HCQ, although exhibited a drop at 1hr followed by recovery

and increase at 4 and 24hr (Fig. 4.3B). Total whole cell concentration of DC661 was increased by a mean of 1.65x at each timepoint when cells were pretreated with 250nM Torin 1 for 16hr hours, suggesting it is also lysosomally-driven, yet seems less perturbed in comparison to Lys05 and HCQ.

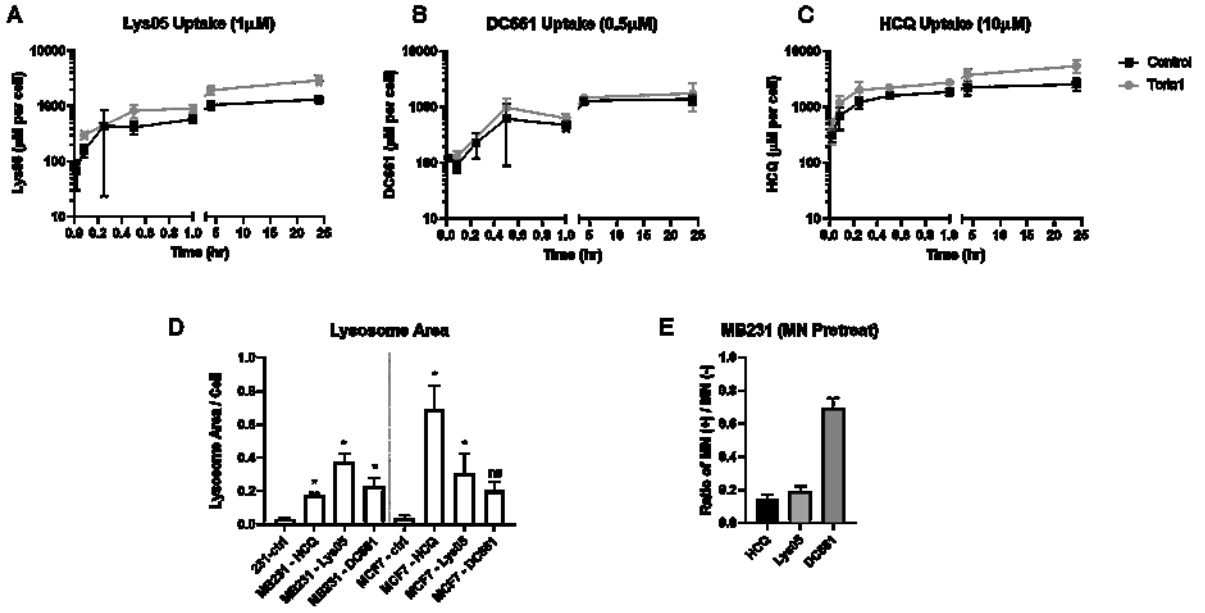

Figure 4.3. Intracellular PK of CQ analogues. MDA-MB-231 cells were treated with Lys05 at 1μM (A), DC661 at 0.5μM (B), and HCQ at 10μM (C) for timepoints ranging from 1 minute to 24 hours (black) or pretreated with Torin1 prior to drug administration (grey), and whole cell concentrations were determined. Lysosome content of cells was probed at 24 hours in MDA-MB-231 and MCF7 cell lines after 24 hours of exposure to the drugs (D). Whole cell concentration ratios of MDA-MB-231 cells pretreated with lysosome ionophore, monensin (MN) or vehicle, prior to 1 hour administration of drugs (E).

Lys05 and DC661, like HCQ, increased the relative lysosome volume in MDA-MB-231 and MCF7 cell lines after 24 hours of exposure (Fig. 4.3D). This suggests that they may also be able to activate the lysosome positive feedback loop which allows them to increase their whole cell concentration over extended exposure times. From

the intracellular PK data illustrated, Lys05 would appear to follow this feedback loop (Fig. 4.3A), whereas DC661 is less apparent (Fig. 4.3B).

MDA-MB-231 cells were pretreated with 25μM MN prior to 1hr exposure to all 3 drugs, and interestingly the decrease in drug uptake of each drug in MN pretreated vs. vehicle pretreated was 0.14 for HCQ, 0.19 for Lys05, and 0.69 for DC661 (Fig. 4.3E). This may indicate that Lys05 and DC661 are less dependent than HCQ on the cytosolic:lysosomal pH gradient to accumulate in cells, suggesting there may be some other binding affect playing a role – potentially due to PPT1 affinity.

Mathematical Modeling of Intracellular PK

To investigate the role of lysosomally-driven PK in the intracellular distribution of Lys05 and DC661, the mathematical model of weakly-basic drug accumulation validated for HCQ from Chapter 3 was applied with appropriate parameters modified. Lys05 and DC661 physicochemical properties have not been determined experimentally, so for the purpose of simulation they were estimated computationally and presented in Table 4.1. LogP values of both drugs were determined using either Molinspiration or ChemDraw. The pKa values were determined by Jaguar through sequential or standard pKa estimation methods. Values used the in the PK simulation were optimized from the estimated values and 2 different combinations were used for each drug.

Table 4.1. Physicochemical properties used in CQ analogue simulations.

Drug	M.W.	LogP (est)	LogP (opt)	pKa (est)	pKa (opt)
HCQ	335.87	3.84	3.84	9.67, 8.27	9.67, 8.27
Lys05	440.37	5.09[1] 7.02[2]	5.9[cond5] 7.02[cond6]	9.57, 7.90, 7.29[3] 9.57, 8.61, 8.61[4]	9.57, 7.90, 7.29[cond5] 9.57, 8.61, 8.01[cond6]
DC661	552.58	8.17[1] 9.48[2]	8.17[cond1] 8.17[cond3]	9.83, 8.40, 7.80[3] 9.83, 8.40, 8.40[4]	9.83, 8.40, 8.40[cond1] 9.83, 8.40, 7.80[cond3]

1 – value estimated by molinspiration
2 – value estimated by Chemdraw
3 – empirical sequential pKa estimated by Jaguar
4 – empirical standard pKa estimated by Jaguar

Simulated versus observed PK of Lys05 and DC661 using the two combinations of pKa and lipophilicity values are shown for MDA-MB-231 cells in Figure 4.4A and B, respectively. With the adjustments made to the base model, outlined in the methods section, the static model of conditions 5 and 6 captured Lys05 uptake kinetics fairly well, aside from 4 and 24 timepoints as was the case in HCQ. DC661 followed a similar pattern.

To investigate the role of the lysosomal pH gradient in uptake of the drugs, I tested the model simulation against conditions representative of MN pretreatment wherein the lysosomal pH is equilibrated with the cytosol (pH = 7.0). Simulated drug treatment with 1μM Lys05 (cond5) and 0.5μM DC661 (cond1) resulted in a lysosomal pH increase to 5.1 and 5.2, respectively (Fig. 4.4C-D). Simulating the MN condition resulted in a whole cell MN (+) / (-) ratio of 0.0026 for Lys05 and 0.00317 for DC661, which were significantly lower than the observed values of 0.19 and 0.60 presented in Figure 4.3E. This again suggests that Lys05 and DC661 whole cell uptake may not be well characterized by the lysosomal pH system, unlike HCQ as outlined in Chapter 3.

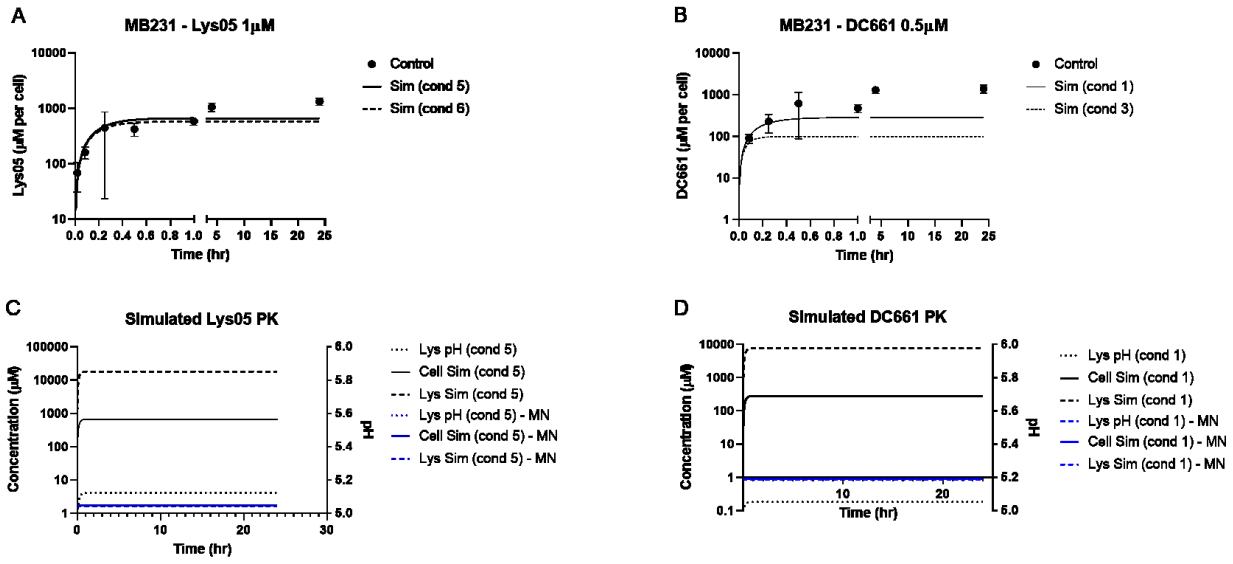

Figure 4.4. Mathematical simulation of acidic ion trap kinetics for Lys05 and DC661. MDA-MB-231 whole cell concentrations of Lys05 and DC661 from Fig. 4.3. compared to simulated cell uptake using Lys05 conditions 1 & 2 (A) and DC661 conditions 1 & 2 (B). Simulation data looking at whole cell uptake and lysosomal uptake of drugs in MN (+) versus (-) conditions for Lys05 (C) and DC661 (D).

Dimeric CQ analogue cell uptake is blunted less by acidic extracellular pH compared to HCQ

Cell interaction with the 3 drugs was tested under standard (N) and more acidified (A) media pH of 7.0 and 7.6, respectively. Drugs were treated at 1 and 10µM for 1 hour in MB231, MB468, and MCF7 cell lines. HCQ whole cell uptake was significantly blunted by the more acidic culture media (Fig. 4.5A) compared to Lys05 and DC661 (Fig. 4.5B-C), such that the concentration of HCQ 1µM (N) was similar to HCQ 10µM (A) for most cell lines. Ratiometric comparisons, presented in Table 4.2, show that the HCQ uptake is decreased by roughly 6.0-fold, where Lys05 and DC661 are decreased by roughly 2-fold. This more pronounced effect for HCQ is observed in cell sensitivity to the drugs in MB231 cells, where HCQ growth inhibiting ability is

completely inhibited (Fig. 4.5D), whereas Lys05 and DC661 maintain some potency under acidic conditions (Fig. 4.5E-F). Simulation of all conditions tested in Figure 4.5A-C show that the mathematical model accounts for reduced uptake of HCQ in most cases for MDA-MB-231, MDA-MB-468, and MCF7 cell lines (Supplementary Figure 4.1A-C). Lys05 conditions 5 and 6 simulation captured the timepoints well at 1μM concentrations in the cell lines, but began to lose accuracy at the higher dose of 10μM (Supplementary Figure 4.1D-F). For DC661, only condition 1 captured the lower concentrations well, but also started to lose accuracy at the higher dose of 10μM (Supplementary Figure 4.1G-I).

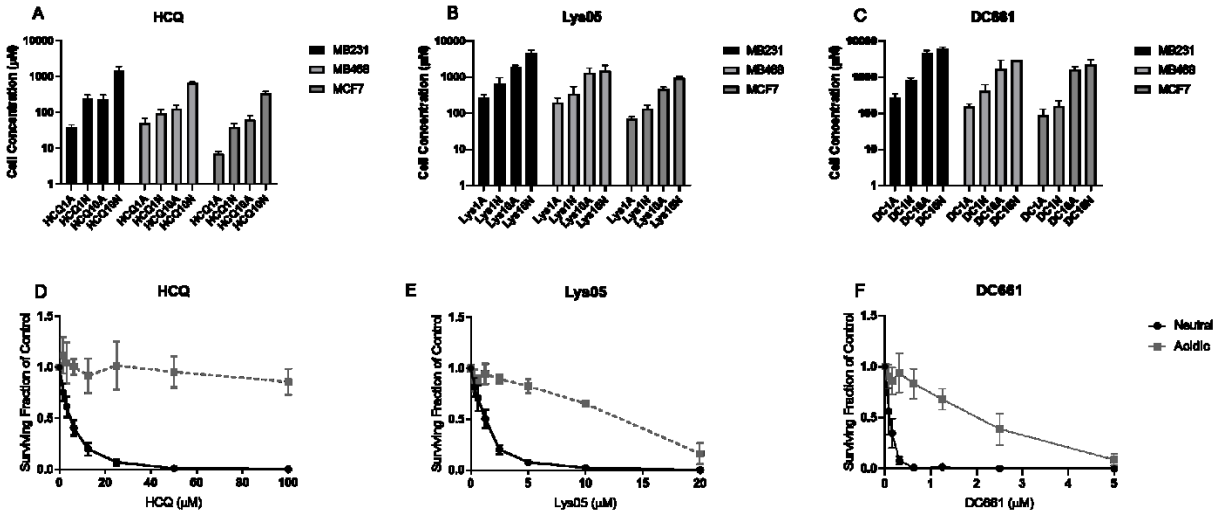

Figure 4.5. Blunting of CQ analogue cell uptake by acidic extracellular pH. Whole cell drug uptake of MDA-MB-231, MDA-MB-468, and MCF7 cell lines treated with 1 or 10μM HCQ (A), Lys05 (B), or DC661 (C) for 1 hour under acidic or neutral media conditions. Cell growth inhibition curves were probed under the same conditions for MDA-MB-231 cell lines using HCQ (D), Lys05 (E), and DC661 (F).

Table 4.2. Ratios for cell lines at different concentrations and pH values

Drug	Conc. Ratio	MB231	MB468	MCF7	Mean	Std. dev
HCQ	1N/1A	8.32	6.80	6.94	*7.35*	*0.84*
	10N/10A	6.38	2.07	5.24	*4.56*	*2.24*
Lys05	1N/1A	2.47	1.72	1.94	*2.04*	*0.38*
	10N/10A	2.33	1.11	2.05	*1.83*	*0.64*
DC661	1N/1A	2.98	2.70	1.79	*2.49*	*0.62*
	10N/10A	1.36	1.69	1.37	*1.47*	*0.19*

To comparatively evaluate the three drugs against each other, simulated uptake of 10μM was tested in MB231 cells for extracellular pH values of 7.6, 7.0, and 6.5 (Fig. 4.6). HCQ cell and lysosomal uptake were significantly decreased the more the extracellular pH was decreased (Fig 4.6A-B), where any alkalinization of lysosomal pH was lost at pH 7.0 (Fig 4.6C). Both conditions for Lys05 had slightly decreased cell and lysosomal uptake between pH 7.6 and 7.0, and more dramatically at pH 6.5 (Fig. 4.6D-E). Condition 5 appeared less blunted by pH between 7.0 and 7.6. Both simulated conditions were able to alkalinize lysosomal pH to some extent under pH 7.0 and 7.6, though condition 6 more so, but most of this was lost at pH 6.5 (Fig. 4.6F). Both simulated conditions for DC661 were barely affected between pH 7.6 and 7.0, but were affected at pH 6.5 (Fig. 4.6G-H). DC661 simulated pH alkalinization suggests that condition 3 is better at alkalinizing lysosomal pH at extracellular pH of 7.6 and 7.0; however, both conditions lose the ability to alkalinize lysosomal pH at extracellular pH of 6.5 (Fig. 4.6I).

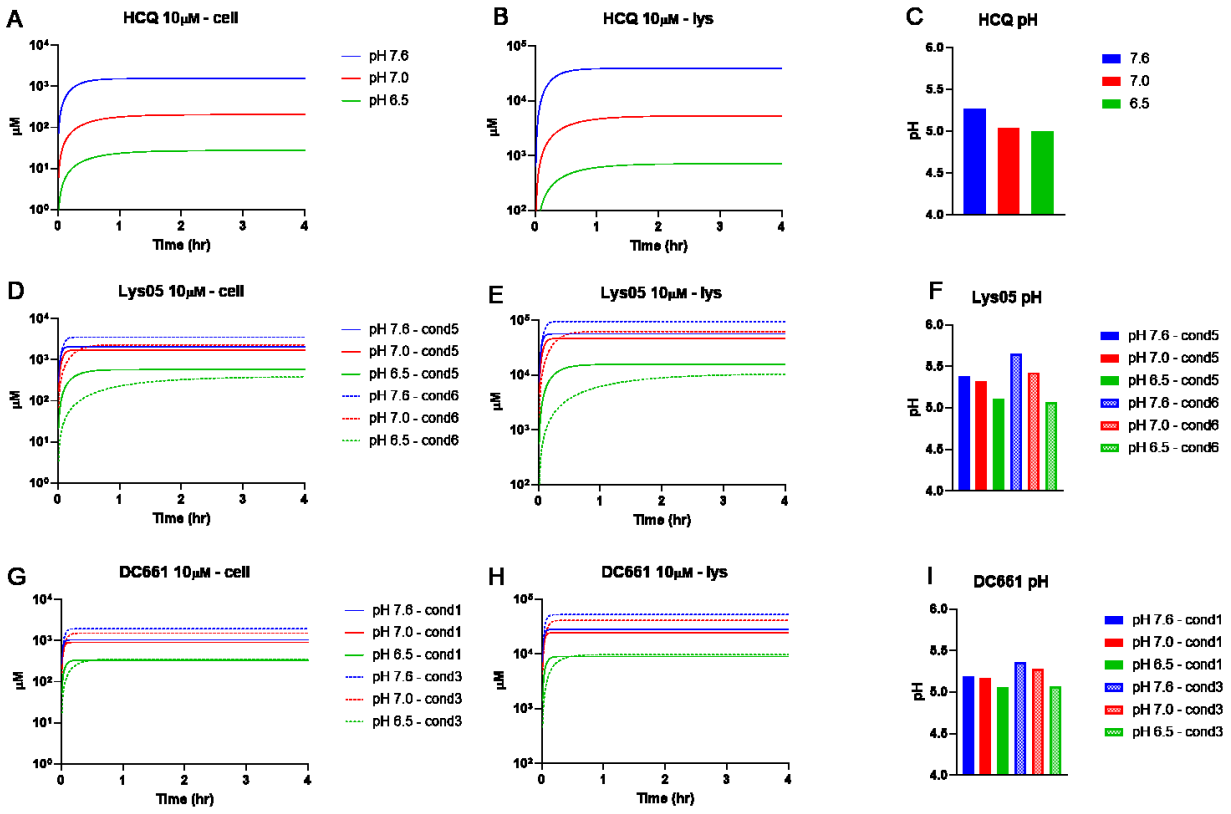

Figure 4.6. Simulation of CQ analogues at different extracellular pH. MDA-MB-231 cell uptake of drugs was simulated at pH 7.6 (blue), 7.0 (red), and 6.5 (green). Simulations were run for HCQ whole cell (A), lysosome (B), and lysosome pH (C); Lys05 whole cell (D), lysosome (E), and lysosome pH (F); DC661 whole cell (G), lysosome (H), and lysosome pH (I).

Mouse Tissue PK of Lys05 and DC661

To investigate the *in vivo* PK of Lys05 and DC661, both drugs were administered to mice intraperitoneally. Lys05 was tested at 5 and 10mg/kg, and DC661 was tested at 3mg/kg, with both drugs tested out to 288hr (12 days). The tissue PK of both drugs were compared to PK data with HCQ at 20, 40, and 80mg/kg from Chapter 2. Lys05 and DC661 were retained in tissue for significantly longer than HCQ (Figure 4.7), and achieved much higher tissue concentrations relative to the dose administered in comparison to HCQ. Lys05 and DC661 were not detected in the brain (Figure 4.7).

Noncompartmental analysis (NCA) of Lys05 and DC661 in Table 4.3 suggest that DC661 is retained in tissue and blood significantly longer than Lys05, despite having mostly lower C_{max} and AUC values for only a slightly lower dose. Comparing half-lives to HCQ, Lys05 was retained in blood 4 times longer and in tissue 4-13 times longer, and DC661 was retained in blood 11 times longer and in tissue 7-61 times longer (Table 4.4).

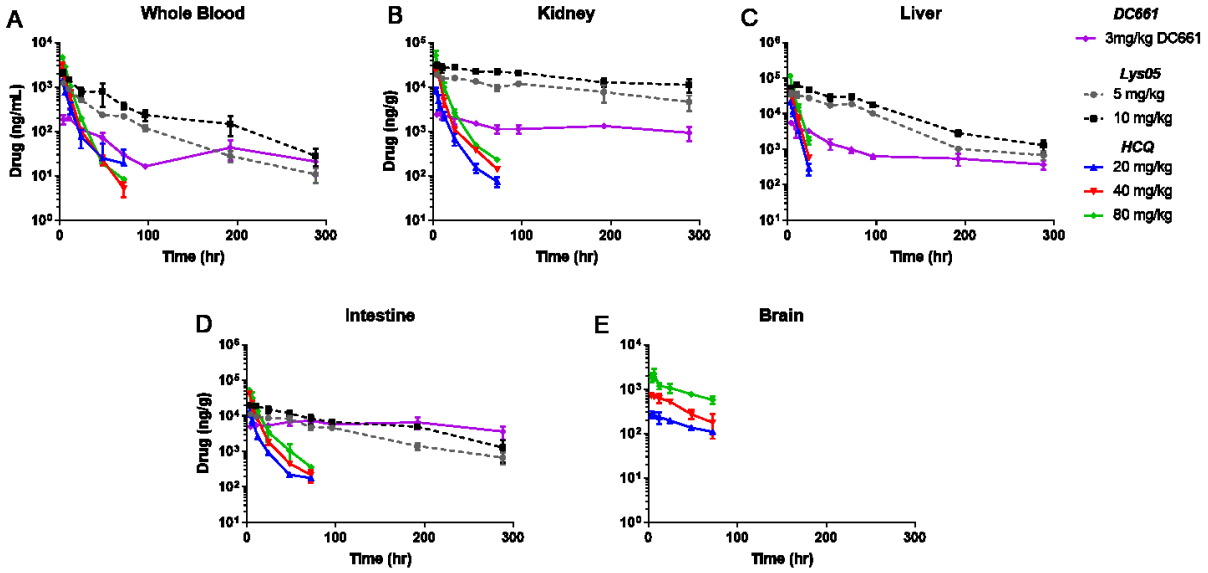

Figure 4.7. Mouse tissue PK of CQ Analogues. Mice were treated with 20, 40, or 80mg/kg HCQ (blue, red, green); 5 or 10mg/kg Lys05 (grey, black); or 3mg/kg DC661 (purple). Tissue were collected between 3-72 hr (HCQ) or 4-288 hr (Lys05, DC661), and concentrations are shown for whole blood (A), kidney (B), liver (C), intestine (D), and brain (E). Lys05 and DC661 were below LLOQ in brain tissue.

Table 4.3. Noncompartmental analysis of Lys05 and DC661 PK data.

Tissue	Cohort	Half-life (hr)		Cmax (ng/g)		AUC (hr*ng/mL)	
		Mean	Std. dev	Mean	Std. dev	Mean	Std. dev
Blood	Lys05 5mg/kg	57.7	7.1	9.28E+02	6.32E+01	3.87E+04	4.84E+02
	Lys05 10mg/kg	65.6	7.0	1.60E+03	2.01E+02	8.43E+04	9.39E+03
	DC661 3mg/kg	179	67.8	2.05E+02	2.49E+01	2.04E+04	7.72E+03
Liver	Lys05 5mg/kg	44.9	3.7	4.01E+04	5.78E+03	2.81E+06	1.27E+05
	Lys05 10mg/kg	48.7	5.9	6.59E+04	6.85E+03	4.87E+06	7.00E+04
	DC661 3mg/kg	182.9	32.1	5.46E+03	2.09E+02	4.11E+05	8.66E+04
Gut	Lys05 5mg/kg	68.9	10.3	1.13E+04	1.28E+03	1.18E+06	6.53E+04
	Lys05 10mg/kg	83.3	20.0	2.05E+04	8.73E+02	2.21E+06	1.09E+05
	DC661 3mg/kg	369.1	96.1	2.49E+03	1.34E+02	9.19E+05	3.34E+05
Kidney	Lys05 5mg/kg	158.5	23.3	1.92E+04	7.76E+02	3.96E+06	5.22E+05
	Lys05 10mg/kg	163.6	34.6	3.22E+04	4.14E+03	7.86E+06	1.17E+06
	DC661 3mg/kg	283	101.2	7.30E+03	9.81E+02	3.34E+06	1.35E+06

Table 4.4. Average tissue half-lives of CQ analogues.

Tissue	HCQ	Lys05	DC661
Blood	15.3	61.7	179.0
Liver	3.6	46.8	182.9
Kidney	15.0	161.0	101.2
Intestine	17.4	65.40	369.1
Brain	47.8	N/A	N/A

Pharmacodynamic Analysis of HCQ, Lys05, and DC661

To investigate the role of HCQ, Lys05, and DC661 in endpoint autophagy inhibition, the MDA-MB-231 cell line was stably transfected with a GFP-mCherry-LC3 reporter construct. The GFP part of the probe is pH-sensitive, and so under normal conditions will be quenched in the acidic lysosome. Endpoint autophagy inhibition by preventing the autophagosome, where LC3 is located, from fusing with the lysosome should therefore prevent GFP from being quenched and ultimately result in higher GFP/mCherry fluorescence in autophagy inhibited cells. Cells were treated with 10 or 50μM HCQ, 1 or 5μM Lys05, 0.5 or 2.5μM DC661, or 100nM Bafilomycin A1 as a positive control under neutral or acidic extracellular conditions for 24 hours prior to live cell imaging. Under neutral conditions 24hr treatment with HCQ 10 and 50μM caused a significant increase in GFP/RFP ratio (Figure 4.8). Lys05 did not cause any significant change, nor did DC661 at 0.5μM; however, DC 2.5μM did. BafA1 did have a significant change relative to control and was most visually apparent.

Under acidic conditions the GFP/mCherry fluorescence ratio comparisons between images were barely changed versus control (Figure 4.9). Lys05 1μM and BafA1 were the only significant conditions. While the quantitative data for most of the dimerics were not significant, they were higher in value relative to HCQ. Visibly, the overall fluorescence in acidic control cells was quite low and the puncta seemed more sparse than neutral control cells. Also, of note is that the overall number of puncta in all acidic treated conditions appeared higher than the control, which may not have been represented in the ratiometric comparison.

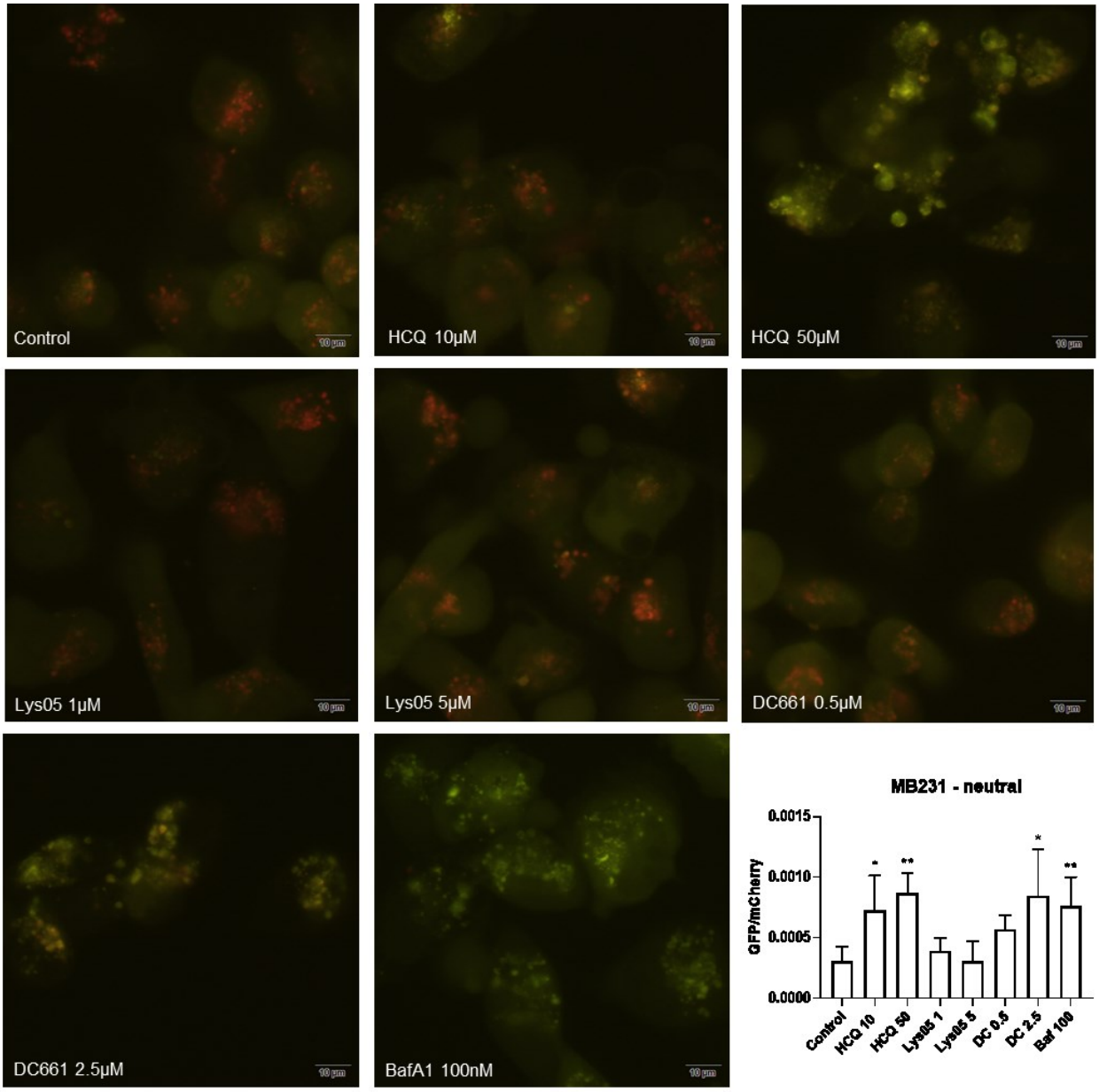

Figure 4.8. MDA-MB-231 LC3-mCherry-GFP cells treated with CQ analogues (neutral). MDA-MB-231 cells transfected with LC3-mCherry-GFP were treated with the indicated drug and concentration in neutral pH culture media for 24 hours prior to live cell imaging at 40x magnification in PBS. Integrated fluorescence density of GFP / mCherry was calculated for each image and condition. Statistical comparisons were made using one-way ANOVA with Dunnett's multiple comparison test relative to control with significance as $P<0.05$. To prepare images for display an equivalent threshold for each channel was applied homogenously to all images.

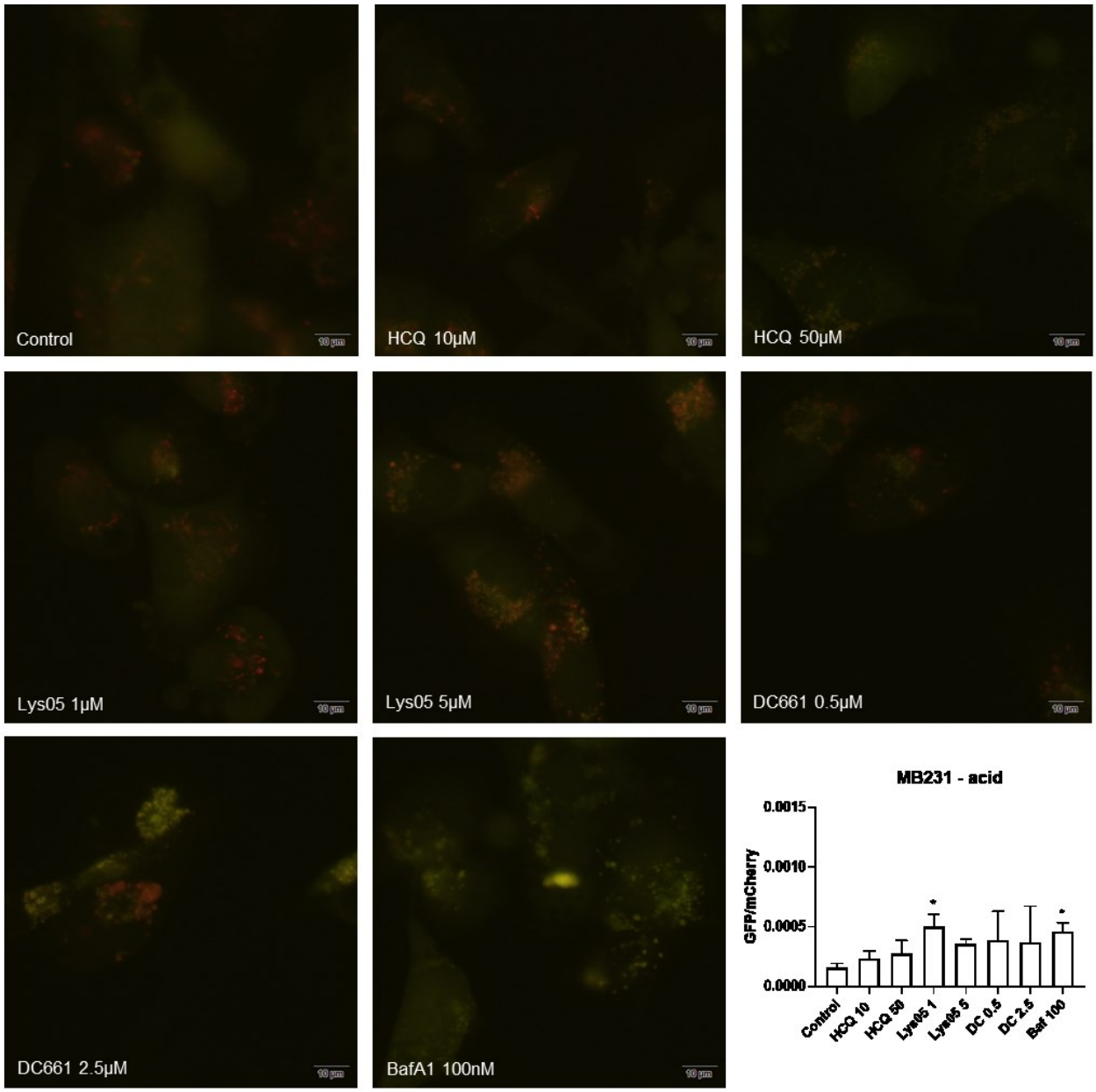

Figure 4.9. MDA-MB-231 LC3-mCherry-GFP cells treated with CQ analogues (acidic). MDA-MB-231 cells transfected with LC3-mCherry-GFP were treated with the indicated drug and concentration in acidic pH culture media for 24 hours prior to live cell imaging at 40x magnification in PBS. Integrated fluorescence density of GFP / mCherry was calculated for each image and condition. Statistical comparisons were made using one-way ANOVA with Dunnett's multiple comparison test relative to control with significance as $P<0.05$. To prepare images for display an equivalent threshold for each channel was applied homogenously to all images.

Discussion

In this chapter I attempt to characterize differences between HCQ and dimeric CQ analogues mainly in the context of pharmacokinetics, and attempt to broadly link pharmacokinetic trends to cytotoxicity and pharmacodynamics. In addition, I attempt to characterize the intracellular pharmacokinetics of dimeric CQ analogues in the same manner as HCQ – based on their physicochemical properties and interactions with the lysosomal system.

All in all, HCQ is similar to Lys05 and DC661 in some regards, but dissimilar in others. The major takeaway is that the behavior of these drugs cannot be mostly characterized by their physicochemical properties, as is the case for HCQ. Under standard conditions, in which these drugs are developed and tested *in vitro*, HCQ, Lys05, and DC661 appear to follow a predictable pattern of cytotoxicity and the trend between cell lines remains the same, i.e. the way the drugs cause growth inhibition appears to be similar. The proposed mechanism is through PPT1 inhibition, which has been identified as the putative target of these drugs (Rebecca et al., 2019). Interestingly, bafilomycin A1 did not follow the same growth inhibition sensitivity trends in cell lines as the CQ analogues, suggesting that growth inhibition is not directly related to endpoint autophagy inhibition by lysosomal pH alkalinization.

Pharmacokinetically, HCQ, Lys05, and DC661 behave similarly under *in vitro* conditions. Their concentrations appear to increase rapidly within the cell, then steadily over time which is likely with induction of some degree of lysosomal biogenesis. This allows them to increase the sequestering capacity of the cell, as the lysosomal compartment becomes larger. Using developed *in vitro* PK models for HCQ one would

expect these drugs to have a higher affinity for the lysosome based on pH-partition theory. Contrary to that assumption, Lys05 whole cell uptake was less perturbed by alkalinizing lysosomal pH with monensin, and DC661 even more so, compared to HCQ. Based on observations from other studies (McAfee et al., 2012; Rebecca et al., 2019), the drugs do appear to alkalinize lysosomal pH like HCQ, but from data within this chapter it would appear that this may not be directly related to their overall cell uptake. It is possible that binding to cell macromolecules, like PPT1, may play a role in this observation as the effect of blunting cell uptake by lysosomal pH alkalinization with monensin is proportional to reported PPT1 inhibiting ability of the drugs (Rebecca et al., 2019). PPT1 chemical binding affinity for the drugs has not been characterized. Another possible explanation is general protein and acid phospholipid binding. HCQ is only about 50% bound to plasma protein, whereas the other two drugs have been observed at >99% bound (personal communication with Ravi Amaravadi). While not directly applicable to *in vitro* observations discussed here, the underlying cause, which is an increase in ionic binding that likely cause the drugs to be more heavily protein bound, may play a role in cells as well. This is also relevant in the context of acid-phospholipids, where the drugs may be shielded from the effects of luminal pH.

A major advantage of Lys05 and DC661, relative to HCQ, is in the context of the acidic microenvironment. Solid tumors generally have non-homogenous extracellular regions with varying pH from 6.3 to 7.0 (Lee and Griffiths, 2020). This physiologically-acidic extracellular pH has been shown to inhibit HCQ, Lys05, and DC661 suggest that the physicochemical properties of HCQ are what allow the acidic microenvironment to inhibit its activity, and that is primarily caused through PK means – i.e. by reduced

overall uptake of the drug into cells. HCQ growth inhibiting capability is completely lost under acidic conditions, but Lys05 and DC661 still maintain some activity. This is connected with a mean reduction in cell uptake of HCQ by 6-fold, versus <2-fold for Lys05 and DC661.

As HCQ is currently the only clinically-approved autophagy inhibitor, this is a major shortcoming in its use. Ironically, autophagy has been suggested as a protective mechanism under acidic extracellular conditions (Marino et al., 2012; Xie et al., 2015), and is suggested to be elevated under acidic extracellular conditions (Tan et al., 2016). This suggests that cells that are more prone to autophagy inhibition are those that HCQ would be unable to target due to acidic extracellular inhibition of its activity, further promoting the advantages of Lys05 and DC661.

In addition, autophagic flux is also suggested to be increased in 3-D *in vitro* cultures relative to 2-D (Follo et al., 2016; Wang et al., 2016; Bingel et al., 2017). In addition, 3-D cultures more closely mimic pH gradients observed *in vivo*, as they have acidic core regions relative to the peripheral regions, and is associated with reduced weakly basic lipophilic drug uptake overall within core regions (Swietach et al., 2012). One would assume Lys05 and DC661 would more effectively permeabilize through the bulk of a 3-D system with an acidifying pH gradient.

From an *in vivo* PK standpoint, Lys05 and DC661 have specific advantages and disadvantages relative to HCQ. The dimeric drugs have much longer half-lives than HCQ, which would allow them to be administered less frequently in a clinical setting assuming that property extrapolates from mice to humans. However, the downside is obvious toxicity concerns as the drugs will maintain concentrations for a longer period of

time. Lys05 and DC661 also were not observed in the brains of mice. This is a potential benefit, as it completely avoids neurotoxic side effects induced by inhibition of PPT1 (personal communication with Ravi Amaravadi). On the other hand, metastatic colonies in the brain cannot be targeted, which is a major area of concern as autophagy inhibition is generally desired in late stage cancers where metastasis is already abundant. Further characterization of the specific mechanism by which Lys05 and DC661 are excluded from the brain are needed, whether it be through impermeability of the blood-brain barrier, or strong affinity for ABCB1 efflux transporters.

From a pharmacokinetics perspective, overall Lys05 and DC661 appear to overcome a major shortcoming of HCQ, which is susceptibility to the acidic microenvironment present in solid tumors. While this is a major benefit, to develop a lead compound, certain aspects of the drugs need to be characterized to understand more specifically how they interact with the cell. Ideally, it would be important to investigate why they do not completely follow the same physicochemically-driven intracellular pharmacokinetics as HCQ. Understanding what drives their distribution on a cellular level would allow development of an ideal lead dimeric CQ analogue, while simultaneously optimizing for properties that give the drug a more optimal clinical PK profile.

References

Abeywickrama CS, Wijesinghe KJ, Stahelin RV and Pang Y (2019) Lysosome imaging in cancer cells by pyrene-benzothiazolium dyes: An alternative imaging approach for LAMP-1 expression based visualization methods to avoid background interference. *Bioorganic Chemistry* **91**:103144-103144.

Barnard RA, Wittenburg LA, Amaravadi RK, Gustafson DL, Thorburn A and Thamm DH (2014) Phase I clinical trial and pharmacodynamic evaluation of combination hydroxychloroquine and doxorubicin treatment in pet dogs treated for spontaneously occurring lymphoma. *Autophagy* **10**:1415-1425.

Bingel C, Koeneke E, Ridinger J, Bittmann A, Sill M, Peterziel H, Wrobel JK, Rettig I, Milde T, Fernekorn U, Weise F, Schober A, Witt O and Oehme I (2017) Three-dimensional tumor cell growth stimulates autophagic flux and recapitulates chemotherapy resistance. *Cell death & disease* **8**:e3013-e3013.

Boone BA, Bahary N, Zureikat AH, Moser AJ, Normolle DP, Wu W-C, Singhi AD, Bao P, Bartlett DL, Liotta LA, Espina V, Loughran P, Lotze MT and Zeh HJ (2015) Safety and Biologic Response of Pre-operative Autophagy Inhibition in Combination with Gemcitabine in Patients with Pancreatic Adenocarcinoma. *Annals of Surgical Oncology* **22**:4402-4410.

Chou TC (2010) Drug combination studies and their synergy quantification using the chou-talalay method. *Cancer Research* **70**:440-446.

Collins KP, Jackson KM and Gustafson DL (2018) Hydroxychloroquine: A Physiologically-Based Pharmacokinetic Model in the Context of Cancer-Related Autophagy Modulation. *The Journal of pharmacology and experimental therapeutics* **365**:447-459.

Follo C, Barbone D, Richards WG, Bueno R and Broaddus VC (2016) Autophagy initiation correlates with the autophagic flux in 3D models of mesothelioma and with patient outcome. *Autophagy* **12**:1180-1194.

Hanahan D and Weinberg RA (2011) Hallmarks of Cancer : The Next Generation. *Cell* **144**:646-674.

Klionsky DJ, Abdelmohsen K, Abe A, Abedin MJ, Abeliovich H, Arozena AA, Adachi H, Adams CM, Adams PD, Adeli K, Adhihetty PJ, Adler SG, Agam G, Agarwal R, Aghi MK, Agnello M, Agostinis P, Aguilar PV, Aguirre-Ghiso J, Aguirre-Ghiso J, Airoldi EM, Airoldi EM, Ait-Si-Ali S, Akematsu T, Akporiaye ET, Al-Rubeai M, Albaiceta GM, Albanese C, Albani D, Albert ML, Aldudo J, Algül H, Alirezaei M, Alloza I, Alloza I, Almasan A, Almonte-Beceril M, Alnemri ES, Alonso C, Altan-Bonnet N, Altieri DC, Alvarez S, Alvarez-Erviti L, Alves S, Amadoro G, Amano A, Amantini C, Ambrosio S, Amelio I, Amer AO, Amessou M, Amon A, An Z, Anania

FA, Andersen SU, Andley UP, Andreadi CK, Andrieu-Abadie N, Anel A, Ann DK, Anoopkumar-Dukie S, Antonioli M, Antonioli M, Aoki H, Apostolova N, Aquila S, Aquilano K, Araki K, Arama E, Aranda A, Araya J, Arcaro A, Arias E, Arimoto H, Ariosa AR, Armstrong JL, Arnould T, Arsov I, Asanuma K, Askanas V, Asselin E, Atarashi R, Atherton SS, Atkin JD, Attardi LD, Auberger P, Auburger G, Aurelian L, Autelli R, Avagliano L, Avagliano L, Avantaggiati ML, Avrahami L, Awale S, Azad N, Bachetti T, Backer JM, Bae DH, Bae JS, Bae ON, et al. (2016) Guidelines for the use and interpretation of assays for monitoring autophagy (3rd edition). *Autophagy* **12**:1-222.

Kornhuber J, Henkel AW, Groemer TW, Stadtler S, Welzel O, Tripal P, Rotter A, Bleich S and Trapp S (2010) Lipophilic cationic drugs increase the permeability of lysosomal membranes in a cell culture system. *Journal of Cellular Physiology* **224**:152-164.

Lee GY, Kenny PA, Lee EH and Bissell MJ (2007) Three-dimensional culture models of normal and malignant breast epithelial cells. *Nature Methods* **4**:359-365.

Lee SH and Griffiths JR (2020) How and Why Are Cancers Acidic? Carbonic Anhydrase IX and the Homeostatic Control of Tumour Extracellular pH. *Cancers (Basel)* **12**.

Levy JMM, Thompson JC, Griesinger AM, Amani V, Donson AM, Birks DK, Morgan MJ, Mirsky DM, Handler MH, Foreman NK and Thorburn A (2014) Autophagy inhibition improves chemosensitivity in BRAF(V600E) brain tumors. *Cancer discovery* **4**:773-780.

Mahalingam D, Mita M, Sarantopoulos J, Wood L, Amaravadi RK, Davis LE, Mita AC, Curiel TJ, Espitia CM, Nawrocki ST, Giles FJ and Carew JS (2014) Combined autophagy and HDAC inhibition: a phase I safety, tolerability, pharmacokinetic, and pharmacodynamic analysis of hydroxychloroquine in combination with the HDAC inhibitor vorinostat in patients with advanced solid tumors. *Autophagy* **10**:1403-1414.

Marino ML, Pellegrini P, Di Lernia G, Djavaheri-Mergny M, Brnjic S, Zhang X, Hägg M, Linder S, Fais S, Codogno P and De Milito A (2012) Autophagy is a protective mechanism for human melanoma cells under acidic stress. *Journal of Biological Chemistry* **287**:30664-30676.

Maycotte P, Gearheart CM, Barnard R, Maycotte P, Gearheart CM, Barnard R, Aryal S and Levy JMM (2014) STAT3-Mediated Autophagy Dependence Identifies Subtypes of Breast Cancer where Autophagy Inhibition can be Efficacious. *Cancer Research* **74**:2579-2590.

McAfee Q, Zhang Z, Samanta A, Levi SM, Ma X-h, Piao S, Lynch JP, Uehara T, Sepulveda AR, Davis LE, Winkler JD and Amaravadi RK (2012) Autophagy

inhibitor Lys05 has single-agent antitumor activity and reproduces the phenotype of a genetic autophagy deficiency. *PNAS* **109**:8253-8258.

Nicastri MC, Rebecca VW, Amaravadi RK and Winkler JD (2018) Dimeric quinacrines as chemical tools to identify PPT1, a new regulator of autophagy in cancer cells. *Mol Cell Oncol* **5**:e1395504.

Onorati AV, Dyczynski M, Ojha R and Amaravadi RK (2018) Targeting autophagy in cancer. *Cancer* **124**:3307-3318.

Pellegrini P, Strambi A, Zipoli C, Hägg-olofsson M, Buoncervello M, Linder S and Milito AD (2014) Acidic extracellular pH neutralizes the autophagy-inhibiting activity of chloroquine Implications for cancer therapies. *Autophagy* **10**:562-571.

Rangwala R, Chang YC, Hu J, Algazy KM, Evans TL, Fecher LA, Schuchter LM, Torigian DA, Panosian JT, Troxel AB, Tan KS, Heitjan DF, DeMichele AM, Vaughn DJ, Redlinger M, Alavi A, Kaiser J, Pontiggia L, Davis LE, O'Dwyer PJ and Amaravadi RK (2014a) Combined MTOR and autophagy inhibition: phase I trial of hydroxychloroquine and temsirolimus in patients with advanced solid tumors and melanoma. *Autophagy* **10**:1391-1402.

Rangwala R, Leone R, Chang YC, Fecher L, Schuchter LM, Kramer A, Tan K-s, Heitjan DF, Rodgers G, Gallagher M, Piao S, Troxel AB, Evans T, Demichele A, Nathanson KL, Dwyer PJO, Kaiser J, Pontiggia L, Davis LE and Amaravadi RK (2014b) Phase I trial of hydroxychloroquine with dose-intense temozolomide in patients with advanced solid tumors and melanoma. *Autophagy* **10**:1-11.

Rebecca VW, Nicastri MC, Fennelly C, Chude CI, Barber-Rotenberg JS, Ronghe A, McAfee Q, McLaughlin NP, Zhang G, Goldman AR, Ojha R, Piao S, Noguera-Ortega E, Martorella A, Alicea GM, Lee JJ, Schuchter LM, Xu X, Herlyn M, Marmorstein R, Gimotty PA, Speicher DW, Winkler JD and Amaravadi RK (2019) PPT1 Promotes Tumor Growth and Is the Molecular Target of Chloroquine Derivatives in Cancer. *Cancer Discov* **9**:220-229.

Swietach P, Hulikova A, Patiar S, Vaughan-Jones RD and Harris AL (2012) Importance of intracellular pH in determining the uptake and efficacy of the weakly basic chemotherapeutic drug, doxorubicin. *PLoS ONE* **7**:1-9.

Tan Q, Wang M, Yu M, Zhang J, Bristow RG, Hill RP and Tannock IF (2016) Role of Autophagy as a Survival Mechanism for Hypoxic Cells in Tumors. *Neoplasia (United States)* **18**:347-355.

Towers CG, Fitzwalter BE, Regan D, Goodspeed A, Morgan MJ, Liu CW, Gustafson DL and Thorburn A (2019) Cancer Cells Upregulate NRF2 Signaling to Adapt to Autophagy Inhibition. *Dev Cell* **50**:690-703 e696.

Trapp S, Rosania GR, Horobin RW and Kornhuber J (2008) Quantitative Modeling of Selective Lysosome Targeting for Drug Design. *European Biophysics Journal* **18**:1317-1328.

Wang Q, Xue L, Zhang X, Bu S, Zhu X and Lai D (2016) Autophagy protects ovarian cancer-associated fibroblasts against oxidative stress. *Cell Cycle* **15**:1376-1385.

Wolpin BM, Rubinson DA, Wang X, Chan JA, Cleary JM, Enzinger PC, Fuchs CS, McCleary NJ, Meyerhardt JA, Ng K, Schrag D, Sikora AL, Spicer BA, Killion L, Mamon H and Kimmelman AC (2014) Phase II and pharmacodynamic study of autophagy inhibition using hydroxychloroquine in patients with metastatic pancreatic adenocarcinoma. *The oncologist* **19**:637-638.

Xie WY, Zhou XD, Li Q, Chen LX and Ran DH (2015) Acid-induced autophagy protects human lung cancer cells from apoptosis by activating ER stress. *Experimental Cell Research* **339**:270-279.

Chapter Five

Conclusions

General Conclusions

HCQ, the touted miracle cure gone flop of the COVID-19 age, may still be the magic bullet for some late stage cancers. Just kidding, magic bullets are what naturopaths sell to you in the form of homeopathic aspirin solutions and concentrated fruit extracts. Hype aside, HCQ does have potential to be a viable combination therapy option for patients with certain late stage cancers. As outlined in this dissertation the shortcomings of HCQ are far and few between, as is often the case with first generation agents. The focus of this dissertation work was motivated by one of the first phase I clinical trials using HCQ to treat solid tumors, led by Rebecca Barnard, a former graduate student in the Gustafson Lab, which highlighted a major roadblock of clinical treatment with HCQ (Barnard et al., 2014). This roadblock was the observation that there was no correlation between HCQ blood concentration and excised tumor concentration in canine patients, referred to multiple times throughout this work as the "HCQ PK/PK disconnect". In a clinical setting, a mathematical relationship is generally assumed between tumor (or peripheral compartment) concentration and that of

blood/plasma. The relationship may be linear or non-linear, or characterized by certain macrophysiological covariates. Generally, there is some way to draw correlation and modify drug dosing if adequate concentrations at the target are not achieved.

The first step I took to approach this problem was to develop a first generation HCQ PBPK model that could characterize PK of HCQ in mice and humans based on physiologic factors. This model also incorporated a lysosomal compartment into the tissue, allowing us insight into the PK of lysosomes, the presumed mechanistic site of action of HCQ, as well as whole tissue. The model was developed by breaking up key tissues in HCQ ADMET into compartments interconnected by blood flow. Within compartments HCQ was trapped within lysosomes, bound to melanin, metabolized, or excreted depending on the tissue being characterized. This complex systems model was characterized largely by physiological and biochemical parameters, with little in the way of unknown parameter optimization, giving it physiologic relevance as an approach to characterizing drug pharmacokinetics. With this model, HCQ PK in mice and humans was described and variabilities assigned to specific, measurable physiological or biochemical factors. The power of this approach is to characterize patient subpopulations directly, based on key parameters within the model. For example, patients with metabolic disorders or renal disease could be simulated directly by modifying relevant parameters. This was a first generation model, and is unproven in the clinic, but with access to more clinical data could be further refined as a valuable tool for individual patient prediction of HCQ PK.

To lay the groundwork for further refinement of this model, particularly attempts to characterize long-term HCQ PK due to trends observed when simulating multiple-

month administration of HCQ, the next step was to define cell-level factors that influenced HCQ PK. The intracellular look at HCQ pharmacokinetics highlighted a few key findings that will drive the way we think about administering this drug going forward. The first is that the sequestering capability of lysosomes is dramatic – in MB231 cells is roughly 92% of total cell uptake. This has implications for other drugs related to HCQ in terms of structure and physicochemical properties. It also highlights that internal or external factors that influence the lysosome will likely also influence HCQ PK. The second is that this lysosomal compartment is dynamic in terms of physical volume fraction of the cell, as well as pH. For the hBC lines examined, the cytosolic/lysosomal pH gradient appeared to be consistent across cell lines; however, the lysosomal volume fraction was different and was correlated with the total uptake of HCQ in the cell. In other cell lines, the pH gradient may be altered in addition to the lysosomal volume fraction. This may have strong implications in vivo as well. As of now, there is minor evidence that lysosomal biogenesis may occur *in vivo* (McChesney, 1983). This needs to be investigated further, but has implications for the way we administer these drugs, especially for long term use or in patients that have been receiving TFEB-activating drugs prior, or in addition to, other drugs that may be candidates for lysosomal sequestration.

It is fairly clear with HCQ that it has some particularly important shortcomings, in terms of distribution. Not only is its uptake and subsequent efficacy blocked by an acidic extracellular space, which is the norm in solid tumors rather than the exception, but it is capable of modulating its own distribution. While yet to be proven *in vivo*, it is an important consideration as the result of this work in considering the HCQ PK/PK

disconnect. Clinical dosing with monoclonal antibodies, such as nivolumab, have been recently observed to have time-varying clearance in human patients, dependent on the state of cachexia (Bajaj et al., 2017; Wang et al., 2017; Wang et al., 2020). In the case of nivolumab, and other monoclonal antibodies like ipilimumab (Sanghavi et al., 2020), clearance is decreased when the patient's health improves, as cachexia and subsequent clearance of the drug is reduced. Lessons from this work, discovered through clinical population pharmacokinetic modeling, can be hypothetically extrapolated to HCQ PK as extended dosing with HCQ may increase the lysosomal volume fraction of tissue and tumor, which would decrease blood clearance of the drug over time. Until a more defined relationship is drawn between HCQ PK in blood and peripheral tumor compartments, the lack of correlation remains cause for concern in clinical dosing as the drug moves into Phase II and III clinical trials.

More importantly, other compounds that behave like HCQ may presumably modify their own volume of distribution and will be subject to these same discrepancies. This is important in developing future drugs, for example in the case of CDK4/6 inhibitors where lysosomal sequestration blunted their efficacy in lysosomally-rich cell lines, and mechanistically-similar compounds were synthesized to side-step this source of resistance (Fassl et al., 2020). Due to the extensive amount of data necessary to characterize HCQ kinetics and dynamic feedback within the non-homogenous tumor microenvironment, it is necessary to consider mechanistically-similar drugs that may minimize or avoid completely the shortcomings of HCQ. Prior to recent findings through target inhibition of PPT1 (Nicastri et al., 2018; Rebecca et al., 2019), the mechanistic action of HCQ was generally assumed to be indirect – through lysosomal deacidification

and/or lysosomal membrane permeabilization. Characterization of mechanistically-similar drugs, then, should be focused on approaches to maximize indirect activity (LMP, deacidification), as well as substrate affinity to PPT1. The focus of Chapter 4 was characterizing mechanistically similar next generation analogues of HCQ in the context of what made them more potent, primarily through characterizing the indirect activity.

Dimeric chloroquine analogues, Lys05 and DC661, showed enhanced potency compared to HCQ. They were also shown, experimentally, to be better suited to maintain potency under acidic extracellular conditions – connected to cellular uptake. Both drugs seem to cause lysosomal biogenesis and have similar in vitro PK profiles to HCQ, suggesting they may also modify their own distribution; however, this potential problem with HCQ may not be as significant of an issue with Lys05 and DC661 if it occurs in vivo. This is due to the extremely long half-life in mice, which would allow the drugs to be dosed less frequently and likely make their PK more predictable. In addition, PK of these drugs would be less influenced by acidic extracellular pH, so if the lack of correlation between tumor PK and blood PK for HCQ observed in canine lymphoma patients is truly due to this factor then it would likely be resolved with Lys05 and DC661. The next step in investigating this mechanism would be to test these drugs in tumor-bearing mice at different dosing levels to directly modify blood concentrations and observe the trend in tumors side-by-side with HCQ. The major downside to these drugs is potential for toxicity. Having such a long half-life would require dose:exposure predictions to be very accurate, working within the narrow therapeutic range of cancer treatment, as side effects from overdoses would be long-lived.

Another potential note to clinical treatment with these drugs is activity within the CNS. HCQ has been linked with psychosis in some patients (Mascolo et al., 2018), and so the observation that Lys05 and DC661 do not accumulate in the brain could be considered a positive attribute of these drugs. The downside of lack of accumulation in the brain is that autophagy-dependency and autophagy-inhibition with HCQ in clinical trials is currently aimed at patients with late stage cancer, where the brain is either the site of a solid tumor or the site of metastatic spread. This poses an obvious potential problem when treating patients with these drugs alone or in combination with other therapies. Whether the drugs are unable to cross the blood-brain barrier, or are strong constituents for CNS efflux transporters is currently unknown. Regardless, this factor is one that is necessary to characterize for clinical administration of these agents, as structural modifications may be appropriate if CNS activity is desired.

Future Directions and Studies

The exciting, and simultaneously frustrating nature of this work is that in answering a few questions we have created many more. The path this work will take going forward can follow multiple different routes, depending on what is deemed most pertinent to characterize. Intrinsic and extrinsic factors relating to HCQ and CQ analogue drug uptake may benefit from further characterization *in vitro* as well as *in vivo*. In addition, other questions formulated as a result of this work may also create interesting projects, specifically around further characterization of TFEB effects on other drugs, further characterization of the lysosomal dye, ETP, and investigation into the interplay between lysosomal pH and HCQ modulation.

From the work described within this dissertation, it is clear that HCQ activates a lysosomal biogenesis feedback loop that increases its own volume of distribution within the cell. The extent to which that feedback loop operates; however, is subject to further characterization. In this work we identified that concentrations as low as 10uM, which are relative maximal concentrations achievable *in vivo*, can induce lysosomal biogenesis significant enough to alter HCQ distribution. From an *in vitro* standpoint, timepoint-based characterization within the 1-24 hour range, as well as out past 24 hours of exposure are necessary to determine the mathematical relationship between HCQ drug uptake and modulation of the lysosomal compartment. In addition, a dose-response study is also warranted. Concentrations between 1-10μM of HCQ are clinically-relevant, and so the *in vitro* PK curve of HCQ at 3-4 concentrations within this range and potentially higher should be evaluated to determine the therapeutic range in which this lysosomal biogenesis effect should be considered. Additionally, this HCQ-altered lysosomal compartment has only been investigated *in vitro*, but the real applicability of this effect would be if it occurs *in vivo*. There is limited data available that observes HCQ tissue PK over long term dosing at multiple timepoints (McChesney, 1983), but this data does suggest that steady-state levels of HCQ in tissue are not achieved at the same time as blood (Wei et al., 1995), if at all. A comprehensive PK study linking steadily increasing tissue PK, steady-state blood PK, and immunohistological characterization of lysosomal biogenesis in tissue/tumor is necessary to truly investigate the role of lysosomal biogenesis in *in vivo* altered distribution of HCQ. Only then can this phenomenon be truly extrapolated to other

lysosomotropic agents and linked with the lysosomal *in vitro* MDR that has been observed in many studies.

On the subject of TFEB-induced lysosomal biogenesis altering volume of distribution of lysosomotropic agents, it would be a rather quick and interesting study to investigate the applicability relative to a panel of such drugs. Experiments would consist of in vitro conditions used for HCQ in Chapter 3, wherein the ability of TFEB, through Torin1, to increase the sequestration of other weakly basic drugs (panel of 8 or so) would be investigated. To strengthen this study, it would be necessary to also test drugs with anionic and zwitterionic structures – drugs not associated with lysosomal uptake.

Further characterization of Lys05 and DC661 is also warranted, both in comparison to HCQ and alone. These drugs appear to activate the same lysosomal feedback loop that alters cellular volume of distribution of HCQ, and so similar experiments as those for further characterization of HCQ should be pursued. Further studies with organoids would have better implications for *in vivo* activity than 2-D studies as well. Specifically, the larger organoids become the more pronounced their internal pH gradient. Investigating organoid size relative to drug uptake of HCQ, Lys05, and DC661 might better explain how they operate *in vivo*. In addition, immunohistological studies investigating drug uptake, lysosomal biogenesis, and autophagy inhibition relative to distance from the organoid periphery might advance our understanding of how these drugs affect localized acidic niches in the *in vivo* tumor microenvironment. To investigate intrinsic factors related to uptake even further it is clear that chemical affinity to PPT1 and the role in which it plays in cellular uptake of

these drugs is warranted. Regarding *in vivo* PK, multiple dose studies, and different dosages are required to determine steady-state levels of these drugs as well as if they follow linear PK with dose.

A rather interesting observation described in recent literature, and observed in some of my experiments (data not included), is around the proposed mechanism of HCQ to alkalinize lysosomal pH. Recent observations suggest the possibility of pH-recovery in lysosomes. Studies with LysoTracker Red, a lysosomotropic fluorescent compound that accumulates in the lysosome due to acidic lysosomal pH, is shown to be quenched upon addition of HCQ to cells preloaded with LysoTracker Red. This observation is consistent with HCQ's proposed mechanism to alkalinize lysosomal pH, and consistent with LysoTracker Red displacement from the lysosome as the pH increases. However, it is observed that treatment with HCQ for 24 hours prior to LysoTracker Red addition still allow for some LysoTracker Red fluorescence within the lysosomal compartment, which is inconsistent with HCQ quenching of lysosome pH over long term continuous exposure. This has been observed in recent studies with CQ as well (Lu et al., 2017; Mauthe et al., 2018). Investigation into the time-based aspect of this phenomena, as well as an underlying mechanistic cause would be extremely valuable data as it contests the proposed mechanism of HCQ autophagy-inhibition as well as the long-accepted mechanism of lysosomotropic drugs to alkalinize lysosomal pH.

References

Bajaj G, Wang X, Agrawal S, Gupta M, Roy A and Feng Y (2017) Model-Based Population Pharmacokinetic Analysis of Nivolumab in Patients With Solid Tumors. *CPT Pharmacometrics Syst Pharmacol* 6:58-66.

Barnard RA, Wittenburg LA, Amaravadi RK, Gustafson DL, Thorburn A and Thamm DH (2014) Phase I clinical trial and pharmacodynamic evaluation of combination hydroxychloroquine and doxorubicin treatment in pet dogs treated for spontaneously occurring lymphoma. *Autophagy* 10:1415-1425.

Fassl A, Brain C, Abu-Remaileh M, Stukan I, Butter D, Stepien P, Feit AS, Bergholz J, Michowski W, Otto T, Sheng Q, Loo A, Michael W, Tiedt R, DeAngelis C, Schiff R, Jiang B, Jovanovic B, Nowak K, Ericsson M, Cameron M, Gray N, Dillon D, Zhao JJ, Sabatini DM, Jeselsohn R, Brown M, Polyak K and Sicinski P (2020) Increased lysosomal biomass is responsible for the resistance of triple-negative breast cancers to CDK4/6 inhibition. *Sci Adv* 6:eabb2210.

Lu S, Sung T, Lin N, Abraham RT and Jessen BA (2017) Lysosomal adaptation: How cells respond to lysosomotropic compounds. *PLoS ONE* 12:1-23.

Mascolo A, Berrino PM, Gareri P, Castagna A, Capuano A, Manzo C and Berrino L (2018) Neuropsychiatric clinical manifestations in elderly patients treated with hydroxychloroquine: a review article. *Inflammopharmacology* 26:1141-1149.

Mauthe M, Orhon I, Rocchi C, Zhou X, Luhr M, Hijlkema KJ, Coppes RP, Engedal N, Mari M and Reggiori F (2018) Chloroquine inhibits autophagic flux by decreasing autophagosome-lysosome fusion. *Autophagy* 0:1-1.

McChesney EW (1983) Animal toxicity and pharmacokinetics of hydroxychloroquine sulfate. *The American Journal of Medicine* 75:11-18.

Nicastri MC, Rebecca VW, Amaravadi RK and Winkler JD (2018) Dimeric quinacrines as chemical tools to identify PPT1, a new regulator of autophagy in cancer cells. *Mol Cell Oncol* 5:e1395504.

Rebecca VW, Nicastri MC, Fennelly C, Chude CI, Barber-Rotenberg JS, Ronghe A, McAfee Q, McLaughlin NP, Zhang G, Goldman AR, Ojha R, Piao S, Noguera-Ortega E, Martorella A, Alicea GM, Lee JJ, Schuchter LM, Xu X, Herlyn M, Marmorstein R, Gimotty PA, Speicher DW, Winkler JD and Amaravadi RK (2019) PPT1 Promotes Tumor Growth and Is the Molecular Target of Chloroquine Derivatives in Cancer. *Cancer Discov* 9:220-229.

Sanghavi K, Zhang J, Zhao X, Feng Y, Statkevich P, Sheng J, Roy A and Vezina HE (2020) Population Pharmacokinetics of Ipilimumab in Combination With Nivolumab in Patients With Advanced Solid Tumors. *CPT Pharmacometrics Syst Pharmacol* 9:29-39.

Wang R, Shao X, Zheng J, Saci A, Qian X, Pak I, Roy A, Bello A, Rizzo JI, Hosein F, Moss RA, Wind-Rotolo M and Feng Y (2020) A Machine-Learning Approach to Identify a Prognostic Cytokine Signature That Is Associated With Nivolumab Clearance in Patients With Advanced Melanoma. *Clin Pharmacol Ther* 107:978-987.

Wang X, Feng Y, Bajaj G, Gupta M, Agrawal S, Yang A, Park JS, Lestini B and Roy A (2017) Quantitative Characterization of the Exposure-Response Relationship for Cancer Immunotherapy: A Case Study of Nivolumab in Patients With Advanced Melanoma. *CPT Pharmacometrics Syst Pharmacol* 6:40-48.

Wei Y, Nygard GA, Ellertson SL and Khalil SKW (1995) Stereoselective Disposition of Hydroxychloroquine and Its Metabolites in Rats. 598404.

Appendix A

Supplemental Material for Chapter Two

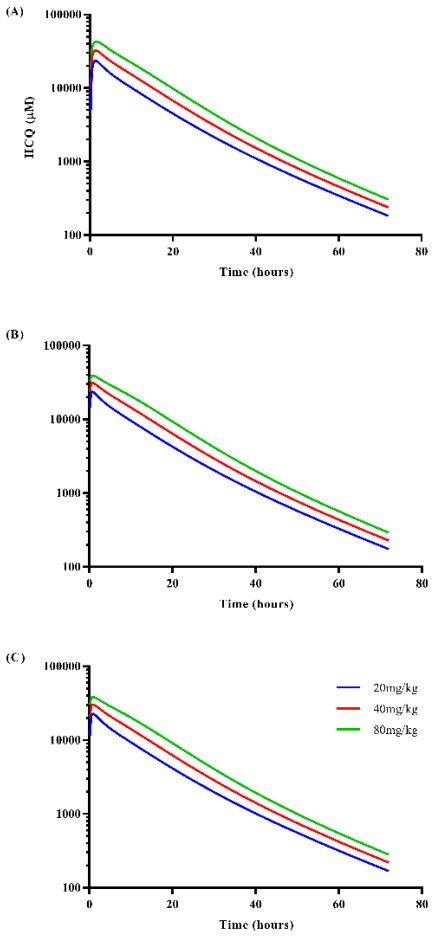

Supplementary Figure 2.1. Simulated lysosomal concentrations in mouse tissue. Simulated lysosomal concentrations of HCQ in mouse liver (A), kidney (B), and gut (C).

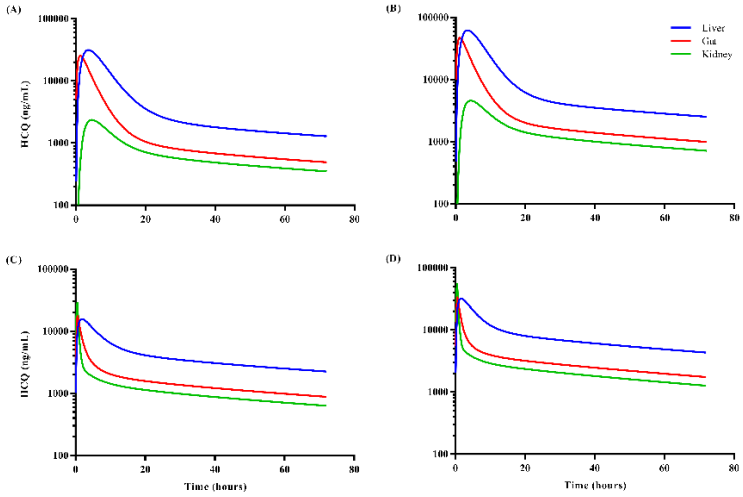

Supplementary Figure 2.2. Simulated concentrations of HCQ in tissue. Simulated HCQ in human liver, kidney, and gut following a single oral dose of 200mg (A), 400mg (B), or IV infusion of 200mg (C), and 400mg (D).

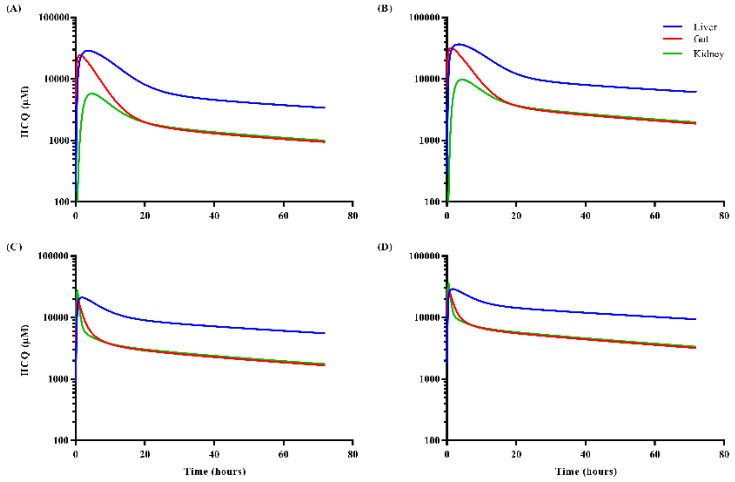

Supplementary Figure 2.3. Simulated lysosomal concentrations. Concentrations of HCQ in human liver, kidney, and gut lysosomes following a single oral dose of 200mg (A), 400mg (B), or IV infusion of 200mg (C), and 400mg (D).

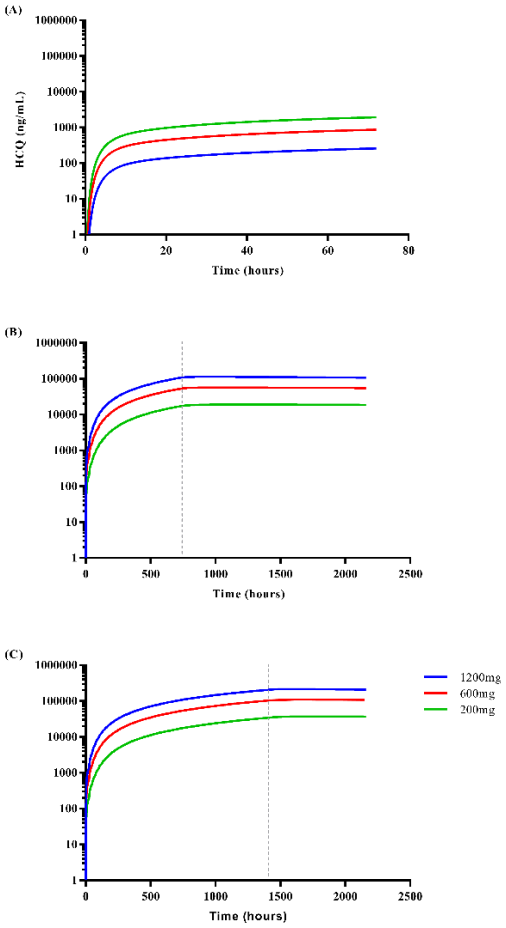

Supplementary Figure 2.4. Simulated concentrations of HCQ in human eyes. Eyes after a single oral dose (A), 30 days of once daily oral dosing (B), and 60 days of once daily oral dosing (C) with 200, 600, and 1200mg HCQ. Grey dotted lines indicate the time when daily dosing was discontinued.

Appendix B

Supplemental Material for Chapter Three

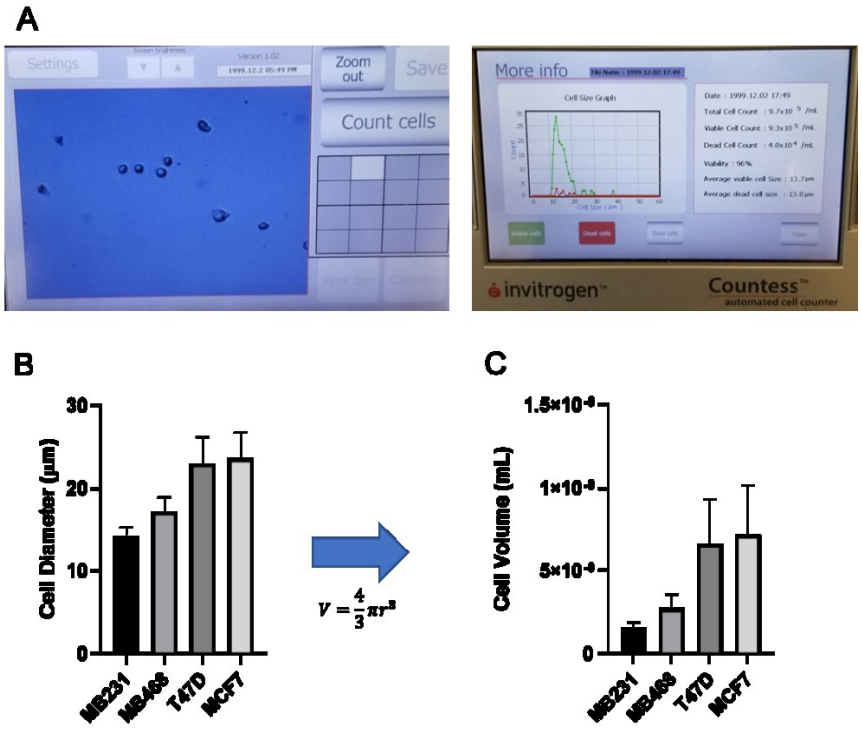

Supplementary Figure 3.1. Calculation of cell volumes. Volume for each cell line was determined by staining with live cell marker Trypan Blue, and then imaging suspended cells on a Countess Cell Counter System (A). Live cell diameter was determined by the mean cell diameter from 4 replicates (B). Cell volume was then calculated from the diameter for each cell line by assuming suspended cells were spherical (C). The geometric mean of the cell volume for each cell line was used in simulation. Data is presented as mean ± sd.

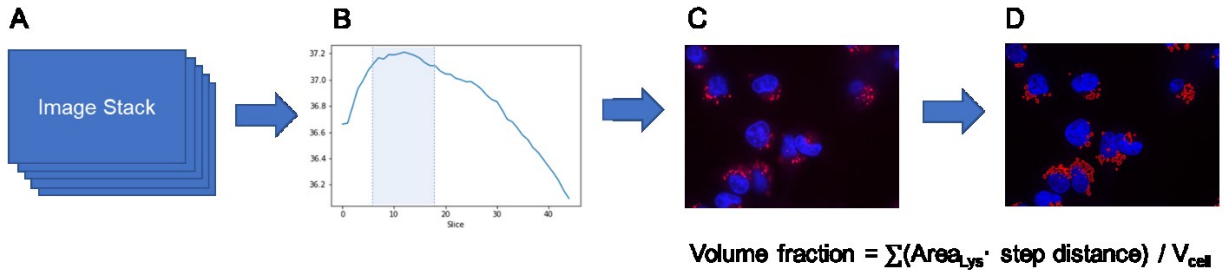

Supplementary Figure 3.2. Calculation of lysosomal volume fractions. Lysosome volume fraction of each cell line was determined by in-house macro methods. Live cells were treated with 1μM ETP for 30 minutes, followed by 10μM Hoechst 33342 for 10 minutes, and then imaging at 60x oil immersion confocal microscopy. 5-10 image stacks were taken per replicate at a step-size of 0.24μm, and 43 slices were taken per image stack on DAPI and Cy3 channels (A). Raw confocal image stacks were converted to .tif files and imported into Python version 3.7.6. Each slice of each image stack was analyzed to determine the peak signal to noise ratio (PSNR) using the sewar module (https://pypi.org/project/sewar/), and the top 10 slices were used for analysis (B). A FIJI macro that calculated the Cy3 (lysosome) area for each raw .vsi image slice based on an algebraic threshold of mean intensity was applied to raw images (C) to generate a lysosome area per slice, which is visualized in (D). Volume fraction for cells was calculated using the following equation: Volume fraction = $\sum(Area_{Lys} \cdot \text{step distance}) / V_{cell}$

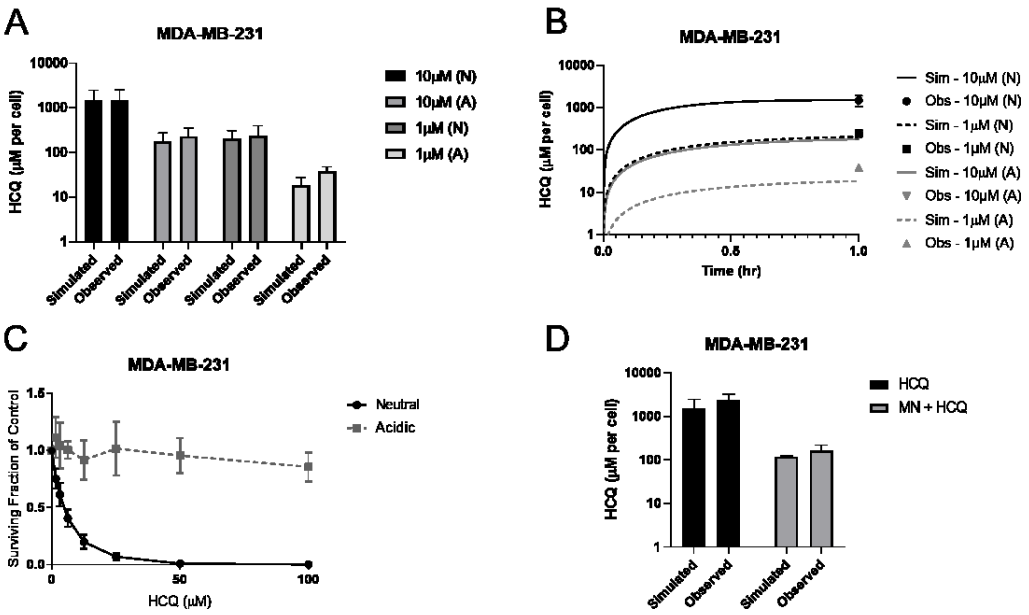

Supplementary Figure 3.3. Static PK Model Accounts for Variability Introduced by Modifying pH Parameters. To further investigate the capability of the model to simulate HCQ PK, we experimentally tested pH parameters within the model to compare to simulation data. We first investigated HCQ whole cell uptake at 1hr in MDA-MB-231 cells at pH_e of 7.6 (N) and 7.0 (A) at 1μM and 10μM for 1 hour and compared to simulation prediction in this cell line (A).

The kinetic uptake curve was not visibly altered between pH_e or concentrations of HCQ μM (B). MDA-MB-231 growth inhibition was almost completely blunted in the presence of the acidic vs. neutral pH after 96hr of exposure (C). The role of the lysosome/cytosol pH gradient in MDA-MB-231 cells by pretreating cells with 25μM monensin (MN) for 30 minutes prior to adding 10μM HCQ for 1 hr (D).

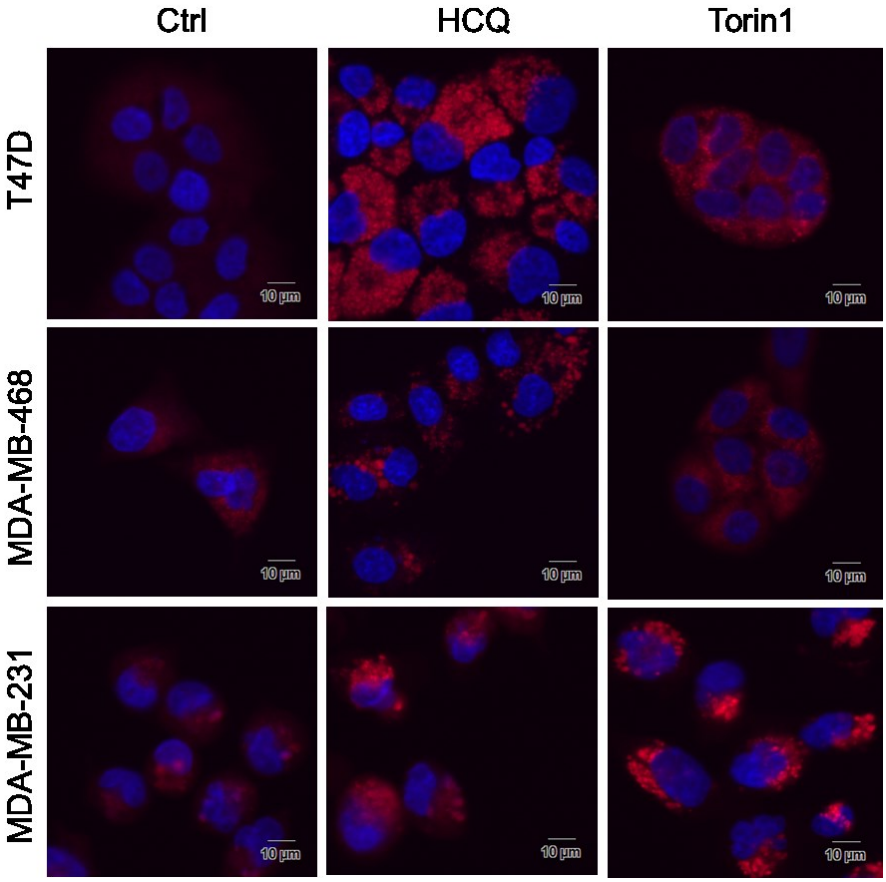

Supplementary Figure 3.4. HCQ and Torin1 treatment causes an increase in lysosomes within the cell. Representative images of T47D (top), MDA-MB-468 (center), and MDA-MB-231 (bottom) imaged with ETP after treatment with HCQ (center) or Torin 1 (right). An increase in lysosomes was visually apparent in all 3 cell lines (in addition to MCF7 – Figure 3) after both treatments. All cell lines appeared to have visibly larger lysosomes in HCQ treated vs. Torin 1 treated images. To prepare figures for publication the raw images threshold was adjusted to the same upper and lower bounds across the entire image for all images shown.

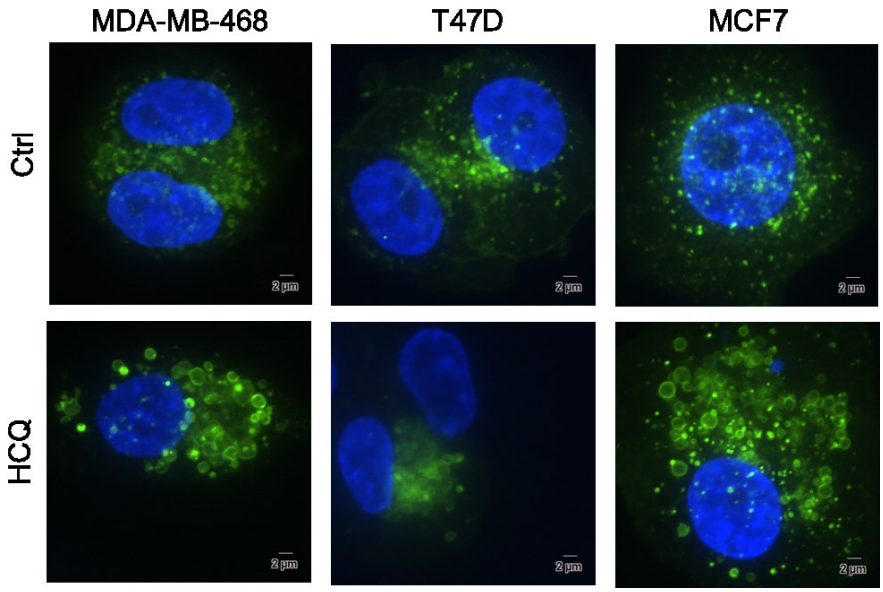

Supplementary Figure 3.5. HCQ treatment causes lysosomal swelling. MDA-MB-468 (left), T47D (center), and MCF7 (right) cells were transfected with GFP-LAMP-1 BacMam and treated with 10µM HCQ for 24 hours. Control cell lines (top) were observed to have LAMP-1 positive (lysosomes) vesicles appearing as small puncta located in the perinuclear region. HCQ treated cells (bottom) were all observed to have lysosomes that were much larger with much more defined membrane edges, though some smaller puncta were still present. To prepare images for publication, the 43-slice image stack was consolidated into a single image using EFI processing on Olympus CellSens software. All images were put through a sharpen filter, and then the GFP threshold was adjusted to the same upper and lower bounds across the entire image for all images shown.

Appendix C

Supplemental Material for Chapter Four

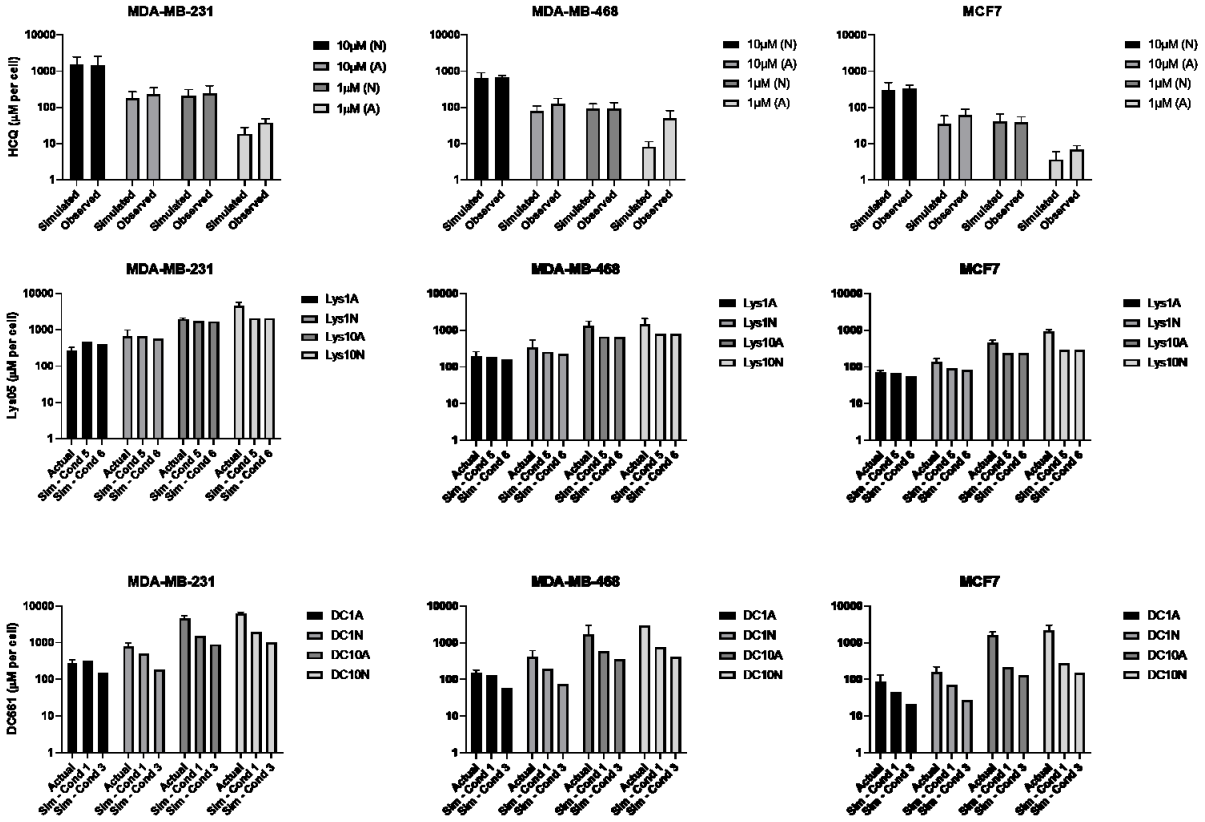

Supplementary Figure 4.1. CQ analogues simulation versus observed data under neutral and acidic conditions. MDA-MB-231, MDA-MB-468, and MCF7 cell lines were treated with 1 or 10 µM of HCQ, Lys05, or DC661 in neutral (N) or acidic (A) media culture conditions for 1 hour. MDA-MB-231, MDA-MB-468, and MCF7 cell line data is displayed in columns left, middle, and right, respectively, with HCQ, Lys05, and DC661 in rows top, middle, and bottom, respectively. The cell PK model was used to simulate neutral and acidic conditions at 1 hour for each cell line using the cell line profile and media pH. HCQ was simulated using the base model presented in chapter 3. Lys05 was simulated using conditions 5 and 6 presented in table 4.1, and DC661 was simulated using conditions 1 and 3 presented in table 4.1.